Bearing Strength Characteristics of Standard and Steel Reinforced GLARE

Bearing Strength Characteristics of Standard and Steel Reinforced GLARE

Proefschrift

ter verkrijging van de graad van doctor
aan de Technische Universiteit Delft,
op gezag van de Rector Magnificus prof. dr. ir. J.T. Fokkema,
voorzitter van het College voor Promoties,
in het openbaar te verdedigen op maandag 1 mei 2006 om 15.00 uur

door

Reinout Gummaris Jacobus
VAN ROOIJEN
ingenieur in de luchtvaart en ruimtevaart
geboren te Bunnik

Dit proefschrift is goedgekeurd door de promotor:

Prof. dr. ir. S. van der Zwaag

Samenstelling promotiecommissie:

Rector Magnificus,	Voorzitter
Prof. dr. ir. S. van der Zwaag,	Technische Universiteit Delft, promotor
Prof. dr. ir. R. Benedictus,	Technische Universiteit Delft
Prof. dr. ir. M.J.L. van Tooren,	Technische Universiteit Delft
Prof. dr. ir. A. Bakker,	Technische Universiteit Delft
Prof. dr. ir. A. de Boer,	Universiteit Twente
Prof. dr. I.M. Richardson,	Technische Universiteit Delft
Prof. ir. L. Katgerman	Technische Universiteit Delft

This research was carried out under project number MC1.01108 (Property-constituent correlation Model for Metal Laminates) in the framework of the Strategic Research programme of the Netherlands Institute for Metals Research (www.nimr.nl).

ISBN-10: 90-77172-21-1
ISBN-13: 978-90-77172-21-6

Keywords: GLARE, Fibre Metal Laminates, Bearing Strength, Pin-loaded Hole, Bolt-loaded Hole, Stainless Steel Reinforcement, Mechanical Joint

Printed in the Netherlands

Contents

Nomenclature

a	half the crack length for a centre crack situation.
a_0	half starter crack length.
a_s	half saw cut length.
$\bar{A}_e$	equivalent shear area affected by the shear deformation.
A_p	cross-sectional area of the pin.
b	delamination height.
C_{cg}	constant in Paris crack growth relation.
C_d	constant in Paris delamination growth relation.
d	degradation factor to describe damage growth in the fibre layer.
da/dN	crack growth rate.
db/dN	delamination growth rate.
D	diameter of the pin.
e	edge distance, i.e. distance between centre of the hole and sheet edge.
e_a	strip width between the centre of the hole and the sheet edge.
e_b	strip width behind the centre of the hole.
E	Young's Modulus.
E_p	elastic modulus of the pin.
G	elastic shear modulus.
$\bar{G}$	average through-the-thickness shear modulus of the laminate.
G_c	critical energy release rate.
Gd	energy release rate for delamination.
G_I	energy release rate for mode I loading.
G_{II}	energy release rate for mode II loading.
G_p	shear modulus of the pin.
I_p	moment of inertia of the pin.
K	foundation or bearing stiffness of plate supporting the pin or bolt.
K	elastic stiffness of the delamination element.
K, K_I	(mode I) stress intensity factor.

K	stress intensity factor at the crack tip.
K_{br}	stress intensity factor as a result of bridging stresses.
K_{eff}	effective stress intensity range.
K_{ff}	stress intensity factor as a result of far field stresses.
K_{pl}	plastic foundation modulus.
K_s	secondary modulus obtained in an hysteris loop after yielding.
$\mathbf{M}$	symmetric stiffness matrix.
M_{pl}	fully plastic bending moment.
M_{rr}	radial bending moment.
n	number of layers.
n_{cg}	power in Paris crack growth relation.
n_d	power in Paris delamination growth relation.
N	interfacial tensile strength.
N	number of fatigue cycles.
N_{pl}	limit force in simple tension.
$\underline{p}$	force vector.
P	applied bearing force.
P_t	pull through load.
r	radius, polar coordinate.
r_c	radius of critical area enabling rivet pull through.
r_e	radius of the area over which lateral displacement takes place.
r_p	pin radius.
R	crack resistance.
R	stress ratio, i.e. $\frac{\sigma_{min}}{\sigma_{max}}$.
R_c	characteristic length for filled hole compression.
R_t	characteristic length for open hole tension.
S, T	(interfacial) shear strength.
S_{br}	bridging stress.
S_{ff}	far field stress.
t	thickness of layer or sheet.
U_c	dissipation of energy on the yield circle r_e.
U_p	potential energy of the pin load.
U_s	energy dissipation in the sheet.
$U_{sb,p}$	strain energy due to bending of the pin.
$U_{s,f}$	strain energy of the Winkler foundation.
$U_{ss,f}$	shear strain energy of the foundation.
$U_{ss,p}$	strain energy due to shearing of the pin.
v	deflection of pin or rivet in direction of loading.

v	crack opening.
v_b	pin deflection due to bearing.
v_{br}	crack opening due to bridgingstress.
v_f	fibre volume fraction.
v_∞	crack opening due to far field opening stress.
v_{pin}	deflection of the pin.
v_s	pin deflection due to shearing.
w	lateral displacement, normal to sheet.
w_{max}	maximum lateral displacement.
W	width of specimen/plate.
X	tensile/compressive strength in principal 11 direction.
Y	tensile/compressive strength in principal 22 direction.
z	through-the-thickness coordinate.

Greek Symbols

α	correction factor for the influence of geometrical parameters on the bearing strength.
α	loading angle of the laminate with respect to the main fibre direction.
β	mode mixity ratio, defining the amount of in-plane shear with respect to normal displacement.
δ_1, δ_2	in-plane shear displacements.
δ_1^f	decohesion displacement for pure mode II.
δ_1^o	damage onset displacement for pure mode II.
δ_2^f	decohesion displacement for pure mode III.
δ_2^o	damage onset displacement for pure mode III.
δ_3	normal displacement.
δ_3^o	damage onset displacement for pure mode I.
δ_e	displacement due to fibre elongation.
δ_m	total mixed mode displacement.
δ_m^f	mixed mode displacement corresponding to decohesion.
δ_m^o	mixed mode displacement corresponding to damage onset.
δ_s	displacement due to fibre shear deformation.
ϵ	tensile or compressive strain.
ϵ_{max}	strain at failure of sheet material.
γ	correction factor for compressive traction.

κ	strain indicator.
κ	ratio of plastic foundation modulus to elastic foundation modulus.
Λ	contact distance through the thickness over which the pin bears in one direction.
λ	correction factor for yield moment for an FML.
λ_s	shear coefficient in Timoshenko's beam theory.
μ	friction coefficient.
ν	Poisson contraction coefficient.
ρ	density.
σ	tensile or compressive stress.
σ_b	bearing stress.
σ_j	joint stress.
σ_y, $\sigma_{0.2}$	tensile or compressive yield stress.
σ_{b_y}	bearing yield stress.
$\sigma_{b_{ult}}$	bearing ultimate stress.
σ_{bn}	blunt notch stress.
σ_{max}	maximum applied fatigue stress.
σ_{min}	minimum applied fatigue stress.
σ_{res}	residual stress in the presence of a sharp notch.
$\sigma_{ult,90}$	ultimate strength of the fibre layer perpendicular to the fibre direction.
σ_{ult}	tensile or compressive ultimate stress.
τ	shear stress.
$\tau_{0.2}$, τ_y	shear yield stress.

Indices

alu	aluminium.
av	average.
c	compression.
lam	laminate.
met	metal.
st	steel.
t	tension.

Abbreviations

ARALL	Aramid Reinforced ALuminium Laminate.
CARE	CArbon fibre REinforced laminate.
GLARE	GLAss fibre REinforced laminate.
TIGR	TItanium GRaphite laminate.
CCT	Centre Cracked Tension (specimen).
CFRP	Carbon Fibre Reinforced Plastic.
CLT	Classical Laminate Theory.
CP	Cross Ply.
FE	Finite Element.
FML	Fibre Metal Laminate.
FRP	Fibre Reinforced Plastic.
L	Longitudinal.
LT	Longitudinal Transverse.
MVF	Metal Volume Fraction.
SEM	Scanning Electron Microscope.
UD	Unidirectional.
UMAT	User MATerial (subroutine).

Chapter 1

Introduction

The original concept and the further development of Fibre Metal Laminates (FMLs) in the 1980-90's was mainly focussed on fatigue critical areas in modern civil aircraft. That research has resulted in an optimised laminated material, which consists of thin metal sheets (typically 0.3 to 0.5 mm thick) bonded together with alternating (unidirectional (UD)) fibre layers as shown in figure 1.1. Typical examples of this concept are aramid and glass fibre reinforced aluminium, commercially available as ARALL and GLARE respectively. Indeed, under realistic fatigue loading, these FML types have proven to be superior to their metallic counterparts. The fibre layers efficiently bridge the fatigue cracks in the metal sheet, resulting in a 10-100 times slower crack growth [1]. The excellent fatigue characteristics, impact resistance [2] and therefore damage tolerance, have led to the commercial application of GLARE in the Airbus A380 fuselage.

An aircraft fuselage is a structure for which the dominant design parameters depend on the location in that fuselage. For a 'metallic' fuselage, the crown section is mainly loaded in (biaxial) tension, the window belt area in shear and the bottom section in compression. Since GLARE is a layered material it can be tailored as much as possible to the specific design requirements. However, in many cases the variations offered by standard GLARE laminates are insufficient compared to monolithic aluminium sheet. Especially, the absolute static strength properties are lower due to the fibre addition. Therefore, new laminate configurations should be defined, which are based upon other constituents than the standard aluminium 2024-T3 sheets and/or the S_2 glass or aramid fibre reinforced epoxy layers.

Several researchers have already investigated other FML concepts, which are presented here to define a framework for this thesis and to highlight a few of the material characteristics that play a role for material selection for aerospace applications.

An FML concept that received considerable attention [3–6] is the so-called CARE or TIGR laminate, which is a combination of titanium sheets with carbon fibre. This material combination can indeed result in an improvement in static strength compared to GLARE, since both the titanium sheet and the carbon fibre have higher strength and stiffness than the respective GLARE constituents. The use of titanium sheets has however several drawbacks compared to aluminium sheets, like material cost, machinability and the difficult pretreatment for laminate bonding. For more demanding applications, with for example high-temperature conditions, this FML is however more suited than GLARE.

In comparison, the combination of carbon fibre with aluminium sheets is generally not used due to the occurrence of galvanic corrosion between these two constituents.

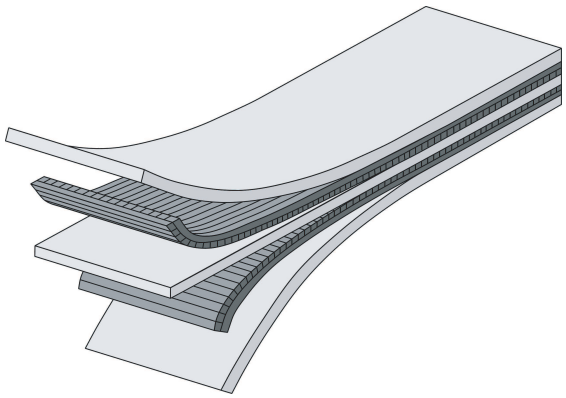

Figure 1.1: *Partially exploded view of a typical build-up of a Fibre Metal Laminate.*

Still, an FML consisting of these constituents had increased stiffness and strength compared to monolithic aluminium sheet [7].

An FML consisting of magnesium sheets combined with carbon fibre layers has also been investigated. This material combination was shown to have improved specific strength compared to an FML with aluminium 2024 sheets in the T0 temper [8]. A comparison with an FML containing 2024 sheets in the T3 temper would have revealed that magnesium is not fit as a fuselage material.

Next to the already mentioned tension/compression and shear properties, several other static strength properties play an important role in fuselage design. A (metallic) fuselage structure is generally constructed of several sheets, which are connected with mechanical (i.e. rivetted or bolted) joints. The reason for the use of these joints is for example the limited width of the metal sheets, the ease of assembly and disassembly and the necessity to join dissimilar materials. An important material parameter for the static strength design of a mechanical joint is the bearing strength, which can be characterised as the resistance of the material to a fastener loaded hole. This resistance depends on the so-called edge distance of the hole, which is the distance between the hole and the sheet edge. Based on the design for minimum weight, the edge distance of a joint should be as small as possible and hence the bearing strength is a critical design parameter. Especially, fibre reinforced materials have a rather low resistance to fastener loads due to their anisotropy and their correlated low shear resistance, requiring a relatively large and undesirable edge distance [9–11].

Fastener holes are also an important cause of local stress concentrations within a fuselage. These stress concentrations can lead to premature failure at load levels below the ultimate strength of the material. This is generally addressed with the blunt notch strength of the material. Blunt notches are typically also more critical for fibre reinforced materials and FMLs than for metals, due to the brittle nature of the fibres and the anisotropic characteristics of the fibre layer, which can result in increased stress concentrations.

The final important static strength characteristic is the resistance to the presence of sharp notches, caused by fatigue or impact damage. This so-called fracture toughness or residual strength defines, to a large extent, the damage tolerance of a material. For fatigue-cracked locations, FMLs perform quite well due to presence of bridging fibres at

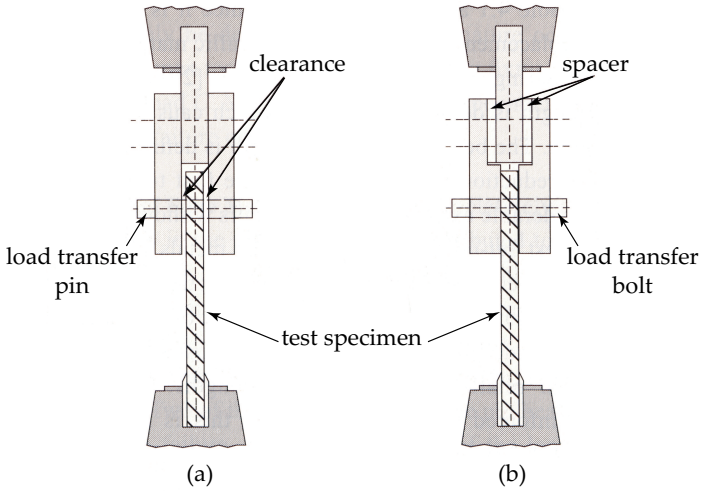

Figure 1.2: *Bearing test setup (source: Slagter [13]): (a) pin bearing, without lateral restraint, applicable to monolithic material and (b) bolt bearing with lateral restraint to prevent delamination for composite material.*

the fatigue locations. However, whenever the fibres are cut, for example due to impact damage, then the residual strength is a more critical parameter for FMLs [12].

The static failure modes of FMLs are detailed further in chapter 2, where more state of the art knowledge is presented. If possible, the FML behaviour is modelled based on the constituents' characteristics. Founded on this knowledge, a first attempt is made to identify areas for new FML types. The behaviour of an FML under certain loading conditions is of course not only related to its constituents' characteristics; interaction effects between the different components also play an important role. In this case, the prediction of laminate properties of new FML types is less straightforward and available test data are then used to define trend lines.

Based on chapter 2 it can be concluded that the state of the art knowledge about bearing strength characteristics of GLARE, or FMLs in general, is rather limited. The main source, next to a limited amount of test data, is the analytical description of bearing strength in [13]. To obtain a better understanding of this failure mode, chapters 3 and 4 cover the bearing behaviour of GLARE laminates both experimentally and numerically. The first covers the so-called bolt bearing strength, where lateral restraint is provided to prevent or minimise delamination around the hole. In chapter 4 this lateral restraint is not provided, hence allowing delamination to occur, which is identified with the so-called pin bearing strength. The difference between these two methods of loading the material are clearly seen in figure 1.2. The material type evaluated, being monolithic or composite material, generally dictates the test method used, but in this thesis both methods are used.

Important feature to be incorporated to correctly model the bolt bearing behaviour of an FML is the failure in the fibre layer. A detailed description of the approach to

cover this in the finite element code is given in chapter 3. To validate the model, the calculated failure zone is compared with the observed damage zone in experimentally loaded GLARE specimens. The fibre failure model is of less importance for correct description of the pin bearing behaviour. In this case, a delamination model based on so-called zero-thickness interface elements [14] is included in the FE model. The characteristics of this delamination model and the validation against experiments are presented in chapter 4. Furthermore, a parameter study is performed to investigate the influence of interface properties on the pin bearing strength.

The bearing strength evaluation in chapters 3 and 4 indeed shows the relatively low strength of GLARE compared to monolithic aluminium sheet. This low strength can mainly be attributed to the low shear resistance of the fibre layer. A novel solution to this problem is presented in chapters 5 to 7, where standard GLARE laminates are locally reinforced with a thin strip of high stiffness and high strength. This solution is based on the principle that the standard GLARE concept performs well for a large part of the fuselage and only for troublesome locations requires (local) reinforcement. In this thesis the thin strip of high stiffness and high strength is materialised as being stainless steel. The laminate obtained is referred to as *steel reinforced* GLARE .

A prerequisite for successful application of the stainless steel type in GLARE is its adhesion to common aerospace epoxies, which is covered in detail in chapter 5. In this chapter both mechanical and chemical adhesion promoting treatments are described. The quality of the adhesion is determined both visually using the Scanning Electron Microscope (SEM) and with the floating roller peel test. The research led to a pretreatment for the stainless steel sheets, which results in adhesion properties comparable to those of the aluminium-epoxy interface.

The successfulness of the local stainless steel reinforcement is investigated in chapters 6 and 7. The first covers the bearing strength evaluation (both bolt and pin loading) of several steel reinforced GLARE laminates, both experimentally and numerically. The numerical evaluation uses the fibre failure model and delamination model in chapters 3 and 4, respectively. The effectiveness of the steel reinforcement is discussed based on a comparison of specific strength properties between standard GLARE and steel reinforced GLARE.

For actual application in aircraft structures, not only the bearing strength but more importantly the static strength of an actual joint requires further attention. Furthermore, it is also important to investigate the fatigue properties since mechanical joints are fatigue critical locations. Both aspects are investigated experimentally for standard and steel reinforced GLARE in chapter 7. Next to the mechanical joints, also centre-cracked tension (CCT) specimens are investigated on their crack growth behaviour. For these CCT specimens, the crack growth and the delamination zones are compared with an analytical model that describes the crack growth in FMLs. A description of the model, the assumptions for the steel reinforced case and the final results are also included in the chapter.

Chapter 2

Property Optimisation in Fibre Metal Laminates

2.1 Introduction

The fibre content in an FML has resulted in improved damage tolerance compared to the monolithic aluminium sheets. However, in FMLs and more generally in hybrid materials, not only the good material properties are combined, but also the moderate to poor ones [15]. While the fibre addition results in improved fatigue properties, it negatively influences several static properties in an absolute sense compared to the monolithic metal sheet.

Especially for biaxial (i.e. cross-ply) laminates a decrease in axial stiffness is found in tension and compression. This lower stiffness also results in a lower yield stress compared to the metal sheet. These two aspects are even more severe under shear loading, resulting in a significantly reduced shear modulus and shear yield stress [16]. Also the strength of a mechanical joint is degraded due to low bearing strength of the UD fibre layers. Especially for relatively small edge distances (i.e. small distance between pin centre and sheet edge), the Fibre Reinforced Plastic (FRP) cannot reach its complete strength resulting in early failure [9, 17, 18]. Finally, also an increase of notch sensitivity is found for both blunt and sharp notches [12, 19]. Holes and cracks therefore become more critical for the design.

As the development of the current FMLs has been led primarily by the optimisation of the damage tolerance, it is interesting to explore the potential for improving other properties by changing the constituents. Possibly but not necessarily these changes will be at the expense of damage tolerance. To do so in an effective manner, theoretical models, linking the FML properties to those of the constituents, can be very useful. The current chapter summarises a number of such analytical or deterministic models and compares the properties of existing FMLs to the predictions. Where no realistic models are available, trend lines, based on experimental data, are generated, which also give guidelines to FML property optimisation. The results of the sensitivity studies are finally used to define future Fibre Metal Laminates.

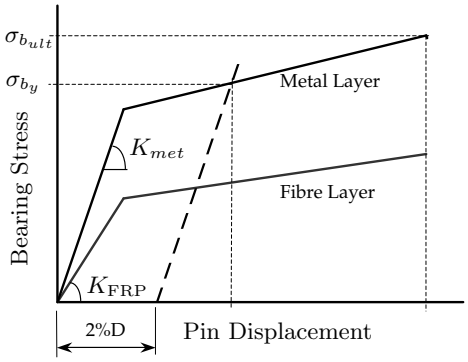

Figure 2.1: *Bilinear bearing behaviour of the metal and fibre layer [13].*

2.2 Methods

To analyse the elastic tensile, compressive or shear properties of a composite material, the Classical Laminate Theory (CLT) can be used. The Young's and shear modulus of the different constituents are combined to obtain the composite properties. Hidde et al. [20] used this approach to define an on-axis model for ARALL. Kawai et al. [21] adopted an equivalent method for the off-axis behaviour of a unidirectional GLARE laminate. In both cases a close approximation with experimentally obtained stress-strain curves was obtained. A generally applicable model is given by De Vries et al. [22], which defines a bilinear stress-strain curve for an arbitrary elastic-plastic FML. Elastic modulus E, yield σ_y and ultimate stress σ_{ult} of the laminate follow quite straightforward from this model:

$$E_{lam} = \mathrm{MVF} \cdot E_{met} + (1 - \mathrm{MVF})\, E_{FRP} \tag{2.1}$$

$$\sigma_{y,lam} = \left[\mathrm{MVF} + (1 - \mathrm{MVF})\frac{E_{FRP}}{E_{met}}\right] \sigma_{y,met} \tag{2.2}$$

$$\sigma_{ult,lam} = \mathrm{MVF} \cdot \sigma_{ult,met} + (1 - \mathrm{MVF})\, \sigma_{ult,FRP} \tag{2.3}$$

The subscripts denote the laminate (lam), metal (met) or fibre layer (FRP). In all equations the total metal thickness with respect to the total laminate thickness is expressed with the so-called Metal Volume Fraction (MVF). The predictions of E_{lam} and $\sigma_{y,lam}$ are quite accurate but the estimate of the ultimate strength is a crude approximation, since it assumes simultaneous failure of all components, which in general is not correct.

To join different FML sheets, generally a mechanically fastened joint is used. The strength of such a joint strongly depends on the bearing strength of the joined materials. Based on the displacement analysis of a pin-loaded hole, Slagter [13] defined a bearing strength model for an arbitrary FML. This model shows a strong resemblance with the bilinear tensile model as defined by De Vries et al. However, unlike the on-axis tensile response, the bearing response of fibre reinforced plastics (FRP) is not linear, but shows a progressive strength decrease. Analogous to the elastic-plastic metal behaviour, this is simplified as a bilinear relation as seen in figure 2.1. For simplicity, it is assumed that the strength decrease of the FRP occurs when the metal starts yielding.

According to the displacement analysis performed, the slope of the bearing response (i.e. bearing stiffness K) is directly proportional to the Young's modulus of the material. The exact relationship depends on geometrical parameters, like edge distance and width. The plastic response was evaluated experimentally, resulting in a reduction factor with respect to the elastic bearing stiffness.

The bearing model can be simplified when it is assumed that this reduction factor (i.e. ratio between plastic and elastic bearing stiffness) is equal for fibre and metal layer. This results in the following two relations for bearing yield σ_{b_y} (stress at 2% permanent hole deformation) and bearing ultimate strength $\sigma_{b_{ult}}$ of the laminate:

$$\sigma_{b_y,lam} = \left[\text{MVF} + (1 - \text{MVF})\frac{E_{FRP}}{E_{met}}\alpha\right]\sigma_{b_y,met} \tag{2.4}$$

$$\sigma_{b_{ult},lam} = \left[\text{MVF} + (1 - \text{MVF})\frac{E_{FRP}}{E_{met}}\alpha\right]\sigma_{b_{ult},met} \tag{2.5}$$

These equations are both comparable to the tensile yield definition, given in equation 2.2. The main difference is the factor α, which corrects for the influence of geometrical parameters on the bearing strength of fibre and metal layers.

The presence of holes, e.g. for fasteners, causes a stress concentration, which generally results in a strength decrease compared to the undisturbed case. For monolithic aluminium sheet, it was seen that a lower amount of strain hardening results in a lower strength decrease [23]. An opposite effect can however occur for FMLs [15, 19] due to the occurrence of delamination, leading to an increase in blunt notch sensitivity [24] with a lower amount of strain hardening.

According to De Vries [12] the delamination in an FML is mainly related to the plastic zone at the notch root in the metal layer. Within the plastic zone, the metal undergoes larger deformations than the elastic fibre layer. These local differences in deformation eventually cause delamination when the maximum shear strain of the adhesive is passed. In this case, a lower yield point results in early creation of the plastic zone and thus promotes delamination, which explains the opposite behaviour of monolithic sheet and FMLs.

Apart from delamination affecting parameters like plasticity and maximum adhesive strain, the ultimate strength of the constituents is also an important parameter. This multiplicity of relevant factors defines the complexity of this failure mode, which complicates the definition of a general constituent based model. This is however also seen for FRP, where generally an experimentally obtained critical length parameter is used to calculate the strength [25]. Therefore test data are used to define trend lines for this failure mode.

During the operational life of a structure, sharp notches can occur due to fatigue or impact damage. These cracks generally cause a larger strength decrease than blunt notches. Due to the laminated build-up of an FML, with alternating metal and fibre layers, the strength decrease is different for fatigue and impact damage [12]. Under fatigue loading, the crack grows in the metal layer while the fibres bridge the crack. These crack-bridging fibres and the delaminated zone around the crack, not only result in good fatigue properties but they also have a positive effect on the residual strength. Impact damage, on the other hand, results in broken fibres (i.e. equal crack length in metal and fibre layer) and nearly no delamination. Both phenomena cause a more critical situation, which requires further attention. The residual strength behaviour after impact damage resembles in several ways the blunt notch characteristics. At the crack tip, a plastic zone develops in the metal layer and related delamination occurs between fibre and metal layer. The main difference is however the occurrence of stable

crack growth before failure.

Vermeeren [19] and De Vries [12] evaluated several fracture mechanics concepts and concluded that the R-curve concept is best applicable for GLARE. This approach has the limitation that for each different laminate the R-curve should be obtained experimentally. Based on curve-fits for experimental GLARE results, De Vries derived an equation to obtain the R-curve for an arbitrary FML. Nevertheless, this model has not been validated yet for other FML types. A more practical approach, which will be used in the next section, has also been defined [12], where the residual strength is defined as a function of the strain hardening of the FML.

2.3 Sensitivity Studies

2.3.1 Tension and Compression

Elastic Modulus

The elastic modulus of an FML under tension and compression is simply related to the elastic modulus of its constituents, as seen in equation 2.1. In this case, the influence of the loading direction is important, since it affects the fibre layer stiffness. For the UD fibre layer it is therefore important to define three different loading cases: in the fibre direction (longitudinal), perpendicular to the fibre direction (transverse) and under an off-axis angle. For each case, the constituent properties influence the total stiffness in a different manner.

The stiffness of the fibre layer in the fibre direction is mainly related to the fibre stiffness, while matrix stiffness plays a less important role. Transverse to the fibre direction, the fibre and matrix stiffness are of comparable importance. Under off-axis loading, the shear modulus of the fibre layer becomes the most important parameter. This shear modulus is related to the fibre and matrix shear modulus and hence to the elastic modulus of these constituents.

The influence of the fibre, metal and matrix stiffness on the FML stiffness for on-axis loading is shown in figure 2.2. To generalise the information, the FML and fibre modulus is normalised with respect to the metal layer. In the figure experimental GLARE data are also plotted. The data points agree well with predicted values. The figure emphasises the influence of metal and fibre stiffness in the fibre direction. Doubling the matrix stiffness has barely an effect and only significantly affects the transverse properties.

Yield Stress

The yield stress of an FML is directly related to the metal yield stress, simply because only the metal layer shows yielding. A first method to increase this yield stress is therefore by using a metal with higher yield stress. A second method is related to the relative stiffness of the fibres, since this defines the net stress level in the metal layer. A higher stiffness of the fibre layer therefore increases the yield stress. This higher stiffness can be obtained according to the previous discussion on elastic modulus of the fibre layer.

Ultimate Stress

The ultimate strength of an FML can generally be affected by either increasing the metal or fibre layer strength. Due to large differences in failure strain, the full strength

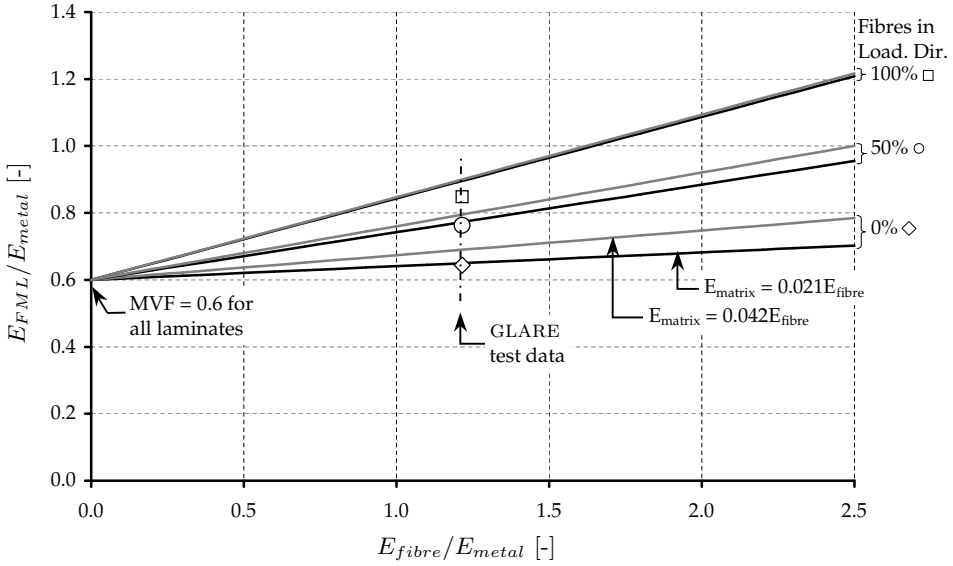

Figure 2.2: *Influence of the fibre, metal and matrix on the elastic modulus of an FML with an MVF of 0.6, where E_{fibre} is the stiffness of the fibre along the fibre direction.* GLARE *test data are used for comparison with the following values: $E_{fibre}/E_{metal} = 1.2$, $E_{matrix}/E_{fibre} = 0.021$ and v_f=0.6.*

level of both components is nevertheless never used. Therefore, it is more important to increase the strength of the component with the lowest failure strain.

For the UD fibre layer a strength increase again requires an evaluation of the longitudinal, transverse and off-axis direction. The longitudinal direction is mainly related to the fibre properties, its strength can therefore be increased with a high strength fibre. For the transverse and off-axis direction, strength is increased with a higher matrix ductility and better fibre-matrix bonding [26].

Figure 2.3 illustrates the influence of all constituents on the ultimate strength, based on the assumption of simultaneous failure of all components. Also in this picture, the FML strength is normalised with respect to the metal layer. The figure shows the strong influence of fibre and metal strength, while the influence of matrix strength is again negligible as seen from the transverse strength ($\sigma_{ult,90}$) influence.

2.3.2 Shear

Shear Modulus

The shear modulus of an FML is determined by the shear modulus of its constituents. Obviously, to increase this stiffness, the shear modulus of the metal or fibre layer should be increased. Due to its isotropic behaviour, a stiffness increase of the metal layer is most efficient. Generally, a low shear modulus is found for the UD fibre layer, due to low matrix stiffness, which does not inhibit fibre shearing. This low modulus can be improved by an increase of shear stiffness of the matrix or that of the fibre. Orientation of the fibres under $\pm 45^\circ$ with respect to the shear load, also results in a

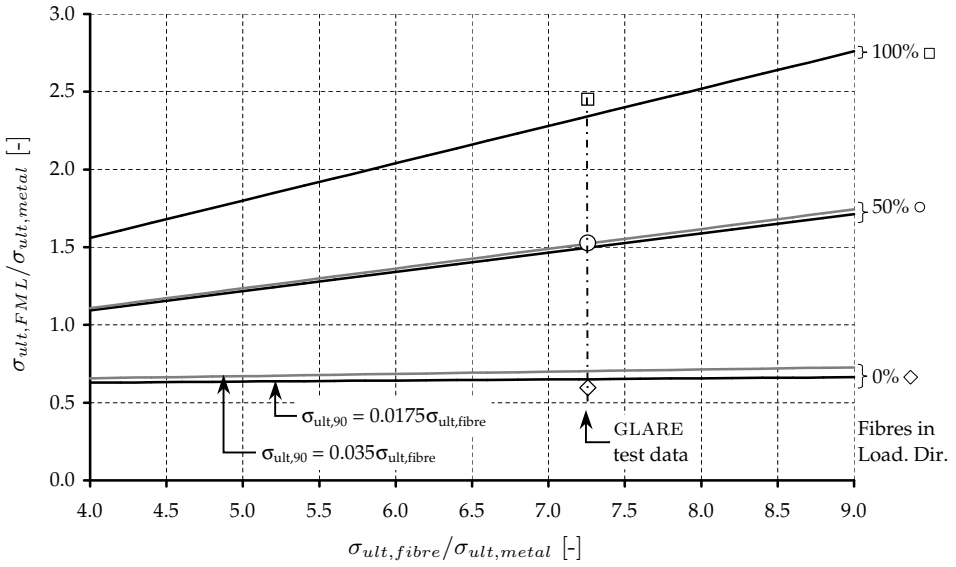

Figure 2.3: *Influence of the fibre, metal and matrix on the ultimate strength of an FML with an MVF of 0.6, where $\sigma_{ult,fibre}$ is the ultimate strength of the fibre.* GLARE *test data are used for comparison with the following values: $\sigma_{ult,fibre}/\sigma_{ult,metal} = 7.25$, $\sigma_{ult,90}/\sigma_{ult,fibre} = 0.0175$ and v_f=0.6.*

large improvement. This is however only an option when the shear load is dominant in that direction.

Figure 2.4 shows the influence of fibre, metal and matrix on the FML shear modulus based on CLT. The low slope of the graph shows the dominance of the metal layer over the fibre layer. Furthermore, it is seen that the influence of the matrix stiffness is comparable to the influence of the fibre stiffness. Unfortunately no test data are available in the literature to validate these trend lines.

Shear Yield Stress

Also under shear loading the yield stress of an FML is directly related to the metal yield stress. A first method to increase this yield stress is therefore by using a metal with higher yield stress. A second method is related to an increased shear stiffness of the fibre layer, to increase the fibre stress at metal yielding. This higher stiffness can be obtained according to the previous discussion on shear modulus of the fibre layer.

Next to standard 2024-T3 based GLARE also shear test results of GLARE with higher and lower strength aluminium are available. As seen in figure 2.5, there is a relationship between tensile and shear yield stress, which surprisingly does not cross the reference point with standard GLARE. The tensile and shear results for GLARE with 2024-T3 were not taken from the same batch, which might explain the small offset.

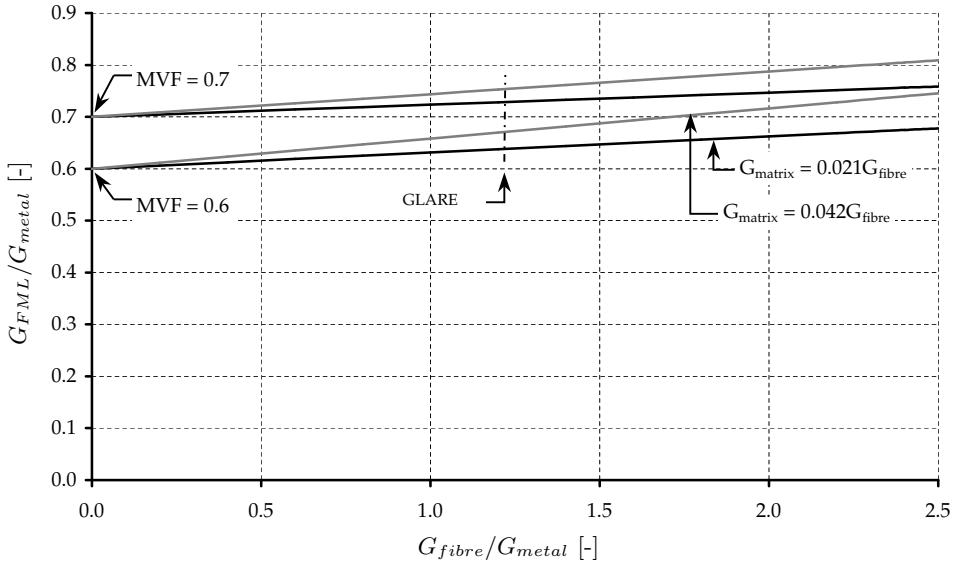

Figure 2.4: *Influence of the fibre, metal and matrix on the shear modulus of an FML with an MVF of 0.6 or 0.7 and v_f=0.6.*

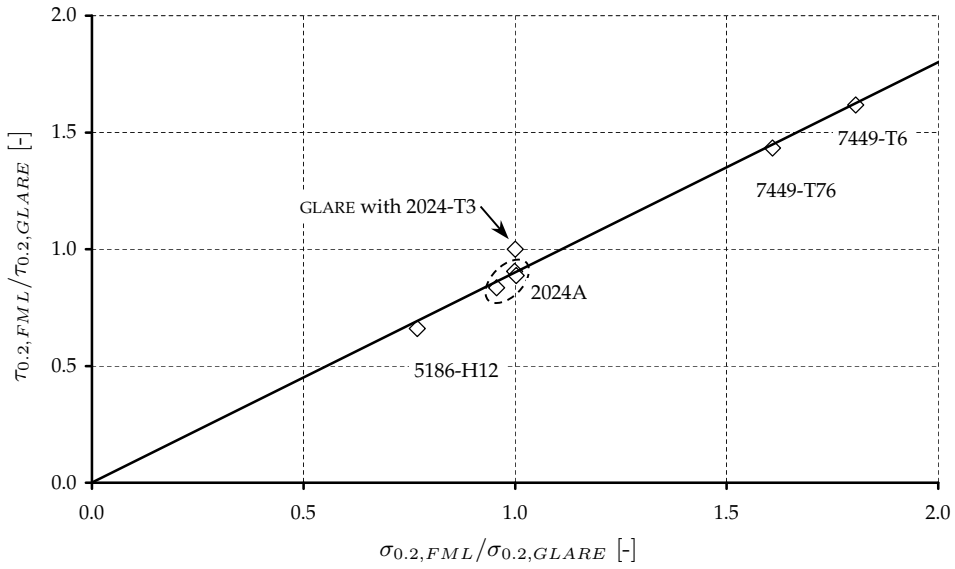

Figure 2.5: *Relation between the tensile yield stress in transverse direction and the FML shear yield for several* GLARE *3-4/3-0.5 laminates with the specified aluminium alloys.* GLARE *2024-T3 test data are used to normalise the test results.*

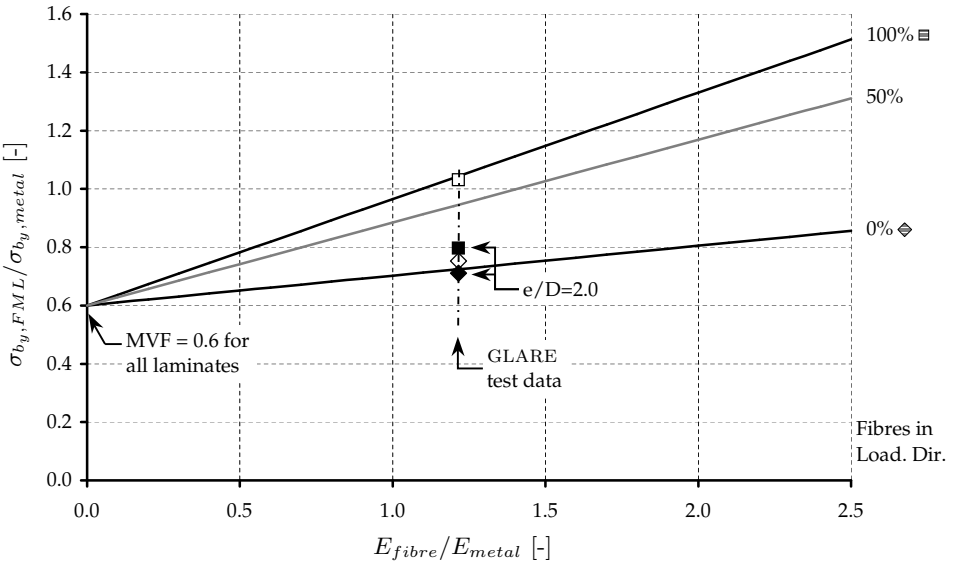

Figure 2.6: *Influence of the ratio E_{fibre}/E_{metal} on the bearing yield strength of an FML with an MVF of 0.6, where E_{fibre} is the stiffness of the fibre along the fibre direction.* GLARE *test data are used for comparison with the following values: $E_{fibre}/E_{metal} = 1.2$, $E_{matrix}/E_{fibre} = 0.021$, v_f=0.6 and e/D=3.0 (otherwise it is stated).*

2.3.3 Bearing

Bearing Yield and Ultimate Stress

The bearing yield and ultimate stress of an FML are dominated by the behaviour of the metal layer. The fibre layer contribution is generally limited, due to its relatively low shear properties. An increase of bearing properties can therefore mainly be achieved with a higher strength metal. The shear properties of the fibre layer can be improved with higher stiffness constituents or with the inclusion of off-axis fibre layers [27].

Figure 2.6 shows the influence of fibre and metal on the FML bearing yield strength for an edge distance ratio (e/D, where e is the distance between the centre of the hole and the sheet edge and D is the fastener diameter) equal to 3. The curves are based on equation 2.4, where α was obtained by curve-fitting GLARE test data. It should be noted that this is a first approximation, requiring additional investigation. To show the performance of the model, GLARE test data are inserted in the graph for edge distance (e/D) equals 2 or 3. The trends indicate the strongest fibre stiffness influence for the case with 100% of fibres in the loading direction. Nevertheless, especially for this case, it is seen that the lower edge distance (e/D=2.0) results in a strong strength decrease due to shear-out failure.

Figure 2.7 shows different trends for the bearing ultimate strength, which are based on equation 2.5. Particularly the case with 50% fibres in the loading direction is influenced with stiffer constituents. The smaller edge distance (e/D equal to 2) now results in a smaller strength decrease. It should however be noted that this is a relative

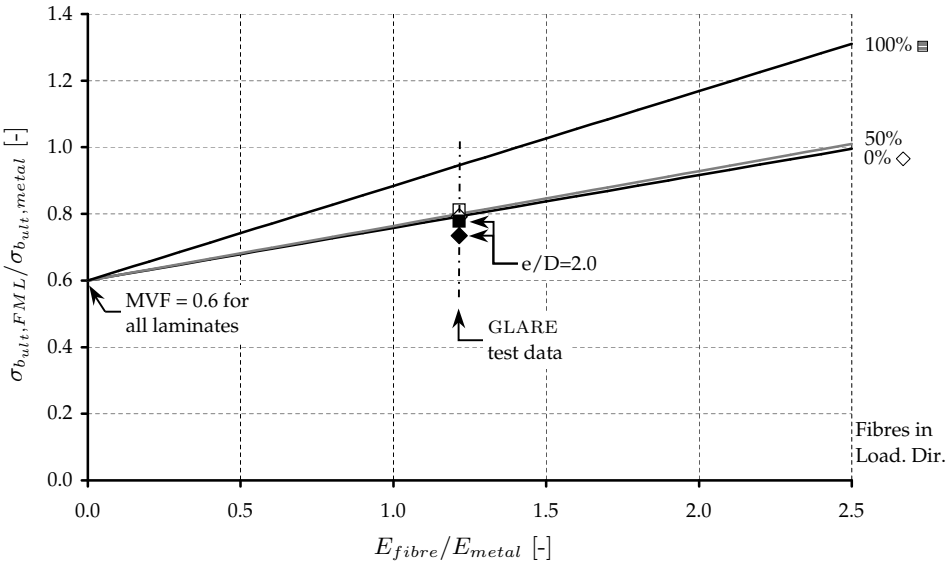

Figure 2.7: *Influence of the ratio E_{fibre}/E_{metal} on the bearing ultimate strength of an FML with an MVF of 0.6, where E_{fibre} is the stiffness of the fibre along the fibre direction.* GLARE *test data are used for comparison with the following values: $E_{fibre}/E_{metal} = 1.2$, $E_{matrix}/E_{fibre} = 0.021$, v_f=0.6 and e/D=3.0 (otherwise it is stated).*

decrease, while the absolute decrease is much larger since also the metal properties decrease.

2.3.4 Blunt Notch

A notch causes a stress concentration, which in general results in a strength decrease of the plate with a blunt notch. Available test data for circular holes demonstrate that this decrease (expressed as notch sensitivity) is comparable for different FML types. It is thus quite apparent that the blunt notch strength increases for a stronger FML. The comparison between several Fibre Metal Laminates in figure 2.8 indeed supports this assumption. Both UD and cross-ply (CP) laminates lie along the same trend line within a small bandwidth. An increase of blunt notch strength can therefore simply be obtained according to the sensitivity study from section 2.3.1. The figure nevertheless shows differences between the aluminium and titanium based laminates, indicating an influence of other material properties on the blunt notch strength.

An evaluation of the blunt notch strength with respect to the laminate yield stress did not reveal an influence of this parameter. This either indicates that delamination occurred for all laminates, or that the creation of a plastic zone and the correlated delamination does not have a distinct influence on the blunt notch strength.

Next to the yield stress, the amount of strain hardening can also be used as a measure for blunt notch behaviour. For plain aluminium sheet, a material with a low amount of strain hardening resulted in a lower notch sensitivity. It was however seen for FMLs

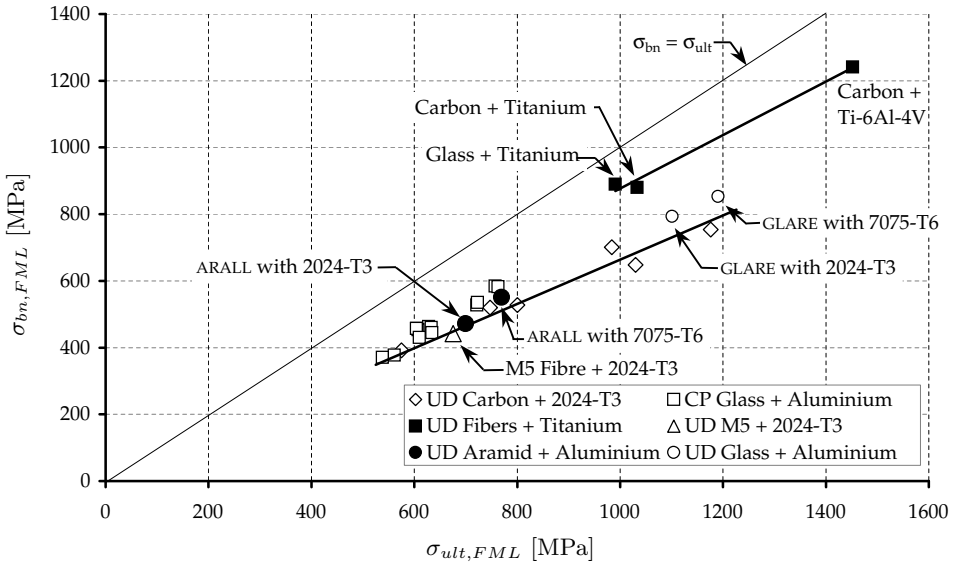

Figure 2.8: *Relation between the ultimate strength of the FML and its blunt notch strength. Comparison of test results for several FMLs with a UD 2/1-0.3 lay-up (MVF=0.706) and for several* GLARE *3-4/3-0.5 laminates (MVF=0.727) with different aluminium layers.*

that an opposite effect can occur due to the occurrence of delamination. In figure 2.9, the influence of the relative amount of strain hardening (i.e. strain hardening divided by the ultimate strength) on the blunt notch strength is illustrated for several FML types. This figure demonstrates both decreasing and increasing trend lines, identifying the complexity of the blunt notch strength and providing proof that other factors than strain hardening play a role.

2.3.5 Residual Strength

The residual strength behaviour of an FML with impact damage can be characterised with two important points: crack initiation and final failure. Crack initiation is related to aspects like fracture toughness, delamination and plasticity but also to crack tip shape [12]. Due to this complex local behaviour, it is too complicated to perform a simple sensitivity study for this parameter.

The final failure point or residual strength should be a function of the strain hardening of the laminate, according to section 2.2. The comparison between several metal-fibre combinations in figure 2.10 indeed supports this statement. It should be noted that this figure compares the residual strength for different relative crack lengths and specimen widths. Since the residual strength depends on these two parameters too, incorrect dependencies could be suggested by just plotting the raw data. However to overcome the geometry limitation, the results in figure 2.10 are normalised with respect to GLARE results with equal geometry. In this way, a general picture is obtained, irrespective of specimen geometry.

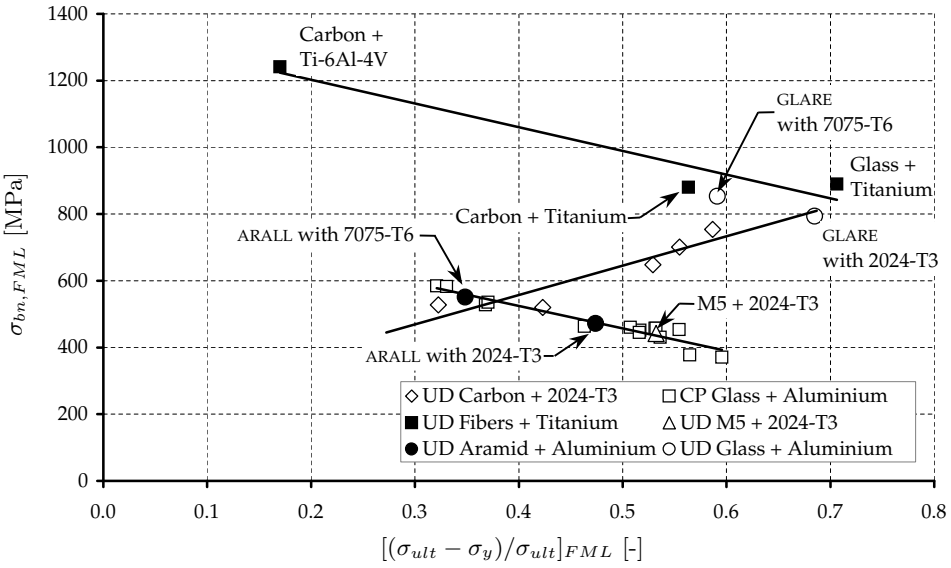

Figure 2.9: *Relation between the relative amount of strain hardening (i.e. with respect to ultimate strength) of the FML and its blunt notch strength. Comparison of test results for several FMLs with a UD 2/1-0.3 lay-up and for several* GLARE *3-4/3-0.5 laminates with different aluminium layers.*

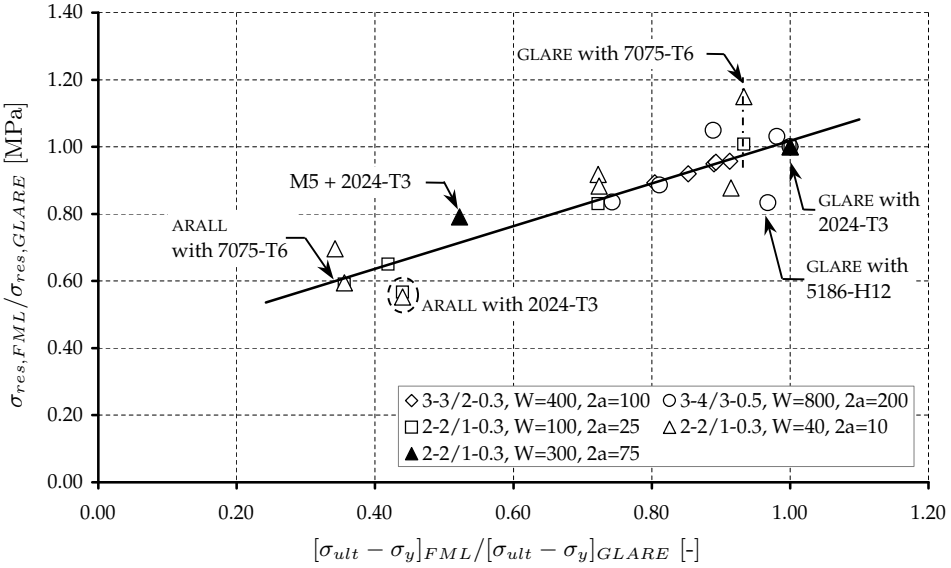

Figure 2.10: *Relation between the strain hardening and the FML residual strength for several specimen geometries. Standard* GLARE *test data, with 2024-T3 aluminium, are used to normalise the test results.*

2.4 Discussion & Concluding Comments

The behaviour of an FML under several static failure modes can be divided into two groups. The first group consists of tension, compression, shear and bearing failure, where interaction between the different layers is on a global scale. In this case, optimisation is relatively simple and can be done on the basis of CLT or CLT like analyses. The second group comprises both blunt and sharp notch failure, where local effects like plastic zone and delamination play an important role. These local effects require a parallel optimisation of all three constituents, which complicates the definition of improvements.

The elastic or shear stiffness can simply be improved by choosing a higher modulus material for each of the components. Compared to many other high-strength metals, aluminium has a modest modulus, but its specific properties (e.g. E/ρ, $E^{1/3}/\rho$) are generally equal or better. Completely replacing the aluminium in GLARE with stiffer metals is therefore not a good option. The weight-penalty is smaller when only a stiff interlayer, made of steel, titanium or nickel, is used.

Carbon, M5 and steel fibres are a few examples to improve the stiffness with respect to the currently used glass fibres. Combining carbon fibres with aluminium sheet causes galvanic corrosion. In this case the use of isolating interlayers or different metals is a requirement. This second option is now more practical due to the higher specific stiffness of carbon. Galvanic corrosion is no issue for other fibre types, but these fibres generally have a lower specific stiffness.

The stiffness of the matrix is of little influence under on-axis loads, but under shear loads its influence increases. Compared to the currently applied thermoset polymer, the stiffness can be improved with either a stiffer polymer or a metallic matrix. Ceramic matrices also improve the stiffness, but its brittle characteristics will negatively influence the blunt and sharp notch behaviour.

Especially for shear related failure (e.g. off-axis tension, shear or bearing), a stiffer fibre and matrix also improve the yield stress for an FML. Further also the lay-out of the fibre layer, for example by using a weave or by stitching the different fibre layers, can affect the shear properties. A stronger influence is obviously obtained from an increased metal yield stress. Next to different aluminium alloys, other possibilities are the already discussed materials like steel, titanium and nickel. Stronger metals also improve the ultimate strength of the FML; also a more ductile matrix increases this strength since it postpones off-axis failure.

The blunt and sharp notch behaviour of an FML can both be characterised with the formation of a plastic zone and delamination. Still, several differences between these two failure modes require a different optimisation.

The blunt notch strength is related to the amount of strain hardening with respect to the ultimate strength. The use of this parameter joins the effect of strain hardening and ultimate strength. With respect to this parameter both an increasing and a decreasing trend is seen for the blunt notch. This shows the complexity of the blunt notch behaviour, which is strongly dependent on the fibre-metal combination.

The residual strength after impact was improved with an increase in strain hardening of the laminate. The use of a metal with a higher amount of strain hardening seems therefore the best option to improve this property. Also a different fibre can result in a lower yield or a higher ultimate stress, but this has a limited influence. A stronger fibre is generally also stiffer than the glass fibres used, leading to a higher ultimate but also to a higher yield stress. Equivalently, a fibre with lower stiffness decreases the yield stress, but in general these fibres are also weaker. Further also delamination has

a positive effect on the residual strength. This is expected to be promoted with a lower maximum shear strain of the adhesive, for example with an epoxy of lower toughness.

Chapter 3

The Bolt Bearing Strength of Fibre Metal Laminates

3.1 Introduction

Aircraft fuselages are generally constructed using mechanical joints (rivets or bolts) joining the individual sheets. The strength of a mechanical joint strongly depends on the edge distance (distance between the centre of the hole and the sheet edge perpendicular to the loading direction) with respect to the fastener diameter.

According to common practice, the optimal strength for metal sheets is generally reached at an edge distance equal to two times the fastener diameter. In this case the joint fails in bearing, in which the hole gradually elongates due to the loaded fastener. Experiments on several aluminium alloys showed that the bearing yield (i.e. stress at 2% permanent hole deformation) has a more or less constant ratio with respect to the tensile yield of the material [28]. Ultimate bearing strength with respect to tensile strength was found to be related to strain hardening of the material, but even more to ductility. Furthermore, for several engineering metals no directional effect (i.e. loading direction with respect to rolling direction) on bearing strength was found [28–30]. This should be attributed to the multi-axial stress state that occurs during bearing.

In contrast, the bearing strength of Fibre Reinforced Plastics (FRP) is strongly influenced by the loading direction due to their anisotropic nature. The anisotropy can also result in low joint strength for small edge distance, hence requiring edge distances higher than three times the fastener diameter to obtain full strength as is clearly described in [9–11].

The elastic stress field around a pin loaded hole in an anisotropic material including friction was defined by De Jong [31]. The influence of edge distance for real joints is however not incorporated since an infinite sheet is assumed. Furthermore it is not possible to include plasticity or local failure in this model, because the model is based on global stiffness parameters.

In general, FE (finite element) calculations are adopted instead of analytical solutions, to tackle the difficulties with the bearing mode. Especially for FRPs, local strength/stiffness degradation plays an important role, which is difficult to model analytically. Several investigations have been performed to model the bearing behaviour of FRP using a progressive strength model [32–34]. In this case the failure progression and correlated strength/stiffness degradation is predicted relatively well up to final failure.

A different FE approach for failure prediction of composite joints has been defined by Chang et al. [35], which is based on global parameters. Comparable to the characteristic length for a blunt notch [36], they defined the so-called characteristic (elliptical) curve. This characteristic curve is defined with the characteristic lengths R_t and R_c, which are obtained from an open hole tension and an open hole compression test. Failure is assumed to occur when the (elastic) stress solution fulfills the failure criterion on this curve. The corresponding location defines the failure mode, i.e. tension, shear-out or bearing. The need to determine characteristic lengths experimentally, forms the major drawback of this model. Since these characteristic lengths are not a material property, they should be evaluated for each different laminate individually.

Fibre Metal Laminates (FMLs) are hybrid materials, which consist of thin metal sheets bonded together with alternating (unidirectional) fibre layers. Due to the fibre addition, an FML is also more sensitive to the edge distance than the metallic counterpart. A higher edge distance is therefore necessary, which results in a weight-increase of the structure.

For the application on FMLs, Slagter [13, 37] defined a model, which is relatively simple compared to methods applied to FRP. The bearing behaviour of both the metal and the fibre layer is modelled as a bilinear relation. This bilinear curve consists of an elastic and a *plastic* part, which for the fibre layer corresponds to progressive failure behaviour. For simplicity it is assumed that the transition of the fibre layer behaviour equals the metal bearing yield point. Major drawback of the model is the assumption of isotropy for the fibre layer, causing a high overestimation compared to actual test results. For a correct description of bearing strength for FMLs it is therefore necessary to define an FE model which includes progressive strength degradation of the fibre layer.

The present chapter first discusses the experimental setup to obtain the bearing strength for aluminium sheet and Fibre Metal Laminates. This is followed by a detailed description of an FE model for bearing strength prediction. Subsequently the results of both these methods are described and compared. Finally the results are used to obtain more insight in the bearing behaviour of FMLs.

3.2 Methods

3.2.1 Experimental Setup

The bearing strength of a metallic material is generally evaluated with the pin type bearing test [38] as shown in figure 1.2a. According to this test standard, the material is loaded by a steel pin without any lateral clamping. Application of this test setup to laminated materials, i.e. composites like FRPs or FMLs, results in delamination due to insufficient clamping. Since delamination leads to premature failure [13, 37], the bolt loading setup [39] with a finger-tight bolt from figure 1.2b, is therefore used for these materials.

The bolt test setup was used to analyse the bearing strength of both aluminium 2024-T3 and a set of typical GLARE laminates, which are listed in table 3.1. GLARE 2-2/1-0.4 laminates consist of two aluminium layers, each one with a thickness of 0.4, and one, 0.25 mm thick, unidirectional fibre layer. This laminate was tested both in the fibre direction (which coincides with aluminium rolling direction L) and perpendicular to the fibre direction (aluminium LT direction). GLARE 3-3/2-0.4 laminates contain three aluminium layers and two crossply fibre layers and it was only tested in the rolling direction of the aluminium. To investigate the influence of clamping, the GLARE

Table 3.1: *Test matrix for the bearing test setup.*

Material	Test setup	Dir.	t [mm]	e/D [-]
Aluminium 2024-T3	bolt	L	1.0	1.0 - 3.0
GLARE 2-2/1-0.4	bolt	L & LT	1.05	1.0 - 3.0
GLARE 3-3/2-0.4	pin & bolt	L	1.7	1.0 - 3.0

3 laminate was also evaluated with a pin bearing test setup.

For each material five different (in steps of 0.5) edge distance ratios (e/D) were evaluated, to investigate the sensitivity of these materials with respect to this parameter. Each test was performed two times to check for consistency of the results. The width of the specimens was taken six times the pin diameter, to prevent net section failure. Although the test standard for metals defines a pin diameter of 8.0 mm, a diameter of 4.8 mm was used instead. In this way the results obtained are more applicable for practical joint design. To prevent delamination during drilling, the specimens were supported with a wood backing and several increasing drill sizes were used. Final diameter was obtained after reaming to an H6 tolerance, which results in a clearance fit with the pin.

The different specimens were loaded with a test speed of 2 mm/min up to failure. Deformation was measured with an extensometer, which was attached on one side to the loading pin and on the other side clamped to the sheet at a distance of 3.25 cm above the pin centre. These same locations were also used in the FE model to obtain the pin displacement.

For several specimens a so-called hysteresis loop was included after yielding to obtain the secondary bearing modulus K_s of the material. This test sequence is comparable to the static strength evaluation of mechanical joints [40], where the secondary modulus is used to obtain the joint yield strength.

Two important properties are obtained from the bearing test: (i) bearing yield (σ_{b_y}) and (ii) bearing ultimate ($\sigma_{b_{ult}}$) of the material; where bearing stress is defined with the following relation: $\sigma_b = P/(Dt)$ where P is the load applied and t the sheet thickness. The yield parameter is defined as the stress at a 2% permanent hole deformation, which is a definition comparable to the tensile yield. Bearing ultimate is defined as the maximum stress reached, which generally was the first maximum load peak.

3.2.2 Fibre Failure Investigation

The behaviour of the fibre layer within an FML under bearing loads has been investigated, to get more insight in this failure mode. For an e/D equal to 2.0, the GLARE 2 laminates, both in L and LT direction, were loaded to predefined pin displacements (v_{pin}). Two specimens were only loaded elastically to obtain the failure initiation point (v_{pin} equal to 0.2 and 0.3 mm) and four specimens were loaded into plasticity (v_{pin} equal to 0.5, 0.7, 1.0 and 1.6 mm). After load removal, the specimen's outer aluminium layer was removed with an etching solution. In this way the failure zone within the fibre layer is revealed. This knowledge can also be used to validate the FE model for bearing strength of FMLs, which is described in the next section.

3.2.3 FE Analysis

Based on the experimental results of monolithic aluminium and the different GLARE laminates it is possible to develop and validate a general FE model for bearing strength of metals and FMLs.

Material Model

For the material model of aluminium 2024-T3 it is assumed that it behaves as an isotropic material with isotropic hardening. Uniaxial tensile test data are simplified into a trilinear behaviour, consisting of (i) an elastic part up to the yield stress of 330 MPa, (ii) a plastic part up to necking (15% plastic strain) with tangent stiffness equal to 1468 MPa, which is followed by (iii) a description of the necking behaviour. Difficulty with this last part is the occurrence of large deformations in the necking zone. Global strain measurements are in this case underestimating the real stress-strain behaviour of the material [41, 42]. For several failure modes this is of little importance since necking occurs after the ultimate strength is reached. For bearing failure this is however not the case, since (local) necking does not immediately result in instability and correlated failure of the specimen. To obtain an ultimate strength prediction, it is therefore necessary to include the large necking deformations. Instead of performing an in-depth analysis of the tensile strength during necking it was decided to approximate the stress-strain relation during necking as a linear relation with a tangent stiffness of 500.0 MPa until 50% strain.

An FML is a combination of isotropic metal layers and anisotropic composite layers. These fibre layers have a completely different behaviour than the metal layers and therefore they require a different material model. In this case it is necessary to differentiate between several intra-laminar failure mechanisms: (i) fibre failure, (ii) matrix failure and (iii) fibre-matrix shearing. Failure initiation rules for these mechanisms used in this work are listed in table 3.2. The fibre-matrix shearing criterion is slightly changed with respect to the original definition [43], since it is assumed that it can also occur for tensile fibre stresses (i.e. $\sigma_{11} > 0$). The fibre failure and fibre-matrix shearing criteria are thus equivalent for fibre tension. Degraded properties and the degradation growth rule are however considered separately after failure initiation.

After damage initiation, damage growth is predicted with a damage growth law. The most simplified growth law is an immediate loss in properties after initiation, i.e. immediate failure, which is generally true for local fibre failure. The two matrix related failures are however progressive, which is characterised as a slow decrease in properties. This damage growth can be predicted according to the following degradation factor, which is comparable to the definition of Hung et al. [32] and Schipperen [44]:

$$d = 1 - e^{\left(0.5 - \frac{\kappa}{\kappa_i}\right)} \tag{3.1}$$

Where κ_i and κ define the initiation and the current strain, respectively. The value of 0.5 is added to the original definition to assure a more realistic stress drop after failure initiation. The exponential degradation factor is also used for fibre failure. While Schipperen used the strain in the fibre direction as relevant strain indicator, it was decided to use the strain in the most dominant failure direction instead. So fibre failure is related to ϵ_{11}, matrix failure to ϵ_{22} and fibre-matrix shearing to ϵ_{12}.

Delamination, which is an interlaminar failure mode between the fibre and metal layers, is not captured with the FE model, since this requires a local loss of interaction between the corresponding plies. A special interface element [45, 46] is in this case

Table 3.2: *Failure initiation criteria [34, 43] for the fibre layer and corresponding degraded properties.*

Failure mode	Criterion	Degraded properties
(i) Fibre failure		
- Tensile	$\left(\frac{\sigma_{11}}{X_t}\right)^2 + \left(\frac{\sigma_{12}}{S_{xy}}\right)^2 + \left(\frac{\sigma_{13}}{S_{xz}}\right)^2 \geq 1$	E_{11}, ν_{12}, ν_{13}
- Compressive	$\frac{\sigma_{11}}{X_c} \geq 1$	
(ii) Matrix failure	$\left(\frac{\sigma_{22}}{Y}\right)^2 + \left(\frac{\sigma_{12}}{S_{xy}}\right)^2 + \left(\frac{\sigma_{23}}{S_{yz}}\right)^2 \geq 1$	E_{22}, ν_{21}, ν_{23}
(iii) Fibre-matrix shearing failure	$\left(\frac{\sigma_{11}}{X}\right)^2 + \left(\frac{\sigma_{12}}{S_{xy}}\right)^2 + \left(\frac{\sigma_{13}}{S_{xz}}\right)^2 \geq 1$	G_{12}

necessary for correct simulation of delamination behaviour. This is however outside the scope of this chapter and will be covered in chapter 4, especially because delamination growth should not occur in the bolt bearing test.

FE Model

The ABAQUS [47] FE code was used to model the bolt bearing behaviour of the different materials. The geometry was taken comparable to the experimental setup, with the edge distance ratio (e/D) as a parameter. To account for tolerances in drilling the hole, the diameter was set equal to $D + 0.05$. Lateral restraint at the hole region, like the bolt loaded setup, is implemented by modelling part of the test fixture as a rigid surface. Since finger-tight clamping is never fully tight, a gap of 0.01 mm was used between specimen and lateral restraint. Based on the relatively high stiffness of the steel pin with respect to the tested materials, the bearing load is exerted by a rigid pin.

To reduce computational time, only a quarter of the full specimen was modelled, which for the GLARE laminates was only possible based on their symmetrical lay-up. A typical mesh of the specimen is shown in figure 3.1, where for clarity the symmetry plane is facing upwards. A sufficiently fine mesh was used at the hole region, to correctly predict the failure within metal and fibre layer. Element size was increased towards the clamped edge to reduce calculation time. Each material layer is modelled separately as a layer of eight-node linear solid elements, i.e. the C3D8 element.

Interaction between pin and hole is not only modelled with a normal bearing load, but also with transverse friction with a friction coefficient μ taken equal to 0.1 to account for a certain roughness of the contacting materials. Calculations showed a modest influence of μ on bearing strength (μ equal to 0.2 results in approximately 20 MPa higher stress levels). Friction between specimen and test fixture is however

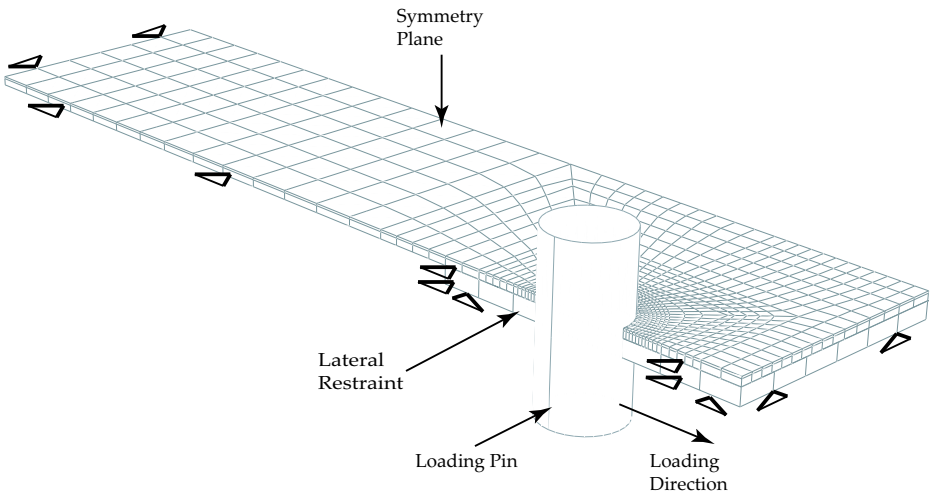

Figure 3.1: *Typical mesh for the bolt bearing strength evaluation of a* GLARE *2-2/1-0.4 laminate, with the symmetry plane facing upwards.*

Table 3.3: *Overview of material properties for aluminium 2024-T3 and the S_2 glass fibre layer.*

Material	E_{11} [MPa]	E_{22} [MPa]	G_{12} [MPa]	ν_{12} [-]	X_t / X_c [MPa]	Y_t / Y_c [MPa]	S [MPa]
2024-T3	72,400	72,400	27,608	0.33	725[a]	725[a]	NA
S_2 glass	53,980	9412	2700	0.33	2429	68	75

[a] true stress value based on the assumption that the engineering stress remains constant during necking.

assumed to be negligible.

Failure of the fibre layers is implemented with a so-called user material subroutine (i.e. a UMAT). The failure criteria from table 3.2 are evaluated with this subroutine after each load increment. Whenever failure initiation is detected, the corresponding properties are decreased. The local tangent stiffness matrix is updated accordingly and the local stresses are calculated.

Material parameters for both the aluminium sheets and glass fibre layers are given in table 3.3. It is assumed that the tensile and compressive properties are equal and that out-of-plane properties are equal to in-plane transverse properties. The residual stresses that occur during manufacturing of the GLARE material are not accounted for in the models.

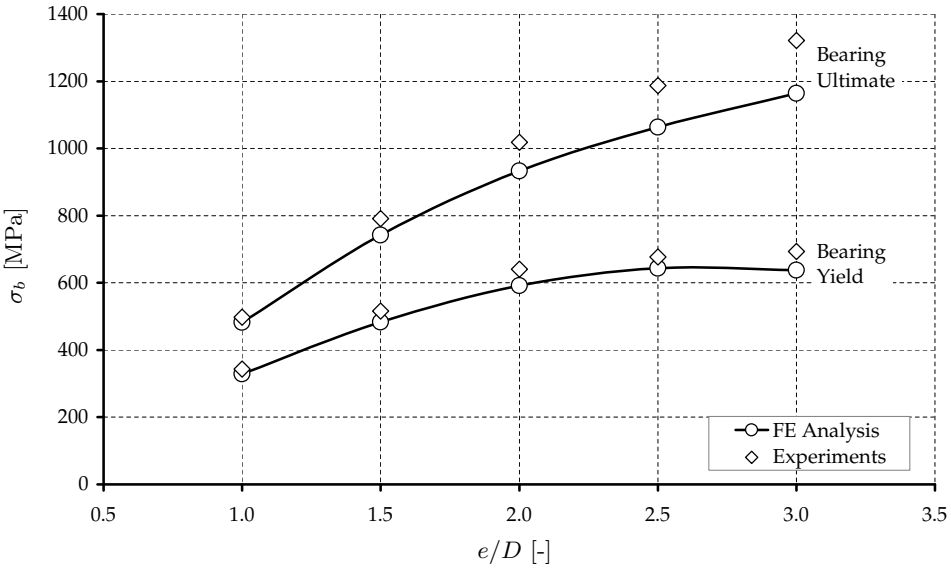

Figure 3.2: *Comparison of experimental and FE results for aluminium 2024-T3 tested in rolling direction with varying edge distance ratio.*

3.3 Results & Discussion

The experimental results in figure 3.2 for monolithic aluminium 2024-T3 show a strong increase in bearing strength with increasing edge distance. While bearing yield reaches an optimum at an e/D equal to 2.0, the ultimate strength still increases beyond this point. Bearing yield is determined by the stiffness ahead of the pin, which is apparently optimal for $e/D \geq 2.0$. For bearing ultimate, the larger amount of material ahead of the pin, postpones shear-out failure and consequently increases the failure strength. This was also seen from the maximum reached pin displacement, which increased with edge distance.

The FE results show comparable trends for the bearing values. The calculated bearing yield values are slightly lower than the experimental ones but they also reach an optimum at e/D equal to 2.0. Ultimate strength is underestimated for all edge distance values, probably due to underestimation of the tensile curve during necking. A necking region was clearly seen in the failed specimen at the sheet edge, where the pin stretches the material outwards.

The bolt tested GLARE laminates have a behaviour, which is comparable to the aluminium sheets, as seen in figures 3.3, 3.4 and 3.5. Even though the bearing yield also reaches its optimum for e/D equal to 2.0, this edge distance is not allowed for an aircraft joint due to the low ultimate strength. For GLARE laminates it is therefore necessary to use a higher edge distance, which of course causes a local weight increase compared to an aluminium structure. A comparison between the different laminates shows almost equal values for bearing yield and ultimate. At first sight this is quite remarkable, since the different fibre orientations should result in different failure behaviour. The different GLARE laminates however contain approximately 70 to 75% aluminium and thus the

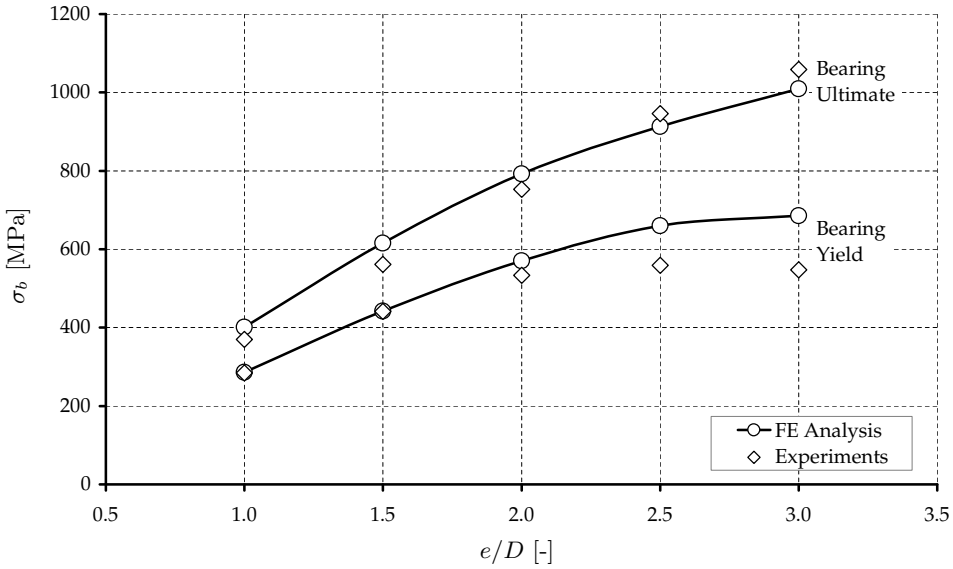

Figure 3.3: *Comparison of experimental and FE results for* GLARE *2 tested in L direction with varying edge distance ratio.*

fibre layer only accounts for a small part of the bearing strength. The different fibre orientations therefore only result in small differences.

The FE results for GLARE 2 tested in the fibre direction (L dir.) show a good approximation for the bearing yield up to e/D equal to 2.0, while at higher edge distance the FE model predicts a higher stress level. The behaviour for high edge distance ratio is clarified in figure 3.6 when the pin and bolt bearing results are compared for the GLARE 3 laminate. Bearing ultimate results from the FE analysis are slightly higher than from the experiments for low e/D and slightly lower for high e/D.

As has been mentioned for monolithic aluminium, the strength of the aluminium layers is underestimated; it is thus inherent that the behaviour of the fibres is actually overestimated in the fibre direction. The occurrence of fibre (layer) splitting, which decreases the load bearing capacity of the fibres, also justifies this statement. Even though matrix (shear) failure is incorporated in the FE model, this does not account for the fibre splitting mode. Fortunately, this failure mode only plays a role for UD fibre layers loaded in the fibre direction.

For GLARE 2 tested perpendicular to the fibre direction (i.e. aluminium LT dir.), the difference between FE results and experiments follows the same trends as the study performed on the aluminium specimens.

The global behaviour of the GLARE 3 laminate under bolt loading is comparable to the GLARE 2L laminate, since also bearing yield is overestimated for e/D higher than 2.0. Bearing ultimate is predicted quite well with the FE model. At small edge distance the ultimate strength is underestimated, comparable to the aluminium behaviour. Because fibre splitting does not occur in this case, the behaviour of the fibres in the loading direction is thus better described. At higher edge distance this conclusion cannot be drawn, since another effect starts to play a role as is clarified below in figure 3.6.

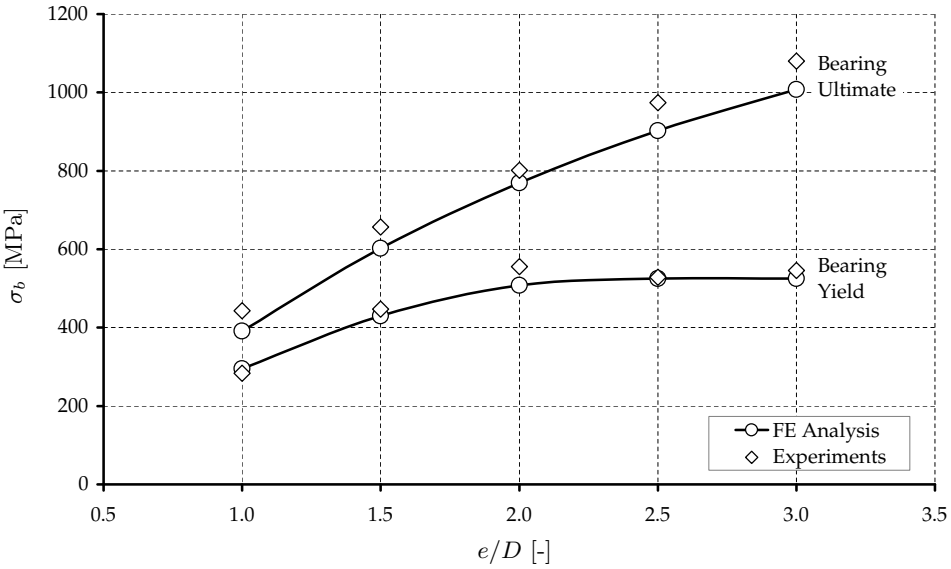

Figure 3.4: *Comparison of experimental and FE results for* GLARE *2 tested in LT direction with varying edge distance ratio.*

Furthermore, it is seen for GLARE 3 that the ultimate strength for the pin loaded case deviates from the bolt loading case reaching a constant value for e/D greater than 1.5, while bearing yield is comparable for both cases. For low e/D there was actually also no difference in actual failure mode: normal bearing failure without delamination. Delamination and buckling of the plies apparently needs a certain load level to initiate, which is not reached for small edge distance. At higher edge distance delamination growth and the correlated strength drop could be clearly observed.

On a global level, i.e. focussing on the yield and ultimate values, the FE model returns a good approximation. It is however important to check whether this is also the case on a detailed level. This can be done by comparing (i) the load-displacement graphs and (ii) the failure progression in the fibre layer as was described in the fibre failure investigation section.

Table 3.4 lists several load-displacement characteristics for e/D equal to 1.5 and 2.0. It shows that in the elastic range the bearing stiffness K is generally twice as high for the FE analysis as for the experiments. This high ratio is however not seen for the secondary modulus K_s, which is probably caused by the following aspects for the initial loading part: (i) setting of the pin in the hole, (ii) out-of-plane deformation due to the pin load and additionally for the GLARE laminates (iii) the inhomogeneity of the fibre layer on a micro-scale resulting in a locally lower stiffness around the hole. Furthermore, the displacement of the pin at maximum load, $v_{pin,\ max}$, is lower for the FE model than for the experiment. This is both due to the difference in elastic stiffness and an underestimation of failure strains of the metal and fibre layer.

The difference in bearing stiffness and the underestimation of the failure displacement, is also seen in figure 3.6, which shows a comparison between experiments and FE analysis for GLARE 3 with e/D equal to 1.5 and 3.0. The main aspect from this figure, is however the large difference between experimental and predicted bearing stress versus

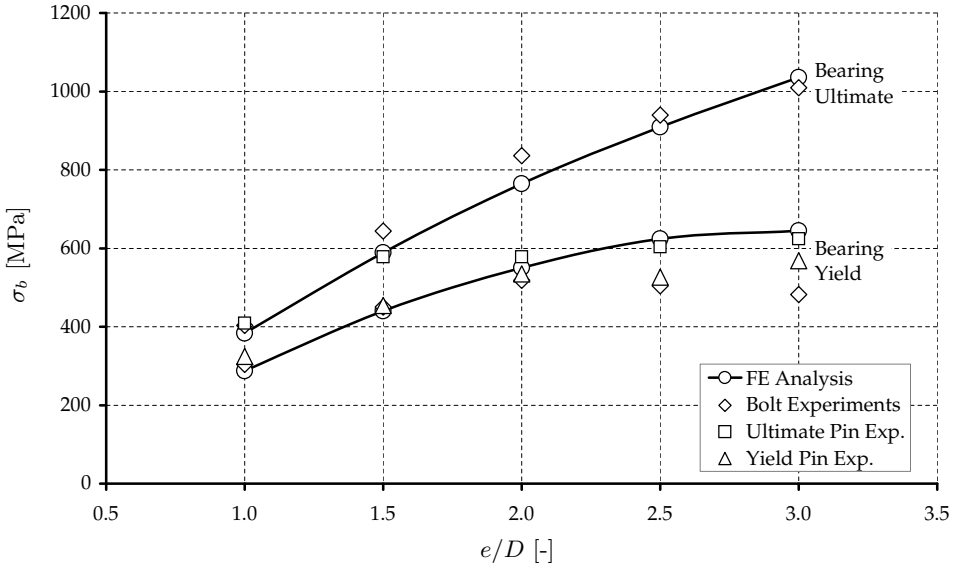

Figure 3.5: *Comparison of experimental and FE results for* GLARE *3 with varying edge distance ratio. The experiments are both pin and bolt loaded tests.*

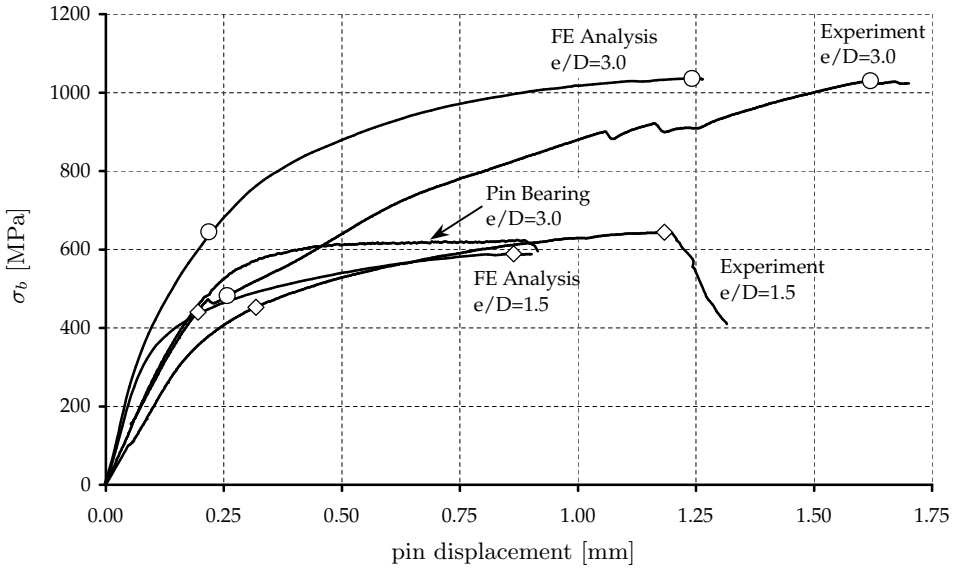

Figure 3.6: *Comparison of experimental and FE bearing stress-displacement curve for* GLARE *3 with e/D equal to* 1.5 *and* 3.0*. For e/D equal to* 3.0 *the experimentally obtained pin bearing curve is also given.*

Table 3.4: *Comparison between experiment and FE analysis of several load-displacement parameters.*

Material	e/D [-]	Experiment $v_{pin,\ max}$ [mm]	Experiment K [MPa/mm]	Experiment K_s [MPa/mm]	FE $v_{pin,\ max}$ [mm]	FE K [MPa/mm]
Aluminium	1.5	1.60	2570	NA	1.38	4700
	2.0	1.88	2920	NA	1.61	5150
GLARE 2L	1.5	1.22	2030	3830	0.93	4610
	2.0	1.59	2590	4540	1.04	5050
GLARE 2LT	1.5	1.52	1900	3643	1.06	4200
	2.0	1.63	2170	4770	1.31	4570
GLARE 3	1.5	1.23	1960	NA	0.86	4230
	2.0	1.34	2210	NA	1.03	4620

pin displacement curves for an edge distance ratio of 3.0. Especially after yielding the experimental curve diverges from the FE model, whereas these curves are comparable for an e/D of 1.5.

A comparison between pin and bolt bearing curve for e/D equals 3.0, shows that the bolt bearing curve levels off approximately at the same moment that the pin bearing tests reaches its maximum load level. This indicates the occurrence of a limited amount of delamination during bolt loading, especially since this behaviour was also seen for an edge distance ratio of 2.0 and 2.5. That the load still increases is simply related to the fact that the clamps prevent further delamination growth. Apparently, finger-tight conditions do not prevent delamination for GLARE laminates, this however only becomes apparent at high edge distance ratios.

The occurrence of delamination is also the reason for overestimation of bearing yield for GLARE 2L and GLARE 3 at high e/D. The influence of delamination on bearing yield for GLARE 2LT is much smaller and hence the model still predicts correct results.

A comparison between experimental and calculated failure in the fibre layer is given in figures 3.7 and 3.8, for GLARE 2 loaded in L and LT direction respectively.

It can be seen that the internal fibre failure prediction for the GLARE 2L laminate approximates quite well the shear-out path from the experiment. Shearing failure and matrix failure are also comparable to the experiment. Even though failure progression is initially overestimated, the failure zones at v_{pin}=1.0 mm are almost identical.

The differences between experimental and FE failure zone are more distinct for the GLARE 2LT laminate. Especially the matrix failure is overestimated, which is either due to a too low matrix failure strength (i.e. Y from table 3.3) or due to the compressive nature of this failure where cracks are not that apparent. The fibre and shearing failure zone seem to be captured better by the model.

Using the FE model it is now possible to define an optimal fibre orientation for the selected GLARE laminates for bearing locations. In figure 3.9 the bearing yield and bearing ultimate are given for an orientation angle α ranging from 0 to 45°. The full range of orientation angles is in this way obtained since GLARE 2LT is rotated 90° with respect to GLARE 2L and GLARE 3 is a cross-ply. The results are obtained for an e/D of 2.0, but it is expected that the trends are comparable for other edge distance ratios.

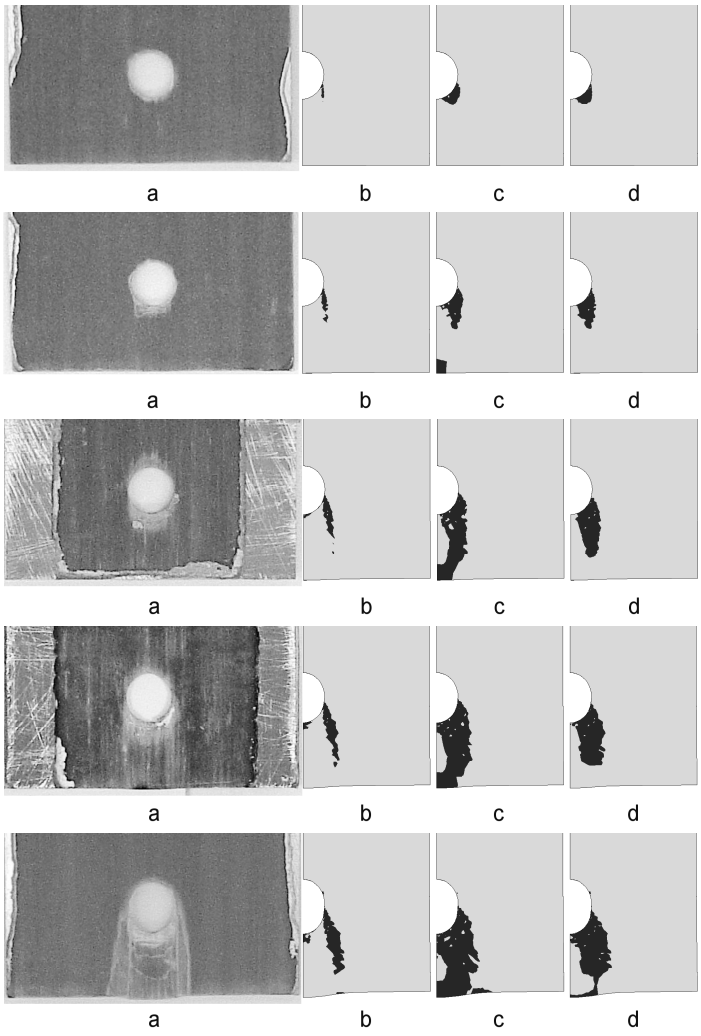

Figure 3.7: *Comparison of failure within fibre layer for several displacement steps for* GLARE *2L. (a) experimental failure zone (grey area near hole), (b)-(d) calculated failure zone (black area near hole), with: (b) fibre failure, (c) matrix failure and (d) fibre-matrix shearing.*

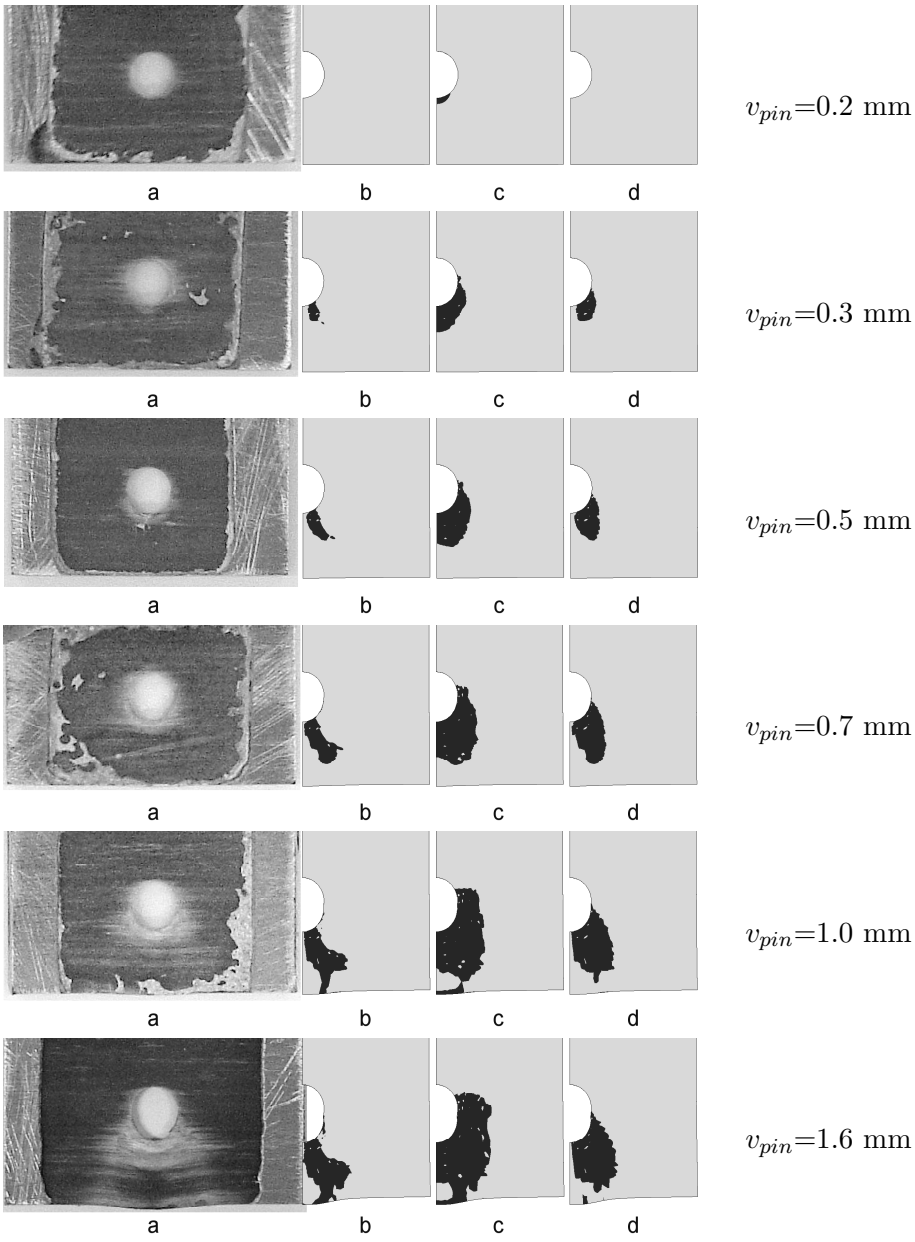

Figure 3.8: *Comparison of failure within fibre layer for several displacement steps for* GLARE *2LT. (a) experimental failure zone (grey area near hole), (b)-(d) calculated failure zone (black area near hole), with: (b) fibre failure, (c) matrix failure and (d) fibre-matrix shearing.*

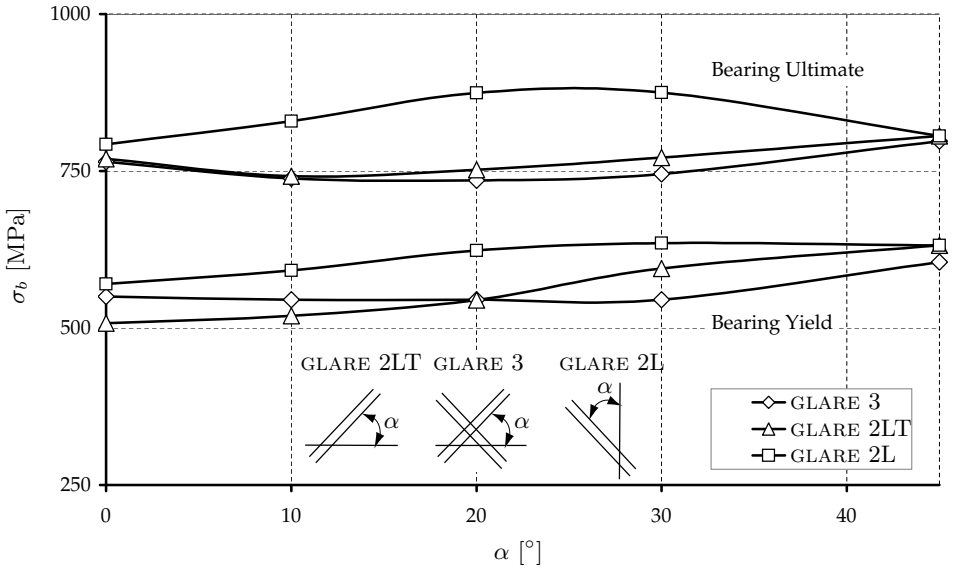

Figure 3.9: *Calculated bearing yield and bearing ultimate for* GLARE *2L,* GLARE *2LT and* GLARE *3 under different loading angles for* e/D=2.0.

For GLARE 3 the orientation under 45° results in the best bearing properties. This is of course related to the higher shear resistance which the 45°-fibres provide. The gain with respect to the standard 0° orientation is however minimal. For a GLARE 2L laminate the influence of orientation angle is more pronounced, reaching its optimum at α equal to 25° (i.e. 65° degrees for a GLARE 2LT laminate).

3.4 Conclusions

An FE model has been developed to describe the bearing behaviour of FMLs with varying edge distance ratio. It was seen that the model returns a good fit with experimental data for several GLARE laminates. Also on a detailed level a good prediction was obtained for the failure zone in the fibre layer.

It was further found that e/D should be equal to 2.5 to obtain sufficient bearing strength for a GLARE laminate. Also under different orientation angles, insufficient bearing strength was predicted for e/D equal to 2.0. The influence of the orientation angle was actually found to be small.

Chapter 4

The Pin Bearing Strength of Fibre Metal Laminates

4.1 Introduction

The bearing strength of monolithic material is generally evaluated without lateral restraint [38] (i.e. with a pin loading configuration according to figure 1.2a). Application of this test procedure on FMLs leads to premature failure due to delamination [13, 37] and generally lateral restraint is provided when pin-loading an FML (i.e. a bolt loading configuration). In an actual structure it is however impossible to obtain full lateral restraint, especially for countersunk holes. Even for the bolt loading configuration it is not possible to obtain full lateral restraint as was seen in chapter 3. Therefore it is important to also investigate the pin bearing behaviour of FMLs.

To describe the pin bearing strength of composite materials Eriksson [48] developed an analytical model. This model is based on the principle that failure occurs when the total energy of the deforming system is minimised. This model was modified to evaluate the behaviour of FMLs [13], showing a quite good comparison with experimental data. The main drawbacks of this approach are however the elastic assumption, which does not seem correct for an FML, and the use of several curve-fit parameters. Tserpes et al. [34] used a numerical approach to study the occurrence of delamination under pin-loads. Delamination initiation and growth was modelled by setting the out-of-plane stiffness of the fibre layer at the delamination location equal to zero. This approach however does not correctly capture the delamination, since delamination also results in a loss of load transfer in the in-plane directions. The advent of so-called interface elements [45] has opened possibilities to describe delamination behaviour correctly. In this chapter these elements are applied to the pin bearing loading of FMLs.

First an overview is given of the FE model developed for calculation of the pin bearing strength. Several laminate configurations are evaluated numerically and verified experimentally with the pin bearing test. Finally a sensitivity study is performed to investigate the influence of the interface properties on pin bearing strength.

4.2 Methods

4.2.1 FE Analysis

FE Model

The pin bearing behaviour was modelled with the ABAQUS [47] FE code. The geometry was based on the ASTM standard for bearing loading of monolithic metal sheet [38], however with a few changes incorporated. The pin diameter D was set equal to 4.8 mm based on actual joint dimensions, while the hole diameter was taken 0.05 mm larger, to account for actual drilling dimensions. The so-called edge distance e between the centre of the hole and the sheet edge in the loading direction was taken equal to 2.5 times the pin diameter. This edge distance ratio (e/D) of 2.5 was based on the bolt bearing experiments from chapter 3, which indicate that delamination starts to play a role at this ratio.

Due to the relatively high stiffness of the steel pin with respect to the evaluated materials, in the model the bearing load is assumed to be exerted by a rigid pin. Friction between the pin and hole is modelled with an anisotropic friction model. Experimentally the out-of-plane friction is expected not to play an important role and because it numerically prevents delamination, it is fully neglected. In the circumferential direction a friction coefficient μ of 0.1 is used, as was employed in chapter 3.

The buckling failure of the different plies under pin loading can either be symmetric (outward buckling in both directions) or asymmetric (outward buckling in one direction). Based on an energy approach Slagter [13] concluded that the symmetric failure mode occurs at a lower stress level and is thus more likely to happen. Since a separate full FE model also showed a symmetric failure mode, it was decided to investigate the symmetric failure type only.

To minimise calculation time, a quarter model with two symmetry planes, was used. A typical mesh is shown in figure 4.1, where at the hole region a finer mesh is used to correctly capture the delamination and the contact situation. Element size was increased towards the sheet edges to reduce calculation time. Each material layer is modelled separately as a layer of eight-node linear solid elements, i.e. the C3D8 element. The outer aluminium layer has two elements through-the-thickness to improve its behaviour under outward displacement.

Several laminates are investigated with the pin-bearing model described. First the behaviour of an aluminium 2024-T3 laminate is analysed, to fully focus on the delamination failure and to omit other failure mechanisms like fibre failure. A so-called 3/2-layup is modelled, which consists of three aluminium sheets and two adhesive layers. The adhesive layer is modelled as being FM94 epoxy (the standard GLARE adhesive) with a thickness of 0.254 mm, which is equal to the cross-ply thickness typically used in GLARE. The aluminium sheet thickness is varied between 0.2, 0.3, 0.4 and 0.5 mm, to investigate the influence of metal layer thickness.

In addition, two different GLARE laminates are investigated: first a GLARE 2-2/1 layup, which contains two aluminium sheets and a 0.254 mm thick unidirectional glass fibre layer. This material is evaluated with the pin load along the fibre direction (indicated with GLARE 2L). Furthermore a GLARE 3-3/2 layup is evaluated, with three aluminium layers and two 0.254 mm thick glass fibre cross-plies. For the GLARE laminates the aluminium thickness is varied similarly to the case of the aluminium laminate.

For simplicity it is assumed that delamination occurs at the metal-adhesive interface and not within the adhesive or fibre layer. As is indicated in figure 4.2 for the symmetric failure mode, this assumption results in two different delamination paths for the alu-

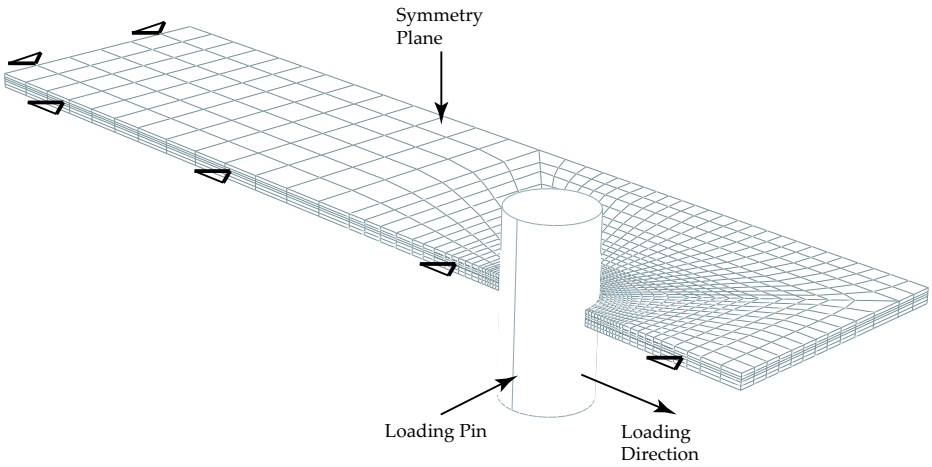

Figure 4.1: *Typical mesh for the pin bearing strength evaluation of a* GLARE *3-3/2-0.4 laminate, with the symmetry plane facing upwards.*

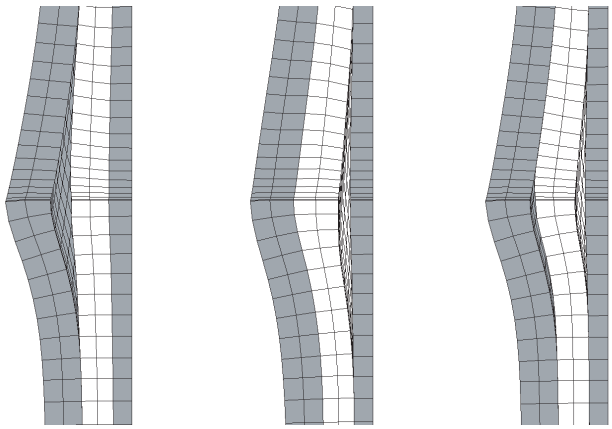

Figure 4.2: *Different delamination paths for the quarter model of a 3/2 layup: (a) at the interface with the outer aluminium sheet, (b) at the interface with the inner aluminium sheet and (c) at both interfaces.*

minium laminate and GLARE 3/2 lay-up: at the interface with (a) the inner metal layer and (b) the outer metal layer. It is of course also possible that both delamination paths are active, which is denoted with option (c). These three failure paths were independently analysed by implementing eight-node zero-thickness linear delamination elements around the hole at the specified interfaces. Even though these interface elements can be used to model crack initiation, still it was found that delamination growth under pin loading only occurs when a small delamination is already present. One element row ahead of the pin was therefore set to be already delaminated. For situation (c), with the multi-delamination path, this initial delamination is located at the outer interface.

Two important properties are normally obtained from a bearing test. First the bearing yield (σ_{b_y}), which is defined as the bearing stress ($\sigma_b = P/(Dt)$) at a 2% permanent hole deformation. And second the bearing ultimate ($\sigma_{b_{ult}}$), which is the maximum bearing stress reached. In this chapter only bearing ultimate is analysed, since this is the critical parameter for pin loading of laminated materials.

Delamination Model and Material Properties

The behaviour of the delamination elements is based on the work of Camanho et al.[14, 45]. Only specific changes with respect to that work are incorporated to model the GLARE and FM94 interface correctly.

An important parameter of the delamination element is the so-called penalty stiffness K, which describes the elastic behaviour of the element in the *interfacial* normal and shear directions. Since the delamination element is used for an elastic-plastic situation, a relatively low value of 70,000 N/mm is used for K. Even though this value does not fully prevent penetration in the elastic part, still it was found to yield stable delamination behaviour.

Under pure Mode I, II or III loading, the onset of damage at the interface is defined by the respective maximum stress allowable. For mixed-mode loading damage onset may already occur before any of the traction components involved reach their respective allowable. It is assumed that the damage onset point is defined by the following quadratic failure criterion:

$$\left(\frac{K\delta_1}{T}\right)^2 + \left(\frac{K\delta_2}{S}\right)^2 + \left(\frac{\gamma K\delta_3}{N}\right)^2 = 1 \tag{4.1}$$

$$\text{with } \gamma = \begin{cases} 1 & \text{if } \delta_3 > 0, \\ 0 & \text{if } \delta_3 \leq 0. \end{cases} \tag{4.2}$$

Where δ_1 and δ_2 are the two in-plane shear displacements, δ_3 is the normal displacement and T, S and N are the respective allowables in the pure mode case. The criterion accounts for the fact that compressive normal tractions do not affect the delamination behaviour. These compressive tractions are described with the penalty stiffness K. When the total mixed-mode relative displacement is defined as:

$$\delta_m = \sqrt{(\delta_1)^2 + (\delta_2)^2 + \gamma(\delta_3)^2} \tag{4.3}$$

and it is furthermore assumed that the in-plane shear allowables are equal (i.e. S=T), then the mixed mode displacement corresponding to damage onset is defined as:

$$\delta_m^o = \begin{cases} \delta_3^o \delta_1^o \sqrt{\dfrac{1+\beta^2}{(\delta_1^o)^2 + (\beta\delta_3^o)^2}} & \text{if } \delta_3 > 0, \\ \\ \delta_1^o = \delta_2^o & \text{if } \delta_3 \leq 0. \end{cases} \tag{4.4}$$

Table 4.1: *Average test results for delamination behaviour between aluminium 2024-T3 and FM94 reinforced with S_2 glass fibre.*

mode	G_I [kJ/m^2]	G_{II} [kJ/m^2]	G_c [kJ/m^2]
mode I	3.23	-	3.23
mode II	-	1.91	1.91
mixed mode ($G_I = G_{II}$)	0.34	0.34	0.68

Where δ_1^o, δ_2^o and δ_3^o are the damage onset displacements in the pure mode case and β is the so-called mode mixity ratio, which is defined as:

$$\beta = \frac{\sqrt{(\delta_1)^2 + (\delta_2)^2}}{\delta_3} \tag{4.5}$$

For the interface between aluminium and fibre reinforced FM94 an allowable normal stress N of 20 MPa is used, while the in-plane shear values S and T are taken equal to 40 MPa. It is assumed for the interface between aluminium and *unreinforced* FM94 that the normal and shear strength are equal to 50 MPa, which is the lap shear strength of the FM94 adhesive [49].

Delamination propagation is generally described in terms of the energy release rates. The energy release rate of the delamination element for the interface between aluminium 2024-T3 and FM94 reinforced with S_2 glass fibre is based on experiments performed by Vesco et al. [50]. Average values from these experiments for pure mode I and pure mode II and mixed mode delamination behaviour are given in table 4.1. An important aspect is the lower total energy G_c for the mixed mode case (50-50) compared to the pure mode I and mode II situations. Both the Benzeggagh-Kenane criterion, as described by Camanho et al., as well as the power law with the power constant equal to 1 or 2 cannot correctly describe the experimental behaviour as obtained by Vesco et al. A better relation for this specific case is the power law with the power equal to one half, i.e.:

$$\left(\frac{G_I}{G_{Ic}}\right)^{0.5} + \left(\frac{G_{II}}{G_{IIc}}\right)^{0.5} = 1 \tag{4.6}$$

With the pure mode I and mode II values from table 4.1 as input parameters for G_{Ic} and G_{IIc}, this relation results in a G_c equal to 1.36 N/mm for a 50% mode mixture. The mixed mode situation still overestimates the experimental value, but unfortunately it is not possible with the current model limitations to get a closer fit.

Since energy release rates are not available for the unreinforced FM94 case, it is assumed that the characteristics are equal to the fibre reinforced case. This probably is an overestimation for the mode I case due to the absence of fibre bridging.

The energy release rates G_I, G_{II} and G_{III} at total decohesion under mixed mode can be obtained from the area under the respective traction versus displacement curves. And hence the mixed mode displacement corresponding to total decohesion can be

Table 4.2: *Overview of material properties for aluminium 2024-T3, FM94 and the S_2 glass fibre layer.*

Material	E_{11} [MPa]	E_{22} [MPa]	G_{12} [MPa]	ν_{12} [-]	$\sigma_{0.2}$ [MPa]	σ_{ult} [MPa]
2024-T3	72,400	72,400	27,608	0.33	350	725[a]
FM94	2189	2189	823	0.33	50	50
S_2 glass	53,980	9412	2700	0.33	250-500	250-500

[a] true stress value based on the assumption that the engineering stress remains constant during necking.

obtained from the power law, resulting in:

$$\delta_m^f = \begin{cases} \dfrac{2(1+\beta^2)}{K\delta_m^o}\left[\left(\dfrac{1}{G_{I_c}}\right)^{1/2} + \left(\dfrac{\beta^2}{G_{II_c}}\right)^{1/2}\right]^{-2} & \text{if } \delta_3 > 0, \\ \sqrt{(\delta_1^f)^2 + (\delta_2^f)^2} & \text{if } \delta_3 \leq 0. \end{cases} \tag{4.7}$$

Where δ_1^f and δ_2^f are the decohesion displacements in the pure mode case. In between the damage onset point δ_m^o and the decohesion point δ_m^f a linear relation is assumed and hence the behaviour of the delamination element is known both in the elastic range and in the propagation range.

The sensitivity of the FE model to delamination parameters is investigated by varying the available mode I and mode II energy and the interfacial strength. It is assumed that the power law, as given in equation 4.6, still holds for these changes.

Material parameters for aluminium 2024-T3 sheets, FM94 adhesive and glass fibre layers are given in table 4.2. It is assumed that the tensile and compressive properties are equal and that out-of-plane properties are equal to in-plane transverse properties. The residual stresses that may occur due to manufacturing of the laminates are not accounted for in the model.

For aluminium 2024-T3 it is assumed that it behaves as an isotropic material with isotropic hardening. This is further simplified into a trilinear behaviour up to a failure strain of 50%, consisting of the following parts: (i) elastic part up to yielding at 330 MPa, (ii) plastic part up to necking (at 15% plastic strain) with tangent stiffness equal to 1468 MPa and (iii) necking plasticity with a tangent stiffness of 500 MPa.

The assumption of isotropic behaviour is also valid for the unreinforced FM94 adhesive. Hardening is however assumed to be negligible and the material is modelled as being ideally plastic.

The anisotropic behaviour of the fibre layers in an FML requires the correct description of several intra-laminar failure mechanisms, like fibre and matrix failure. These failure modes are quite often described with a progressive failure model, which consists of an initiation rule followed by a degradation definition. Initiation rules can either be separate mode or interactive criteria [51].

Even though the separate mode criteria are preferred, as was also discussed in chapter 3, still it was found that they cause numerical instability problems when combined with

Table 4.3: *Test matrix for the pin bearing test setup.*

Material	Dir.	t [mm]	e/D [-]
aluminium-3/2-0.4	L	2.1	2.0 & 3.0
GLARE 2-2/1-0.4	L	1.05	1.0 - 3.0
GLARE 3-3/2-0.3	L	1.7	2.0
GLARE 3-3/2-0.4	L	1.7	1.0 - 3.0

the delamination element definition. The main difficulty is the definition of the elastic stiffness of the delamination element, which is strongly dependent on material stiffness.

To overcome this problem the fibre layer is described with a Tsai-Hill interactive failure criterion, while post-failure behaviour is described as being ideally plastic. The large difference in fibre failure stress (i.e. 2429 MPa) and matrix failure stress (i.e. 67.9 MPa) however results in a stretched failure ellipsoid with high aspect ratio, which causes numerical difficulties. A lower aspect ratio is therefore implemented, with a failure stress of 250 MPa perpendicular to the fibre direction and 500 MPa in the fibre direction. This fibre failure model was verified on a global level for the bolt loading case, by comparing it with the separate mode criteria as described in chapter 3. Only for large pin displacements the behaviour is slightly overestimated, but this is no issue for pin loading where failure occurs at low pin displacement.

4.2.2 Experimental Validation

To validate the FE model, several laminates were evaluated experimentally, which are listed in table 4.3. These tests were performed according to the ASTM standard for bearing loading of metals [38], involving the modifications as described for the FE model.

GLARE 2L-2/1-0.4 and GLARE 3-3/2-0.4 specimens were evaluated for five different edge distance ratios (e/D), to obtain the edge distance at which buckling failure occurs. The influence of aluminium sheet thickness was examined by comparing GLARE 3-3/2-0.3 to the GLARE 3-3/2-0.4 specimens. Furthermore an aluminium-3/2-0.4 laminate was tested, which was obtained by bonding three 0.4 mm aluminium sheets together. The adhesive plies contain a carrier to obtain a minimal thickness of 0.254 mm. Due to the applied autoclave pressure, the excess of adhesive however could not fully flow out, resulting in locations with higher thickness than the GLARE 3-3/2-0.4 laminate. For comparison, the bonded aluminium was also tested according to the bolt bearing setup [39], i.e. with lateral restraint to prevent delamination.

The specimen holes were drilled with a wood backing and with step-wise increasing drill sizes to prevent initial delamination. Finally the hole was reamed to an H6 tolerance, to obtain a clearance fit with the pin. The width of the specimens was taken to be six times the pin diameter, to prevent net section failure.

The bearing test was conducted at a speed of 2 mm/min up to the maximum load level. To measure the deformation, an extensometer was attached on one side to the loading pin and on the other side clamped to the sheet at a distance of 3.25 cm above

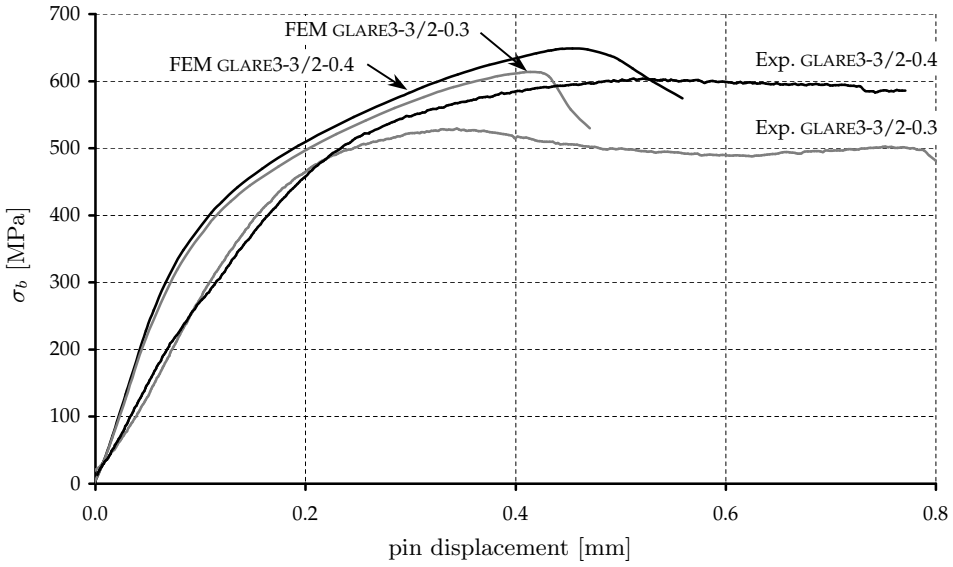

Figure 4.3: *Bearing stress versus pin displacement curves for pin loading of* GLARE *3-3/2-0.3 and* GLARE *3-3/2-0.4.*

the pin centre. These same locations were also used in the FE model to obtain the calculated pin displacement.

The internal damage of the specimens after pin bearing failure was investigated ultrasonically. With this method the acoustic damping of the material is measured, which gives an indication of the quality of the bond line within the laminate. Furthermore, some of the GLARE 3-3/2-0.4 and aluminium-3/2-0.4 specimens were investigated under the Scanning Electron Microscope (SEM) to obtain a more detailed overview of the extent of the delamination. To this aim a cross-section was made along the centre-line of the specimen, where the largest out-of-plane deformations were seen.

4.3 Results & Discussion

The comparison between FE analysis and experimental behaviour is given in figures 4.3 and 4.4. It is seen that the results for the different laminates compare reasonably well, both in stress level and in pin displacement at ultimate load. In general the model overestimates the experimental results, except for the aluminium laminate where the model is conservative.

An important overall difference is, the considerably lower stiffness in the elastic region for the experimental results. This was also seen for the bearing behaviour with lateral clamping in chapter 3, whereas for pin loading the out-of-plane deformation due to the pin-load is of course more severe. It is furthermore seen in figure 4.3 that the influence of aluminium thickness is slightly underestimated.

The influence of aluminium ply thickness is further investigated numerically and results are shown in figure 4.5 for different delamination paths. The results of the GLARE 2L laminate are not shown in the figure, since it had comparable trends to the GLARE

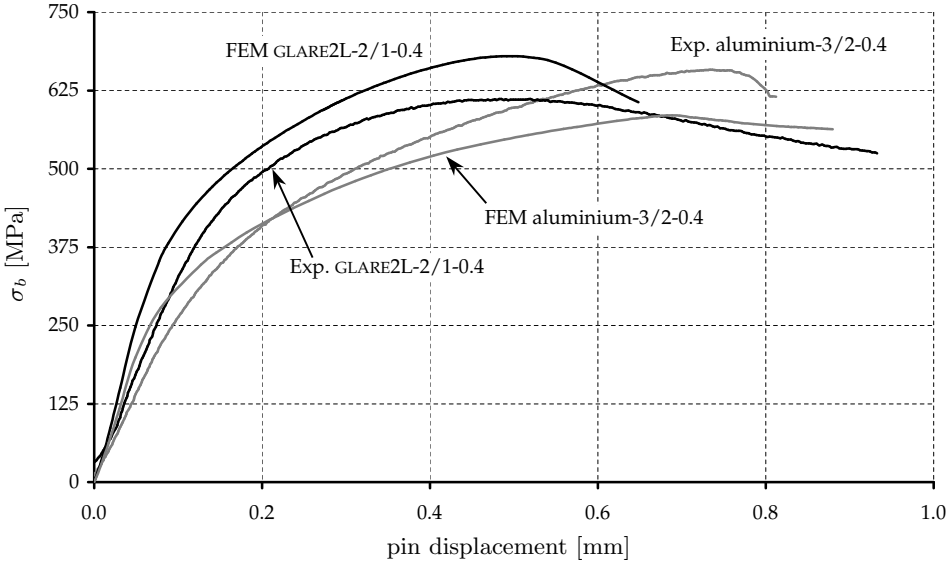

Figure 4.4: *Bearing stress versus pin displacement curves for pin loading of* GLARE *2L-2/1-0.4 and aluminium-3/2-0.4.*

3 case. The numerical results show a linear relation between the bearing strength and the aluminium layer thickness. This differs from the behaviour of a simply-supported monolithic sheet in the elastic regime, where the buckling stress is linearly related to the second power of the sheet thickness (i.e. $\sigma_b \sim t^2$). However, the behaviour of the pin loaded-laminate is different due to the presence of the adhesive interface and the occurrence of plasticity in the metal layer before buckling occurs. Also in this figure it is seen that the influence of the metal sheet thickness is not correctly captured for the GLARE 3 laminates. The trend lines for the bonded aluminium laminate actually compare much better to the GLARE 3 case. The behaviour under pin loading of the fibre layer is apparently much closer to that of the unreinforced adhesive.

Figure 4.5 also shows the effect of delamination path on the bearing ultimate of GLARE 3-3/2 and aluminium-3/2. Clearly delamination path 'b' returns the highest stress levels in both cases, which is related to the higher total thickness of the delaminating ply. For the aluminium laminate there is no difference seen between case 'a' and 'c' since delamination path 'b' did not become active for the multi-path analysis. The results for GLARE, however, show that the lowest results are obtained if both delamination paths become effective. The different trend for delamination path 'a' for the GLARE laminate is related to the fact that the fibre layer does not delaminate and therefore does not loose its load bearing capabilities. Since failure occurs at a higher pin displacement for an increase of aluminium thickness, the fibre layer effectively carries a higher stress.

The influence of edge distance (e/D) on the bearing strength is given in table 4.4. The comparison between pin and bolt loaded test results from chapter 3 indicates at which e/D value delamination starts to play a role. For the GLARE laminates this is approximately at e/D equal to 1.5 or 2.0. For the aluminium laminate this occurs at slightly higher value, which is related to the higher interface strength of the unreinforced

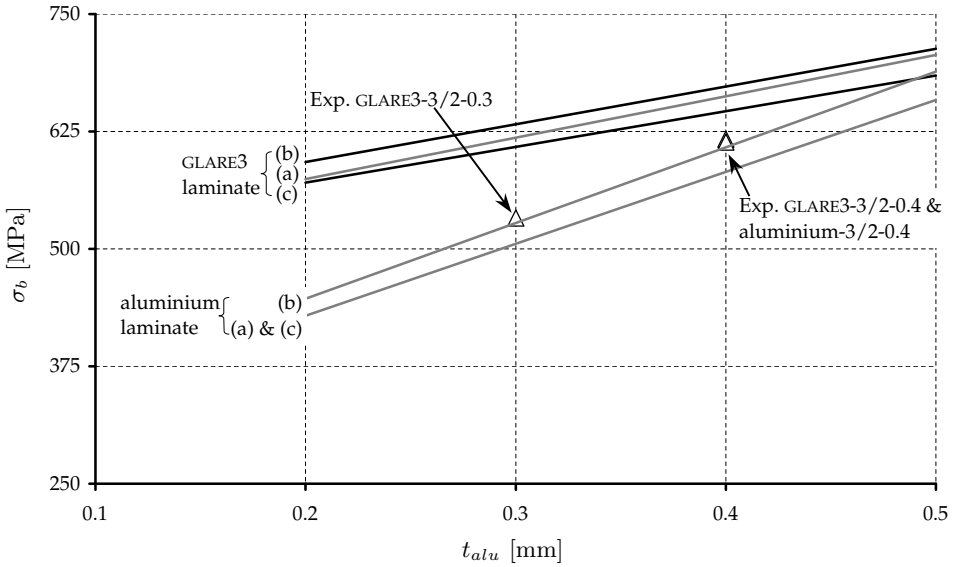

Figure 4.5: *Influence of single aluminium sheet thickness and delamination path on the laminate pin bearing strength of* GLARE *3-3/2 and aluminium-3/2 laminates. The delamination paths a, b and c are defined in figure 4.2.*

adhesive. Based on these results the assumption to model pin bearing behaviour at an e/D of 2.5 seems appropriate.

The actual extent of the delamination zone and the delamination path was investigated for several laminates with ultrasound and the SEM. Figures 4.6 and 4.7 show these characteristics for a pin-loaded GLARE 3-3/2-0.4 and aluminium-3/2-0.4 and a bolt-loaded aluminium-3/2-0.4, respectively. Due to edge effects close to the hole, the full delamination zone cannot be measured with ultrasound. Still the results indicate a similar failure zone for both loading cases on the aluminium laminates, while the zone is slightly smaller for the GLARE specimen. The cross-section at the failure location, as obtained with the SEM, however reveals the largest failure zone for the GLARE specimen.

More importantly, the cross-sections show the failure characteristics of the different materials and loading conditions. Several similarities are seen in the failure pattern of the different specimens. In all cases, the delamination is multi-path and the deformation pattern is not fully symmetrical. Differences are however seen in the exact delamination location. The GLARE specimen fails experimentally mainly within the fibre layer close to the so-called adhesive rich zone (i.e. the small region in the fibre layer close to the metal ply that has a relatively higher adhesive content). In the model failure can only take place at the metal-fibre layer interface. The bonded aluminium delaminates at the interface between aluminium and primer, which is equal to the modelled delamination location. Nevertheless in both cases, failure indeed takes place at the weakest interface.

Given the reasonable agreement between FE predictions and experimental values it is now possible to do a parameter study on the influence of interface properties on the pin bearing strength of a GLARE 3-3/2-0.4 laminate. As a reference state we use the case with interfacial shear strength (S) and tensile strength (N) equal to 30 MPa and

Table 4.4: *Comparison of experimentally obtained ultimate bearing strength for pin and bolt loaded laminates with varying edge distance ratio.*

Material	e/D [-]	Pin $\sigma_{b_{ult}}$ [MPa]	Bolt $\sigma_{b_{ult}}$ [MPa]	Difference [%]
aluminium-3/2-0.4	2.0	564	592	-5
	3.0	573	774	-26
GLARE 2L-2/1-0.4	1.0	380	369	+3
	1.5	574	561	+2
	2.0	637	753	-15
	2.5	611	946	-35
	3.0	596	1059	-44
GLARE 3-3/2-0.3	2.5	533	-	
GLARE 3-3/2-0.4	1.0	409	404	+1
	1.5	578	644	-10
	2.0	578	836	-31
	2.5	604	969	-38
	3.0	624	1010	-38

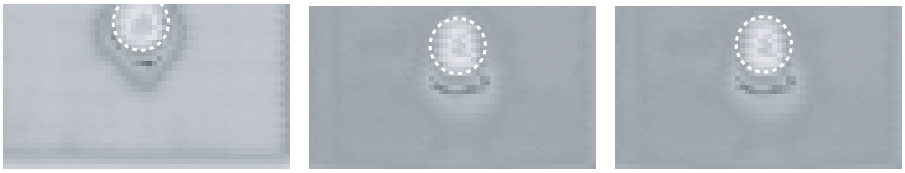

(a) **(b)** **(c)**

Figure 4.6: *Overview of the failure zone obtained with ultrasound for (a) pin loaded* GLARE *3-3/2-0.4, (b) pin loaded aluminium-3/2-0.4 and (c) bolt loaded aluminium-3/2-0.4, showing the delamination ahead of the (dashed) hole.*

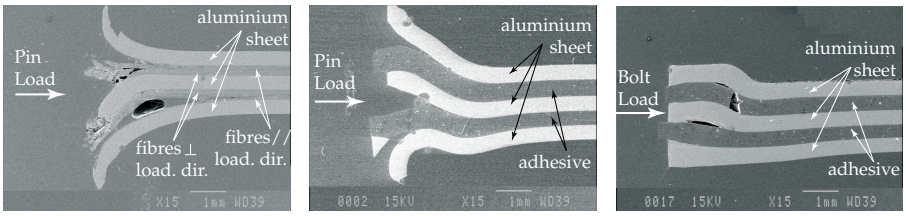

(a) **(b)** **(c)**

Figure 4.7: *Overview of the failure zone obtained with the SEM for (a) pin loaded* GLARE *3-3/2-0.4, (b) pin loaded aluminium-3/2-0.4 and (c) bolt loaded aluminium-3/2-0.4.*

Table 4.5: *Influence of interface properties on the calculated bearing ultimate of* GLARE *3-3/2-0.4. Parameters varied with respect to the reference situation are indicated in bold characters.*

N [MPa]	S [MPa]	G_{I_c} [kJ/m^2]	G_{II_c} [kJ/m^2]	$\sigma_{b_{ult}}$ [MPa]
30	30	3.23	1.91	654
60	30	3.23	1.91	663
30	**60**	3.23	1.91	687
60	**60**	3.23	1.91	707
30	30	**1.91**	**3.23**	654
30	30	**6.46**	1.91	654
30	30	3.23	**3.82**	657

energy release rates G_{I_c} and G_{II_c} equal to 3.23 and 1.91 kJ/m^2, respectively.

Data in table 4.5 clearly indicate that a higher interface strength leads to higher bearing ultimate values, since it postpones delamination initiation. More specifically, interfacial shear strength plays a bigger role than the interfacial tensile strength . This is due to the fact that initiation is mainly a mode II or shear phenomenon related to the in-plane pin load. The influence of energy release rate is found to be almost negligible. As buckling failure already occurs at a small amount of delamination, such a minimal effect is to be expected.

4.4 Conclusions

The FE model presented shows good agreement with the pin bearing behaviour of several GLARE and bonded aluminium laminates. Delamination is shown to play a major role. The model predicts that pin bearing strength can be improved by increasing the interfacial shear strength. Interfacial tensile strength is shown to play a minor role, while the influence of energy release rates is almost negligible.

Chapter 5

Improving the Adhesion of Thin Stainless Steel Sheets

5.1 Introduction

The use of (stainless) steel sheets for aerospace applications has long been considered as not being viable because of the relatively high density of this material. Even though its specific stiffness (i.e. elastic stiffness per unit weight) is comparable to aluminium alloys, its application would result in a too low sheet thickness, resulting in a higher sensitivity to compression loading. Laminated materials open up new possibilities for steel application in the aerospace field, where a combination of high density steel sheet and low density fibre layers can lead to required total thickness and improved properties.

A material well suited for steel incorporation is the commercially available Fibre Metal Laminate called GLARE. The use of stainless steel sheet with high specific strength properties (e.g. yield and ultimate strength per unit weight) can result in improvement of several static strength characteristics of GLARE as was already highlighted in chapter 2. An important aspect for successful application of stainless steel as a reinforcement layer in Fibre Metal Laminates is its adhesion.

ASTM standard D2651 [52] describes several methods, both mechanical and chemical, to pretreat stainless steels to improve adhesion. The methods are described in general, without showing the effectiveness of a treatment. The performance should, therefore, be determined experimentally for each specific adhesive-metal combination. Bouquet et al. [53] investigated different surface treatments to bond AISI 304 steel. Either etching alone or etching followed by anodising were applied to the steel. Initial adhesion was comparable for all treatments, but differences were seen in durability tests. Only for the nitric acid and the sulphuric-chromic acid anodising procedures excellent bond durability was observed. To determine the most effective bonding treatment for stainless steels, Gaskin et al. [54] pretreated different stainless steel types, (namely AISI 301, 347 and 15-5). No consistent effectiveness was, however, found for the different steel types, each showing an optimum adhesion by a different pretreatment. It was, however, concluded that sulfuric acid pickling followed by desmutting using nitric-hydrofluoric acid had the potential to be generally applicable to all stainless steel types.

As indicated above, the stainless steel type dictates, to a large extent, the pretreatment that should be used. A description of the stainless steel used and the selected

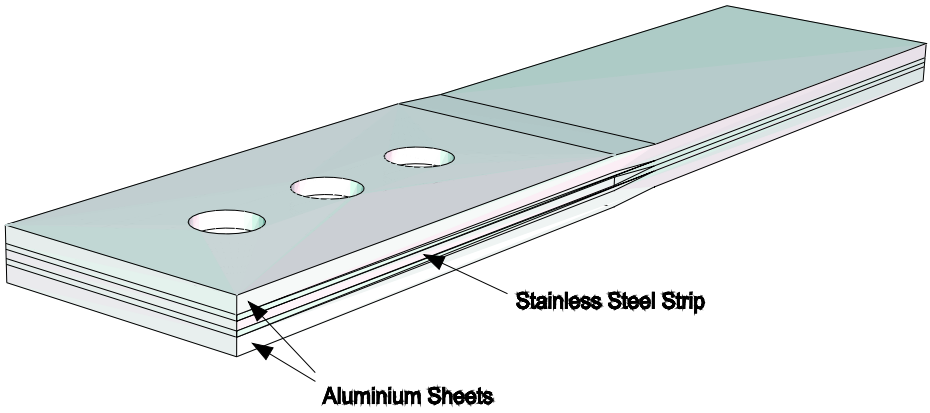

Figure 5.1: *Schematic representation of a* GLARE *laminate reinforced at the fastener holes with a thin steel strip in between the fibre layers.*

chemical pretreatments is given in the next section. To compare the effect of chemical modification of the sheet surface it was decided to apply a mechanical treatment also, via gritblasting, to improve adhesion. To overcome possible difficulties with stainless steel bonding, aluminium coated stainless steel was also investigated. Both surface analysis after pretreatment as well as adhesion study were performed on these materials to investigate the adhesion characteristics.

5.2 Methods

5.2.1 Materials Description

Improvement in static strength properties of GLARE can be achieved by application of a stainless steel sheet with high specific strength properties. Since the application area of GLARE is mainly aerospace, it is also important to have excellent fatigue characteristics. Based on these requirements, the austenitic AISI 301 spring steel with added molybdenum was selected for investigation. The molybdenum increases corrosion resistance, but it can also increase resistance to chemical pretreatment.

Since the density of steel is three times higher than that of aluminium, it was decided to use a thickness approximately three times less than that used for the aluminium sheet. Thus the weight increase due to adding a stainless steel sheet is comparable to using an aluminium sheet. A second reason for the lower thickness is that it results in a smaller thickness increase when incorporated as a local (interlaminar) reinforcement. Especially to increase the strength of mechanical joints, only a small strip at the fastener locations is necessary. This is illustrated in figure 5.1, where a GLARE laminate is locally reinforced with a thin strip of steel.

Based on standard aluminium thickness in GLARE of 0.3, 0.4 and 0.5 mm, a thickness of 0.1 mm was selected for the steel strip. Furthermore, 0.28 mm thick AISI 301 steel sheet was also investigated, but without the molybdenum content. These sheets are referred to as thin (t=0.1 mm) and thick (t=0.28 mm) throughout the text.

As the requirements for aluminium pretreatment for FML applications are well

known, it was decided to also investigate the properties of aluminium coated AISI 301 steel sheet. The aluminium coating, of approximately one micrometer thickness, was deposited by evaporation on both thin and thick steel sheets.

5.2.2 Materials Preparation

Two different chemical treatments were selected to create a desirable surface condition on the uncoated stainless steel strips. The first was a sulfuric acid-sodium dichromate solution treatment as described in ASTM standard D2651 [52]. Specimens were immersed for 15 min. at approx. 63°C, followed by rinsing in water to remove the residue.

The second was comparable to the work of Gaskin et al. [54], where acid pickling was followed by a desmutting treatment. In this case, a 50% sulfuric acid solution was used at a temperature of approx. 60°C. Since the effectiveness of this treatment was not known beforehand, etching times of 1, 2 and 3 minutes were used. Subsequently, the specimens were immersed for 10 minutes in a 25% nitric acid solution as described in ASTM standard A967 [55] to desmut the material.

In addition to these stainless steel treatments, also a treatment for the aluminium coated steel was investigated. In this case, the standard pickling solution for aluminium was used, which is a sulfuric acid-dichromate solution. Due to the limited thickness of the aluminium top layer, the pretreatment could not be executed at the prescribed 65°C, since this would remove the coating in a too short period. The bath was, therefore, kept at room temperature for a relatively low chemical activity. Specimens were etched for 5 and 10 minutes, since preliminary investigations showed that a 15-minute procedure completely removed the coating.

Furthermore, the material was also treated mechanically via gritblasting, using angular aluminium oxide particles with particle size between 149 and 210 μm. An investigation into the influence of pressure and blasting distance resulted in an optimum pressure of 200 kPa at a distance of approximately 5-10 cm. These process conditions were therefore, used for further investigation.

To improve the adhesion of the pretreated surfaces, several samples were post-treated with a 1% aqueous silane solution. The silane selected was 3-glycidoxypropyltrimethoxysilane, which is used as a coupling agent to improve the adhesion of organic resins (specifically epoxies) to inorganic surfaces [56, 57].

5.2.3 Test Description

To investigate the surface characteristics of the pretreated material, scanning electron microscopy (SEM) was used. Samples were analysed using magnification ranging from 250 to 10,000 times at an acceleration voltage of 10 kV.

The adhesion of the adhesive-metal combination was analysed with the floating roller peel test, which is described in ASTM standard D3167 [58]. Specimens were prepared by bonding the pretreated AISI 301 sheets to a rigid aluminium plate, which was pretreated with a standard sulfuric acid-dichromate solution to ensure good bonding. As a reference, peel experiments were also conducted on thin pretreated 2024-T3 aluminium sheets.

To compare the adhesion of the AISI 301 steel sheets to the existing GLARE material, the Cytec FM94 epoxy-based adhesive was used for bonding. An adhesive film with a carrier fabric was used to ensure an adhesive thickness of 0.1 mm. The specimens were cured at 120°C at a pressure of 100 kPa.

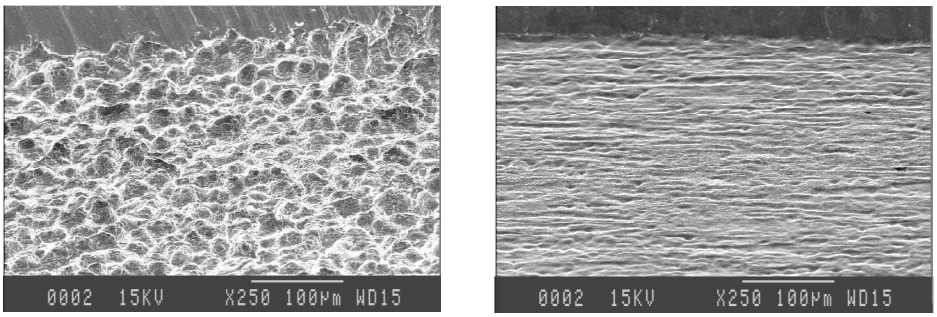

(a) **(b)**

Figure 5.2: *Etched surface as observed with an SEM: (a) thick AISI 301 steel sheet (t=0.28 mm) after etching for 15 minutes in a sulfuric acid-sodium dichromate solution, (b) thin AISI 301 steel sheet (t=0.1 mm) after etching for 3 minutes in sulfuric acid.*

By peeling off the thin AISI 301 steel sheet at a controlled angle, a relatively severe loading condition is introduced on the interface with the adhesive. This either results in a cohesive failure in the adhesive or in interfacial failure, corresponding, to respectively good or poor surface treatment. Hence, the peel test provides a good indication of the quality of the pretreatment.

An important advantage of the peel test is the relatively long loading trajectory, since peel strength is measured over the full strip length. This results in reliable test values from a minimal number of specimens. A disadvantage, though, is that it is not possible to compare peel strengths of different sheet thicknesses or material types, since the sheet characteristics influence the peel strength.

5.3 Results & Discussion

5.3.1 Effect of Etching

The sulfuric acid-sodium dichromate solution was applied to both thin and thick (uncoated) AISI 301 steel sheets. To obtain a first indication of etching effectiveness, the specimens were weighed before and after the etching procedure. For a 15-minute etching procedure it was seen that the weight of the thick steel sheet decreased by 40%, while no decrease was found for the thin AISI 301 sheet. This difference was also clear from the difference in chemical activity, where no reaction was seen for the thin AISI 301 sheet, while the thick version showed a strong exothermic reaction. An SEM micrograph of the thick sheet surface is shown in figure 5.2a, which clearly shows surface roughness. The chemical resistance of the thin AISI 301 sheet is probably due to the molybdenum content, which results in a higher corrosion resistance for relatively high sulfuric acid concentrations [59].

The application of sulfuric acid to the thin sheet was much more successful. Although the passivation layer provided initial chemical resistance, still a strong exothermic reaction occurred after approx. 30 seconds. Meanwhile the outer surface was blackened with smut, which, however, dissolved in the nitric acid solution. A typical surface after 3 minutes of etching is shown in figure 5.2b. Clearly the roughness is not comparable to

Table 5.1: *Peel test results on differently treated thick AISI 301 steel sheet as well as aluminium coated version (t=0.28 mm). A pretreated 2024-T3 aluminium sheet (t=0.3 mm) was used as a reference.*

Material	Pickling time [min]	Silane applied	Peel Strength [N/mm]	Failure
AISI 301	-	yes	7.1	cohesive/interfacial
AISI 301	-	no	1.1	interfacial
Alu coated	-	yes	6.8	cohesive
Alu coated	5	yes	7.8	cohesive
Alu coated	10	yes	7.3	cohesive
2024-T3	-	no	6.4	cohesive

figure 5.2a, but still the effect of the treatment can be seen. During this 3-minute treatment the weight loss was approximately 10% and longer etching periods are, therefore, not really an option for this thin sheet.

5.3.2 Adhesion Investigation

Both interface strength and properties of the bonded sheet play important roles in the peel strength. Especially, because of deformation of the bonded sheet, it is difficult to compare the peel strengths of specimens with different sheet thicknesses. Hence, the results of thin and thick stainless steel types are described separately.

The results for the thicker steel sheets are shown in table 5.1 and in figure 5.3. The results are comparable for all but the untreated steel, showing a strong influence of the silane treatment. The fact that the 2024-T3 aluminium has a slightly lower peel strength is not related to the silane but simply to the difference in material properties of the bonded sheet. Besides the comparison in peel strength the surfaces of the tested specimens were examined to check for the type of failure: interfacial or cohesive. Based on this investigation it was concluded that the pickled coated surface resulted in more cohesive failure and, therefore, had the best adhesion properties.

For the thin sheets much lower peel strength values were obtained, as can be seen from table 5.2 and figure 5.4. As already mentioned this is inherent to the peel test, because a thicker sheet simply requires a higher load to *peel it off*. More important is that the failure mode for the untreated silanated steel sheets was in this case interfacial. The corresponding peel strength was so low that the specimens already failed during the initial preloading stage. Since the loading conditions are comparable for both sheet thicknesses, this difference should be attributed to different surface qualities related to the difference in thickness decrease during sheet production. Only after sufficient etching, in this case 3 minutes, the outer surface is largely removed from the thin sheet and the failure becomes more cohesive.

The peel test on the thin aluminium coated steel sheet resulted in early failure at the interface between aluminium coating and the stainless steel sheet. Apparently also in this case, the surface quality of the thin AISI 301 steel sheet played an important role. Further investigation was conducted with the SEM to investigate this interface. In figure 5.5a clearly a poor interface with the stainless steel is indicated, where some

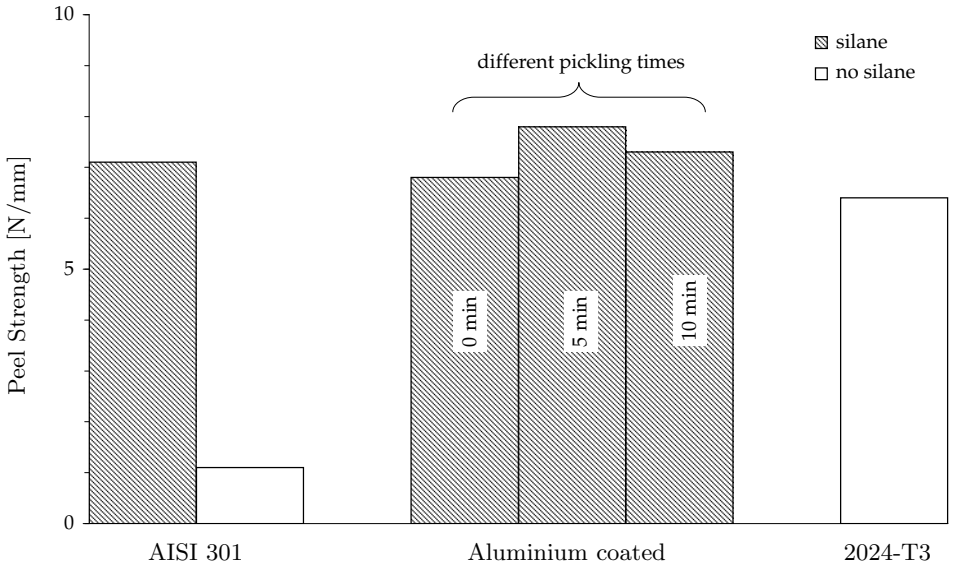

Figure 5.3: *Comparison of peel strength values for differently treated thick AISI 301 steel (t=0.28 mm) and 2024-T3 aluminium sheets.*

Table 5.2: *Peel test results on differently treated thin AISI 301 steel sheet as well as aluminium coated version (t=0.1 mm).*

Material	Pickling time [min]	Silane applied	Peel Strength [N/mm]	Failure
AISI 301	-	no	NA	interfacial
AISI 301	-	yes	NA	interfacial
AISI 301	1	yes	NA	interfacial
AISI 301	2	yes	NA	interfacial
AISI 301	3	yes	0.74	cohesive/interfacial
gritblasted AISI 301	-	yes	1.62	cohesive
Alu coated	-	no	0.23	interfacial
Alu coated	-	yes	1.28	cohesive/interfacial
Alu coated	5	no	0.31	interfacial
Alu coated	5	yes	NA	coating failure
Alu coated	10	no	0.24	interfacial
Alu coated	10	yes	NA	coating failure

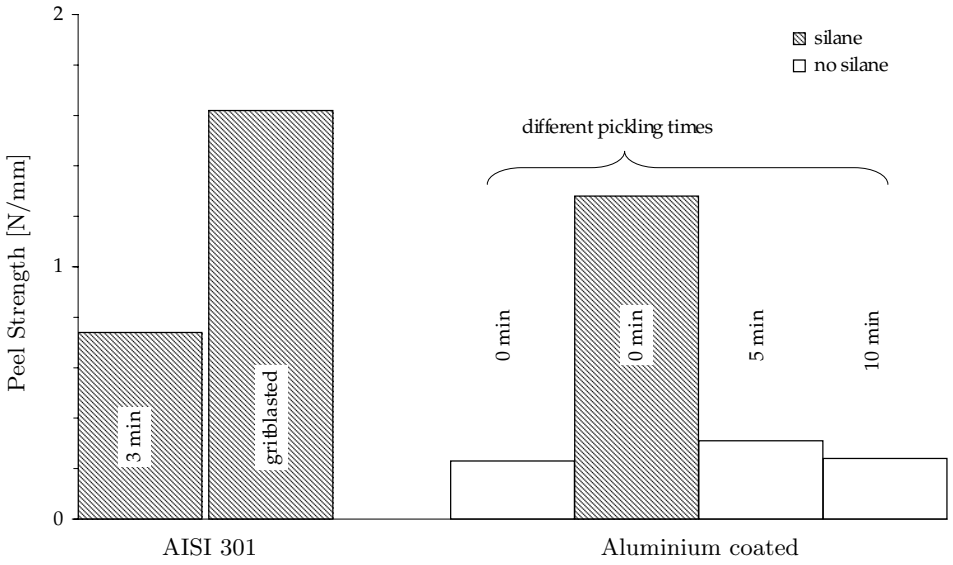

Figure 5.4: *Comparison of peel strength values for differently treated thin AISI 301 steel sheets (t=0.1 mm). The uncoated AISI 301 steel sheet was either pickled for 3 minutes or gritblasted.*

debonding is apparent already. In comparison, figure 5.5b shows a stronger interface for the thicker sheet.

Clearly gritblasting, which results in relatively high peel strength values and cohesive failure, is more effective than the chemical treatment. Moreover, for this manual process a quite reproducible surface quality was obtained, since comparable behaviour was found for several specimens. In figure 5.6 a cross section of the gritblasted sheet after the peel test is presented, which clearly shows a good interface between the stainless steel sheet and the adhesive. Further research should be conducted to see the influence of gritblasting on the mechanical properties of this thin sheet.

5.4 Conclusions

It was shown that a good initial adhesion of a common aerospace epoxy based adhesive can be obtained to molybdenum containing AISI 301 steel sheet by gritblasting it followed by a silane surface treatment. Further research should, however, be conducted to investigate the durability of this treatment. Chemical pretreatment of the AISI 301 steel sheet surface did not result in the initial adhesion level required for FML application.

Coating the stainless steel with aluminium holds considerable promise. However, in our experiments the bond strength between the aluminium layer and the steel substrate proved insufficient for thin (t=0.1 mm) AISI 301 steel sheet.

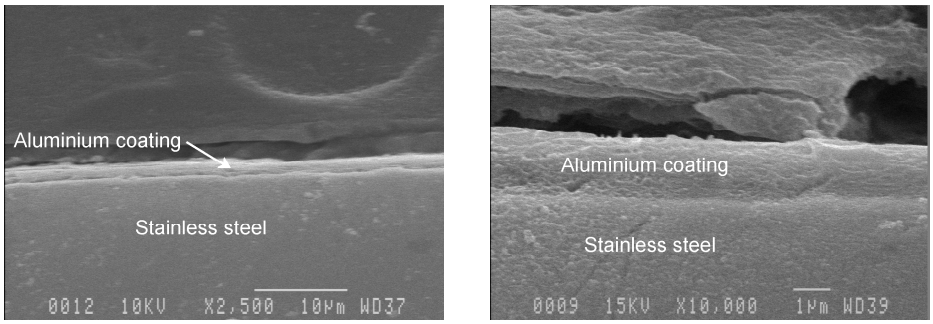

(a) **(b)**

Figure 5.5: *Cross sections of (a) thin (t=0.1 mm) and (b) thick (t=0.28 mm) aluminium coated AISI 301 steel sheets showing the interface between the coating and the substrate.*

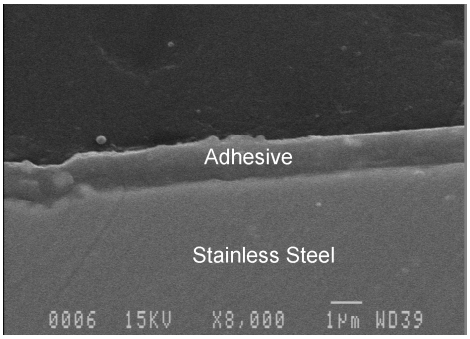

Figure 5.6: *Cross section of the gritblasted AISI 301 steel sheet after the peel test showing the interface with the adhesive.*

Chapter 6

Increasing the Bearing Strength of Glare

6.1 Introduction

The increasing use of Fibre Metal Laminates (FMLs) to replace monolithic aluminium fuselage structures is mainly driven by improved fatigue resistance and damage tolerance. Mechanical joints, with the fastener holes acting as stress concentrations, are critical fatigue locations within a fuselage. Application of FMLs at these locations results in a decrease in crack growth rates due to the crack bridging fibres within an FML.

The static strength of mechanical joints made of Fibre Metal Laminates is, however, negatively influenced in absolute numbers by the fibre content. Especially, the bearing strength of an FML is relatively low due to the fibre addition. As was discussed in chapter 3, an increased distance between fastener hole and sheet edge is necessary for GLARE to obtain sufficient bearing strength.

Also for fibre-reinforced composites the presence of fastener holes leads to high stress concentrations and hence results in a local weakness. Several ways of reinforcement have been studied for these materials. An effective way to increase the bearing strength was found to be fibre steering, where the fibres are locally directed in accordance with the principal stress trajectories. Although, the bearing strength of a CFRP was increased up to 36% with this procedure [60], the costs and the reparability of this production process restrict large scale applicability. A different method to increase the strength of bolted composite joints is by bonding a metallic insert to the surface of the hole to redistribute the bolt load over the full hole circumference. Due to early adhesive failure at the interface between the hole and the insert this method was found to have a negligible influence [61, 62]. In comparison, local reinforcement by means of interlaminar titanium strips was shown to result in a significant increase in bearing and joint strength for a CFRP laminate as has been studied by Fink et al. [63].

In this chapter a comparable principle is used to improve the bearing characteristics of GLARE. Thin stainless steel strips are in this case added within several GLARE laminates as is outlined in the next section. Subsequently, a description of the experimental setup is given, which includes both pin and bolt loading. These experiments are then used as a validation for two FE models for pin and bolt bearing strength prediction, respectively.

6.2 Methods

6.2.1 Experimental Setup

The bearing strength of a material can either be evaluated with or without lateral restraint of the specimen near the hole. The pin bearing test without lateral clamping [38] is generally used for monolithic metal sheet. Application of this test method to laminated materials, leads to delamination and premature failure due to insufficient clamping. The bolt loading setup [39] with a finger-tight bolt, is therefore used for these materials. For real aircraft structures the application of a torqued bolt or a squeezed rivet results in lateral restraint close to the bolt loading condition. Nevertheless, since both test methods provide insight into the bearing behaviour, they were both applied to several steel reinforced GLARE specimens.

The evaluated steel reinforced GLARE laminates are modifications of standard GLARE 2-2/1-0.3 and GLARE 3-3/2-0.3 laminates. A standard GLARE 2-2/1-0.3 lay-up consists of two aluminium sheets, each one with a thickness of 0.3 mm, and two, 0.127 mm thick, unidirectional glass fibre layers. This laminate was reinforced with one stainless steel strip at the sheet edge in between the two fibre layers as indicated in figure 6.1a. The fibres were either oriented along the aluminium rolling direction (a standard GLARE 2A laminate) or perpendicular to the aluminium rolling direction (a so-called GLARE 2B laminate). Furthermore, the standard GLARE 3-3/2-0.3 laminate, which consists of three aluminium sheets of 0.3 mm thickness and two crossply fibre layers of 0.25 mm thickness, was reinforced at the sheet edge with two stainless steel strips within the crossply as shown in figure 6.1b. All material was evaluated along the aluminium rolling direction.

Two different stainless steel types were used for the reinforcement strip: austenitic AISI 301 spring steel with added molybdenum with a thickness of 0.1 mm and so-called Nanoflex of 0.08 mm thickness, which is a stainless steel material with good formability. Both material types were selected based on their high specific strength properties combined with excellent fatigue characteristics. To investigate the influence of adhesion on bearing behaviour, the AISI 301 sheets were pretreated with two different methods. The first being a mechanically pretreatment by gritblasting with aluminium oxide particles. The second was a 3-minute chemical pretreatment in a sulfuric acid solution, followed by 15 minutes immersion in nitric acid to remove the residue. The effectiveness of the pretreatment was investigated in chapter 5 with a peel test, showing a better adhesion of the AISI 301 sheet after gritblasting. For the Nanoflex sheet the same chemical pretreatment was used, however with the etching period in the sulfuric acid shortened to 2 minutes.

After pretreatment, the stainless steel sheets were treated with a 1% aqueous silane solution to improve the adhesion. This was followed by application of BR-127 (an epoxy based corrosion inhibiting primer), which is also used for the aluminium sheets in GLARE to improve durability.

An important parameter for the bearing strength is the edge distance e with respect to the pin diameter (i.e. e/D), where e is defined as the distance between the centre of the hole and the sheet edge in the loading direction. Also the influence of lateral restraint, i.e. pin or bolt loading, is related to the e/D ratio. At high e/D values the pin loaded test results in lower strength than the bolt loaded test as was seen in chapter 4. Therefore the influence of edge distance ratio (e/D) was only investigated for the bolt-loaded test: for each material five e/D values were evaluated, ranging from 1.0 to 3.0. The pin bearing test was only performed at an e/D equal to 2.5.

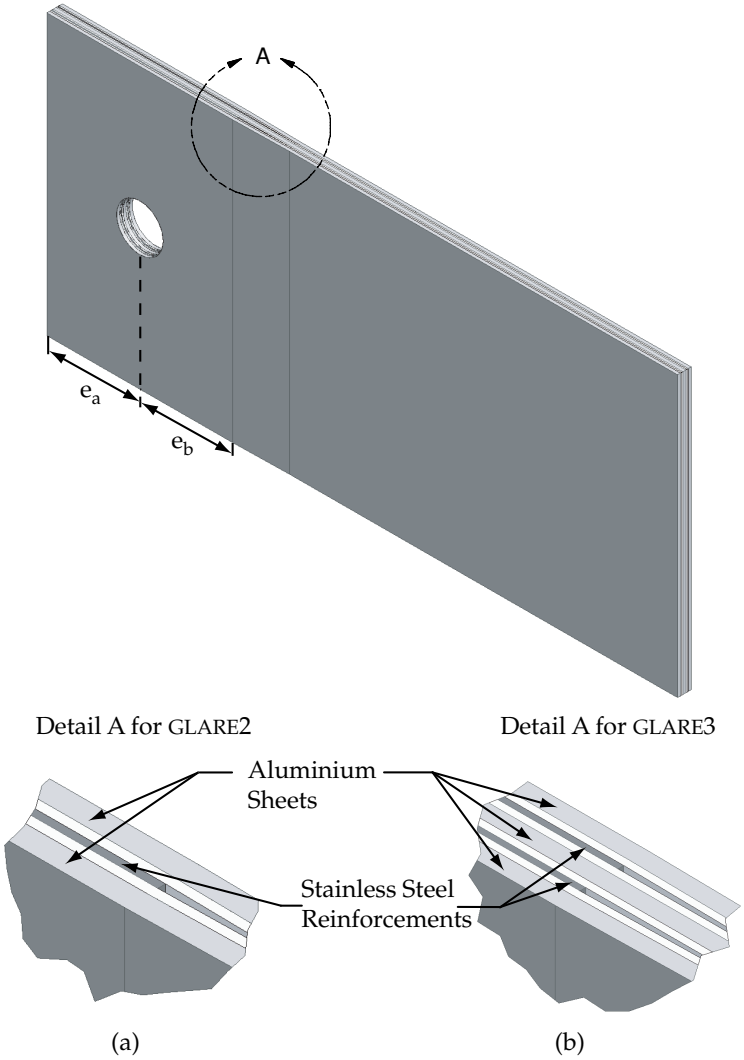

Figure 6.1: *Layout of the specimen used for bearing evaluation of steel reinforced* GLARE*, with the location of the steel reinforcement as indicated in (a) for* GLARE *2 and in (b) for* GLARE *3.*

Table 6.1: *Test matrix for all steel reinforced* GLARE *laminates.*

e/D [-]	e_a/e_b [-]	Test setup
1.0	0.5 & 1.0	bolt
1.5	0.5 & 1.0	bolt
2.0	> 1.0	bolt
2.5	> 1.0	pin & bolt
3.0	> 1.0	bolt

For e/D equal to 1.0 and 1.5 the influence of the strip width behind the hole was also analysed. The ratio of strip width ahead of the pin centre with respect to the width behind the pin centre (i.e. e_a/e_b, where e_a is equal to the edge distance e) was in this case either 0.5 or 1.0. For higher e/D values, the strip width was not expected to play a major role and therefore a relatively wide strip was used.

The test matrix for the steel reinforced GLARE laminates is shown in table 6.1. This test matrix is valid for all the GLARE laminates and reinforcement strips, except for the GLARE 2 laminates reinforced with gritblasted 301 strip. In that specific case, all but pin bearing experiments were performed.

To prevent net section failure the specimen width was equal to six times the pin diameter. Based on actual joint dimensions, a pin diameter of 4.8 mm was used. To prevent delamination during drilling of the hole, the specimens were supported with a wood backing and several increasing drill sizes were used. Final hole diameter was obtained after reaming to an H6 tolerance, which results in a clearance fit with the pin.

The specimens were loaded with a speed of 2 mm/min up to failure. For the bolt loaded specimens a so-called hysteresis loop was included after yielding to obtain the secondary bearing modulus K_s of the material. This test sequence is comparable to the static strength evaluation of mechanical joints [40], where the secondary modulus is used to obtain the joint yield strength. An extensometer was attached to the specimen to measure the local deformation between the pin and the sheet at a distance of 3.25 cm above the pin centre. These same locations were also used in the FE model to obtain the pin displacement.

Two important properties are obtained from the bearing test: (i) bearing yield (σ_{b_y}) and (ii) bearing ultimate ($\sigma_{b_{ult}}$) of the material. The bearing stress itself is defined with the following relation: $\sigma_b = P/(Dt)$ where P is the load applied and t the sheet thickness. The yield parameter is defined as the stress at a 2% permanent hole deformation, which is a definition comparable to the tensile yield. Bearing ultimate is defined as the first maximum load peak, which generally was the maximum stress reached.

6.2.2 FE Analysis

Several laminate configurations were modelled with the ABAQUS [47] FE code. A comparable model was used for the pin and bolt loaded situation, with only specific

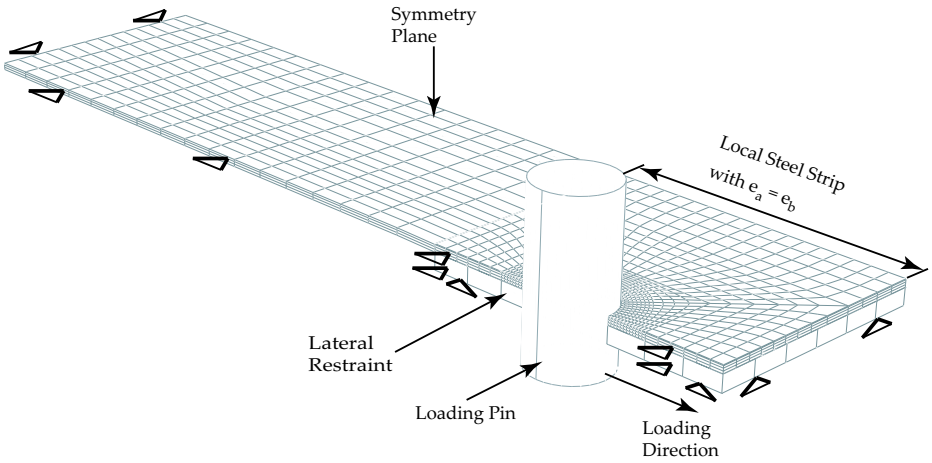

Figure 6.2: *Typical mesh for the bolt bearing strength evaluation of a steel reinforced* GLARE *2-2/1-0.4 laminate.*

changes incorporated to model the appropriate boundary conditions. To a large extent the dimensions were based on the experimentally used geometry.

To account for drilling tolerances, the hole was modelled 0.05 mm larger than the pin diameter D. The steel pin itself was assumed rigid based on its relatively higher stiffness compared to the aluminium and glass fibre layer and the thin stainless steel strip. Friction between the pin and the hole was modelled with an arbitrary constant in-plane friction coefficient μ equal to 0.1. Friction in the out-of-plane direction was not included since it prevents delamination for the pin bearing case. In comparison, this friction component does not have a large relevance for the bolt loaded FE model, since it is assumed that no delamination occurs under bolt loading as is detailed below.

The lateral restraint was included for the bolt loaded case with a rigid surface at the hole region. This surface was positioned with a gap of 0.01 mm with respect to the specimen to account for finger-tight clamping, which is never fully tight. Friction between specimen and lateral restraint was assumed to be negligible.

Based on the symmetrical lay-up of the evaluated materials and to reduce computational time, only a quarter of the full specimen was modelled. Also for the pin bearing case this decision is justified since the symmetrical buckling mode was found to be the most likely to occur as has been discussed in chapter 4.

As shown in figure 6.2, a finer mesh was used around the hole to improve the description of failure within the fibre layer and the occurrence of delamination for the pin bearing case. Element size was increased towards the clamped edge to reduce calculation time. Each material layer was modelled as a layer of eight-node linear solid elements. Only for the pin bearing case the outer aluminium ply had two elements through the thickness to improve the behaviour under outward displacement.

Delamination was only covered for the pin loaded case, since the lateral restraint should prevent delamination in the bolt loaded case. According to the results in chapter 4, delamination was found to occur mainly within the fibre layer, but close to the interface with the aluminium sheet for standard pin loaded GLARE laminates. This beha-

Table 6.2: *Overview of material properties for aluminium 2024-T3, stainless steel 301, Nanoflex and the S_2 glass fibre layer.*

Material	E_{11} [GPa]	E_{22} [GPa]	G_{12} [GPa]	ν_{12} [-]	$X_{T/C}$ [MPa]	$Y_{T/C}$ [MPa]	S [MPa]	ρ [g/cm^3]
2024-T3	72.4	72.4	27.6	0.33	725[a]	725[a]	NA	2.77
301	185.0	185.0	69.6	0.33	2000	2000	NA	7.87
Nanoflex	185.0	185.0	69.6	0.33	1400	1400	NA	7.87
S_2 glass	54.0	9.4	2.7	0.33	2429	68	75	1.98

[a] true stress value based on the assumption that the engineering stress remains constant during necking.

viour is simplified as delamination at the interface between fibre layer and metal sheets. Eight-node zero-thickness linear delamination elements were therefore implemented at all the metal-glass fibre layer interfaces, so also at the interface with the stainless steel strips.

Material Properties and Delamination Model

The material behaviour of the GLARE constituents is to a large extent already described in chapter 3, but they are summarised below for completeness. Material parameters for the different materials are given in table 6.2. It is assumed that the tensile and compressive properties are equal and that out-of-plane properties are equal to in-plane transverse properties. Furthermore, the residual stresses that occur during manufacturing of the laminates are not accounted for in the models.

Aluminium 2024-T3 is described as an isotropic material with isotropic hardening. Based on uniaxial tensile test data a trilinear true stress-strain relation was defined. In the elastic region this relationship is governed by the elastic modulus up to the yield stress of 330 MPa. The plastic behaviour is defined with a tangent stiffness equal to 1468 MPa until necking occurs at 15% strain. After necking it is assumed that the engineering stress remains constant up to 50% strain, which results in an ultimate true stress of 725 MPa. This last part is especially important for a correct bearing description since necking does not lead to immediate failure.

The plastic description of the stainless steel types is relatively simpler, since it can be modelled as ideally-plastic behaviour. The main difference between the two types is the maximum stress level, which is almost 50% higher for the 301 type.

For the glass fibre reinforced epoxy it is important to differentiate between the following intra-laminar failure mechanisms: (i) fibre failure, (ii) matrix failure and (iii) fibre-matrix shearing. The failure initiation rules used for these mechanisms are listed in table 6.3. The fibre-matrix shearing criterion is slightly changed with respect to the original definition [43], since it is assumed that it can also occur for tensile fibre stresses (i.e. $\sigma_{11} > 0$). The fibre failure and fibre-matrix shearing criterion are thus equivalent for fibre tension.

After damage initiation, the corresponding 'degraded properties' are slowly decreased to zero. After Hung et al. [32] and Schipperen [44] the following degradation factor was used to describe this decrease:

Table 6.3: *Failure initiation criteria [34, 43] for the fibre layer and corresponding degraded properties.*

Failure mode	Criterion	Degraded properties
(i) Fibre failure		
- Tensile	$\left(\frac{\sigma_{11}}{X_t}\right)^2 + \left(\frac{\sigma_{12}}{S_{xy}}\right)^2 + \left(\frac{\sigma_{13}}{S_{xz}}\right)^2 \geq 1$	E_{11}, ν_{12}, ν_{13}
- Compressive	$\frac{\sigma_{11}}{X_c} \geq 1$	
(ii) Matrix failure	$\left(\frac{\sigma_{22}}{Y}\right)^2 + \left(\frac{\sigma_{12}}{S_{xy}}\right)^2 + \left(\frac{\sigma_{23}}{S_{yz}}\right)^2 \geq 1$	E_{22}, ν_{21}, ν_{23}
(iii) Fibre-matrix shearing failure	$\left(\frac{\sigma_{11}}{X}\right)^2 + \left(\frac{\sigma_{12}}{S_{xy}}\right)^2 + \left(\frac{\sigma_{13}}{S_{xz}}\right)^2 \geq 1$	G_{12}

$$d = 1 - e^{\left(0.5 - \frac{\kappa}{\kappa_i}\right)} \tag{6.1}$$

Where κ_i and κ define the initiation and the current strain, respectively. The value of 0.5 is added to the original definition to have a slightly slower stress drop after failure initiation. It was decided to use the strain in the most dominant failure direction as relevant strain indicator. So fibre failure is related to ϵ_{11}, matrix failure to ϵ_{22} and fibre-matrix shearing to ϵ_{12}.

For the pin bearing case numerical instability was seen when the fibre failure model was combined with the delamination model and the contact conditions at the pin loaded hole. The first element row around the hole therefore has a different material model. In this case a Tsai-Hill interactive failure criterion is used, with ideally-plastic post-failure behaviour. Equal to the pin bearing description in chapter 4 a failure stress of 250 MPa perpendicular to the fibre direction and 500 MPa in the fibre direction is used for the Tsai-Hill definition.

A detailed description of the behaviour of delamination elements is given by Camanho et al. [14, 45]. To model the interface between the glass fibre layer and the aluminium or stainless steel sheet correctly, several changes were incorporated in this definition, which are described in section 4.2.1. Since the properties for the stainless steel-glass fibre interface are not available, it is assumed that they are equal to the aluminium-glass fibre interface.

6.3 Results & Discussion

A comparison between experiments and FE results for varying edge distance is given in figures 6.3-6.5. These figures show the bearing yield and bearing ultimate for 301

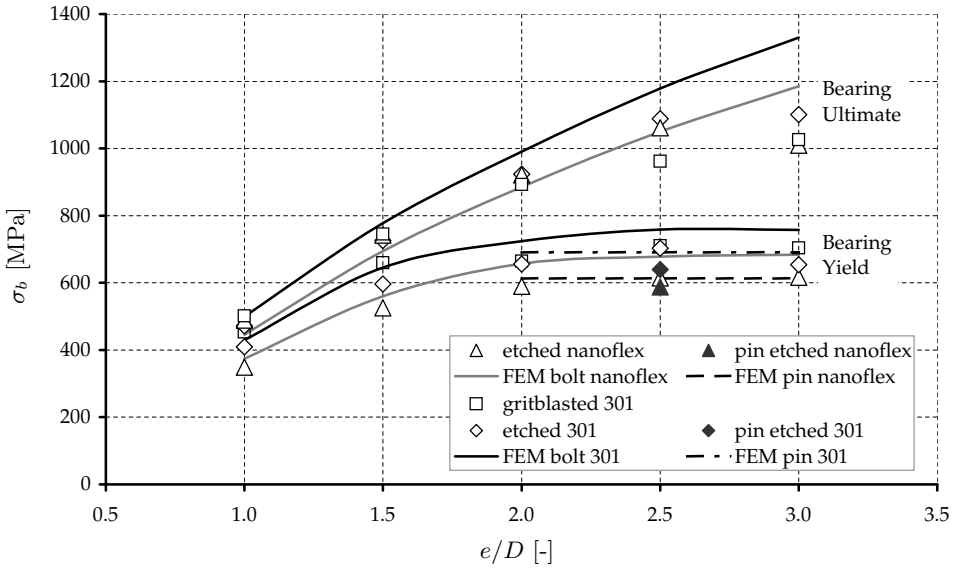

Figure 6.3: *Comparison of experimental and numerical pin and bolt bearing results for steel reinforced* GLARE *2B with varying edge distance ratio.*

and Nanoflex reinforced GLARE types for the bolt loaded case. For the pin loaded case the yield value is plotted whenever this is lower than the bearing ultimate, which was actually only the case for the GLARE 2B model. To differentiate clearly between the pin and bolt loaded results, they are addressed throughout the text as pin bearing and bolt bearing yield and ultimate, respectively.

The bolt experiments did not show any influence of the strip width ratio, i.e. e_a/e_b, and therefore the results of the different strip width ratios were simply averaged. Apparently already at a ratio of 0.5, the strip is sufficiently wide to transfer the load to the fibre and aluminium layers.

For the reinforced GLARE 2B specimens a quite good prediction of bolt bearing yield and ultimate stress is obtained. Only for high e/D the bolt bearing yield is slightly overestimated. The results for the pin loaded case, both experimentally and numerically, actually describe the bolt bearing yield much better for $e/D \geq 2.0$. The incorrect yield values in the bolt bearing case should therefore be attributed to the occurrence of delamination and correlated out-of-plane deformation of the different lamina, as was also discussed for the bolt bearing behaviour of standard GLARE in chapter 3.

As seen in the figure the experimentally obtained bolt bearing ultimate reaches a maximum at e/D equal to 2.5, while this is not seen for the FE model. This difference is related to the net section failure of most specimens, which is not included in the FE model. This failure mode occurs due to the low ultimate strain of the metal sheets. Especially, for the GLARE 2B laminates this plays a role, since all fibres are oriented perpendicular to the loading direction and, therefore, provide no loading capacity at the net section.

For the reinforced GLARE 2A, larger differences are seen between the experiments

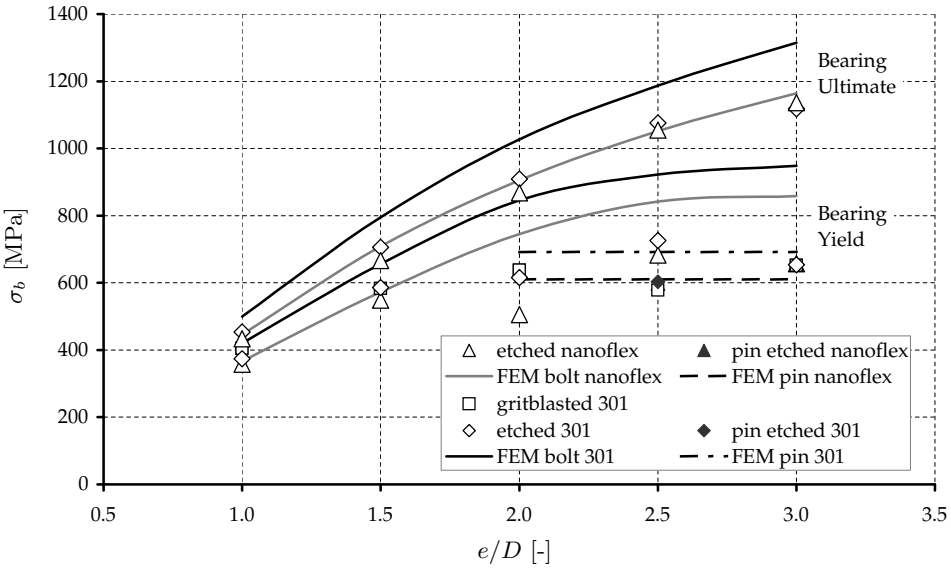

Figure 6.4: *Comparison of experimental and numerical pin and bolt bearing results for steel reinforced* GLARE *2A with varying edge distance ratio.*

and the FE model for the bolt loaded case. Especially the bolt bearing ultimate of the 301 reinforced laminates is overestimated. This was also seen for standard GLARE 2L in chapter 3 and is probably related to the occurrence of fibre (layer) splitting which decreases the load bearing capacity of the fibres when loaded in this direction. Remarkably, the model compares better with the results for the Nanoflex reinforced material.

The large difference between calculated bearing yield and measured values for the bolt loaded case of reinforced GLARE 2A shows the strong influence of delamination and buckling of the different plies. Also for reinforced GLARE 2A the calculated pin bearing results compare quite well with the bearing yield for bolt loading and the experimental pin results.

The differences between experimental and calculated bolt bearing strength are smallest for the reinforced GLARE 3 material. Only for e/D equal to 3.0 the bolt bearing ultimate for the 301 reinforced cases drops off due to net section failure. For high e/D the bolt bearing yield again is according to the calculated pin bearing results.

Actually, the GLARE 3 material is the only case where really a difference can be seen between the etched and the gritblasted 301 specimens. The gritblasted version performs better in the bolt experiments, which is possibly related to its better adhesion. However, this conclusion is not valid for the pin loaded case, where comparable results are obtained.

Even though for all cases on a global scale the predicted results differ only slightly from the experiments, on a detailed scale bigger differences are seen. Especially for high e/D values a different load versus displacement was seen, which is of course related to the buckling of plies.

A typical bearing stress versus displacement relation for the bolt loaded case is

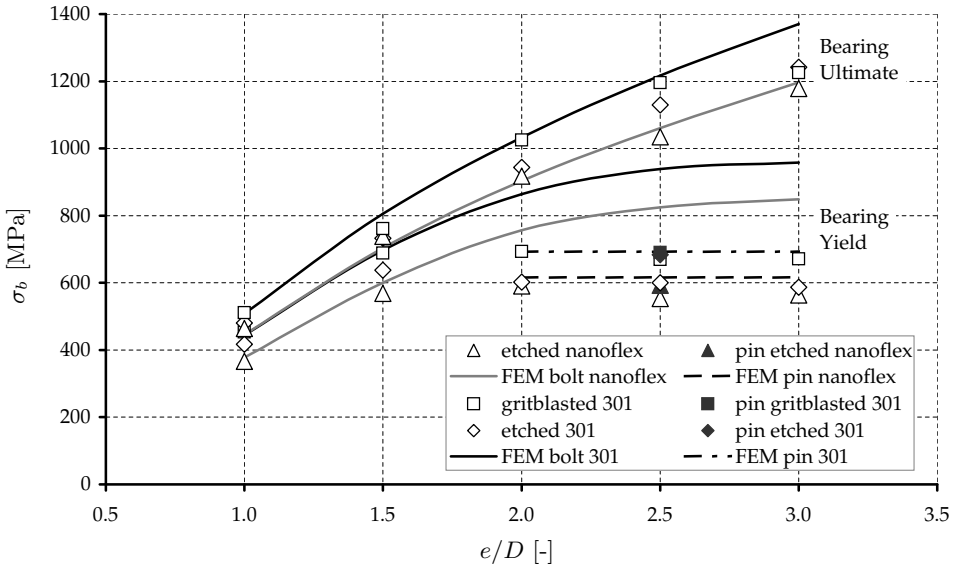

Figure 6.5: *Comparison of experimental and numerical pin and bolt bearing results for steel reinforced* GLARE *3 tested in L direction with varying edge distance ratio.*

given in figure 6.6 for two reinforced GLARE 3 laminates at e/D equal to 3.0. Both the Nanoflex and the gritblasted 301 experiments show load drops at comparable pin displacements, which are highlighted with the numbers in parentheses. Load drop *1* is the onset of the pin bearing failure mode, where the presence of the lateral restraint prevents further load decrease. Clearly, the bearing yield line (at 2% permanent hole deformation) crosses the experimental curves exactly at this first load drop and hence explains the overestimated yield point for bolt loading. Increasing the pin displacement results in another drop at point *2* followed by final failure at point *3*. A comparable behaviour was seen for almost all specimens with an $e/D \geq 2.0$. This behaviour is not seen for the FE results for bolt loading, since delamination and buckling of the plies is prevented.

The bearing stress versus pin displacement for several pin loaded laminates is given in figure 6.7. Due to the absence of lateral restraint the material fails at the first load drop, which is seen both for the experiments and the calculations. The main difference between the modelled behaviour and the experiments is the considerably lower stiffness in the elastic range. Based on the small difference in figure 6.6 for the bolt loaded specimens, this stiffness difference should be related to the absence of lateral restraint and hence the out-of-plane instability of the specimens.

The influence of edge distance (e/D) on the failure behaviour under bolt loading of GLARE 3 reinforced with gritblasted 301 was investigated with an SEM. Figures 6.8 and 6.9 show SEM micrographs taken at the hole and at the sheet edge, respectively.

Clearly, the micrographs of areas near the hole show increasing deformation with increasing edge distance. Since the cases with $e/D \geq 2.0$ had a comparable deformation shape, only the situation with an e/D of 2.0 is shown. While at e/D equal to 1.0 there

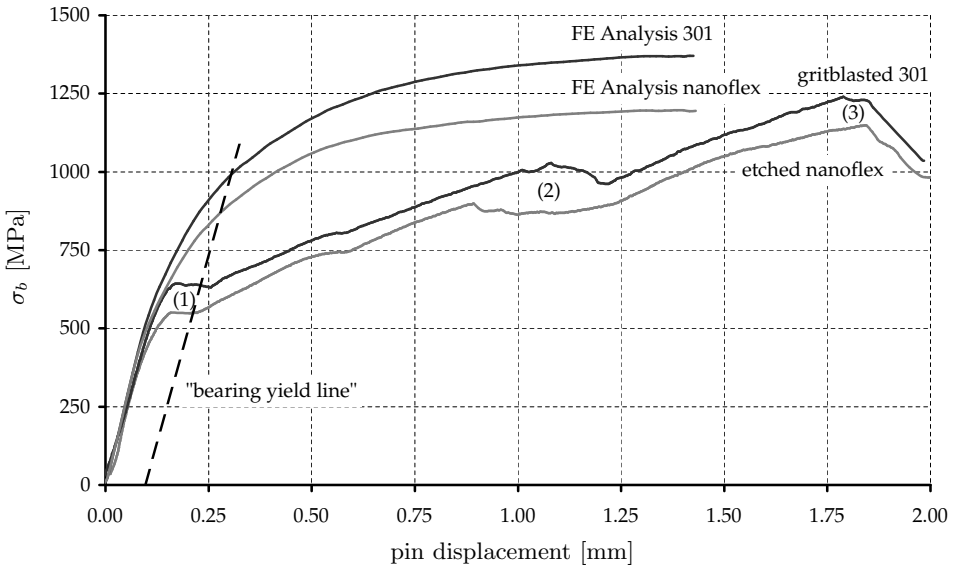

Figure 6.6: *Comparison of experimental and FE bearing stress-displacement curve for bolt loaded 301 and Nanoflex reinforced* GLARE *3 with e/D equal to 3.0. The different load drops are highlighted with numbers in parentheses.*

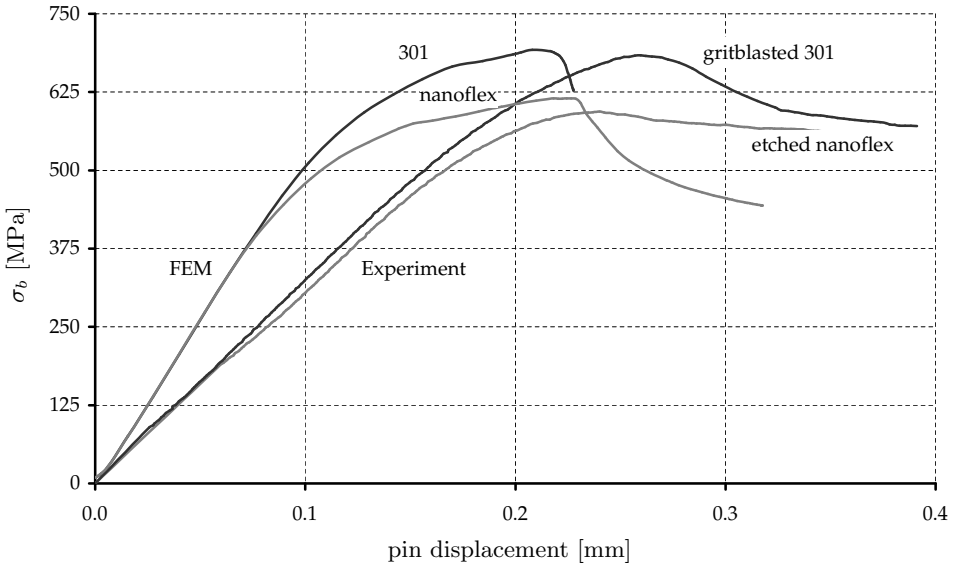

Figure 6.7: *Comparison of experimental and FE bearing stress-displacement curve for pin loaded 301 and Nanoflex reinforced* GLARE *3 with e/D equal to 2.5.*

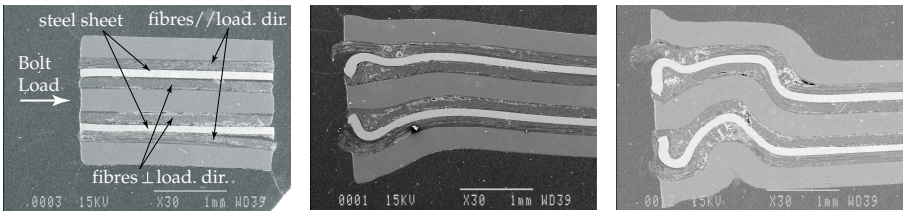

(a) e/D=1.0 **(b)** e/D=1.5 **(c)** e/D=2.0

Figure 6.8: *Deformation of the* GLARE *3-3/2-0.3 specimens with gritblasted 301 strips at different edge distance ratios obtained with the SEM at the area near the hole.*

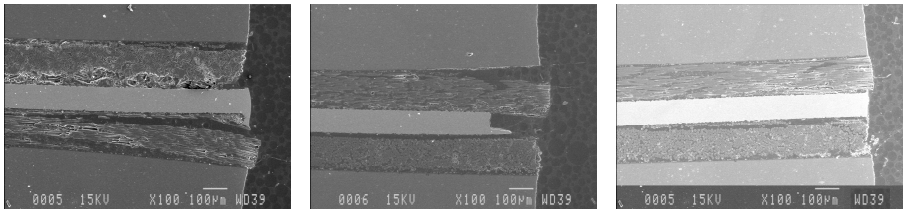

(a) e/D=1.0 **(b)** e/D=1.5 **(c)** e/D=2.0

Figure 6.9: *Deformation of the* GLARE *3-3/2-0.3 specimens with gritblasted 301 strips at different edge distance ratios obtained with the SEM at the area near the edge of the sheet.*

is almost no out-of-plane deformation, already at e/D equal to 1.5 delamination and buckling of the stainless steel strips is present. At higher edge distance the out-of-plane deformation is more severe, which should be the cause for the load drops that are seen in figure 6.6.

In comparison, the micrographs at the sheet edge show a decrease of deformation with increasing edge distance. Only for small edge distances the pin displacement results in stretching of the material at the sheet edge, while at higher edge distance the deformation is more localised around the hole. Actually, the specimens with small edge distance failed due to failure of the stainless steel strip at the sheet edge. The delamination, which is seen on the micrographs, is possibly caused by the elastic springback of the failed steel strip.

The pin loaded GLARE 3 specimens were also investigated after failure with an SEM. Since no major differences were seen between the different reinforcements, only the Nanoflex reinforced version is presented. In figure 6.10 quite big differences are seen in deformation between the experiment and the FE calculations. In the model the stainless steel strip reaches a maximum out-of-plane deformation at the edge of the hole, while in reality this maximum occurs a small distance away from the hole. Furthermore, the experiments show a high thickness increase of the fibre layer perpendicular to the load, while the model predicts delamination between this fibre layer and the stainless steel strip.

To define the effectiveness of the steel reinforcement it is important to compare it to the unreinforced GLARE case. Based on the design for minimal weight for aerospace

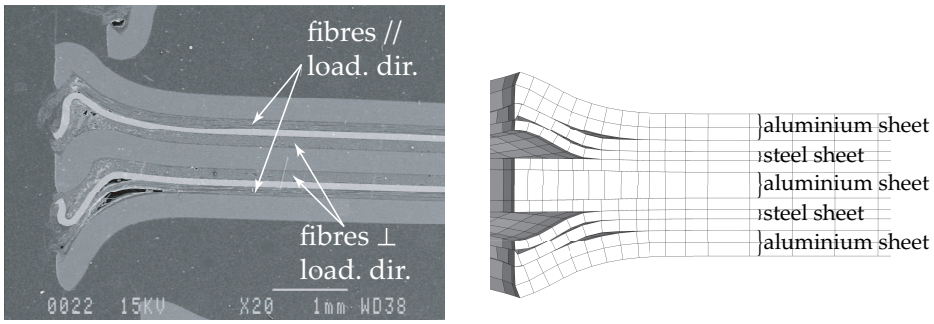

(a) *experiment* **(b)** *FE model*

Figure 6.10: *Deformation of the pin loaded specimen with etched Nanoflex: (a) obtained with the SEM, (b) according to the FE calculations.*

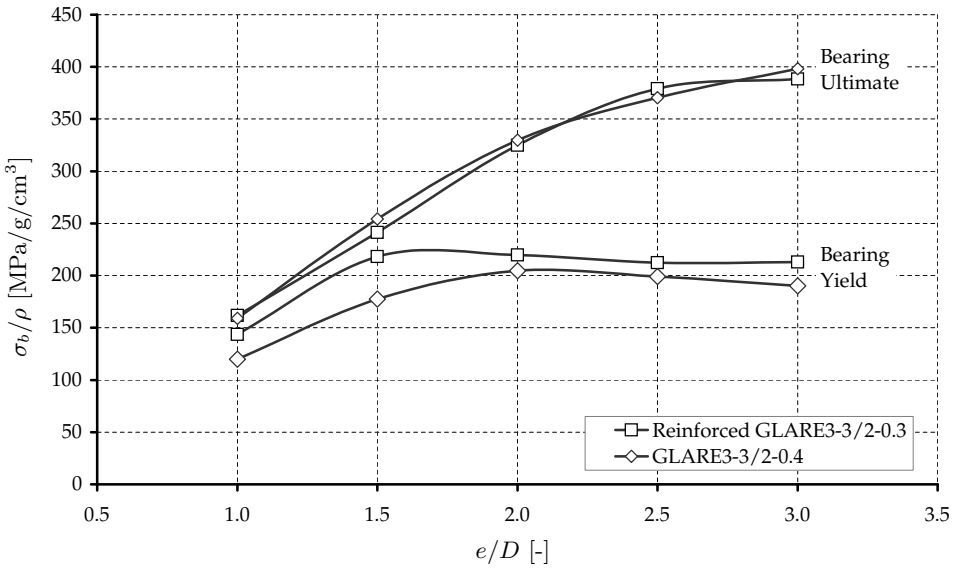

Figure 6.11: *Comparison of experimental bearing characteristics per unit weight for* GLARE *3-3/2-0.4 and gritblasted 301 reinforced* GLARE *3-3/2-0.3.*

applications, this comparison is best done on a 'per weight' basis. These specific results (i.e. per density) for the bolt loaded GLARE 3-3/2-0.3 reinforced with gritblasted 301 and standard GLARE 3-3/2-0.4 laminates taken from chapter 3 are compared in figure 6.11. Both result sets show almost identical behaviour, only for specific bolt bearing yield the influence of the stainless steel strips is clear. The specific bolt bearing yield is slightly higher and it is reached at a lower e/D value for the stainless steel reinforced GLARE type. The small difference in specific bolt bearing ultimate should be related to the low ultimate strain and hardening of the stainless steel strip.

The comparison between specific strength properties does not cover several secondary aspects. It should be kept in mind that the steel strip is a local reinforcement, which only locally results in a weight increase. Still, the specific strength comparison, shows that a comparable strength increase can be obtained with equal weight aluminium strips. These aluminium strips are, however, approximately three times thicker and result in an increase of eccentricity within a mechanical joint. This increased eccentricity has a negative effect on the fatigue behaviour of the joint, since it results in higher stress levels at the mating aluminium sheets.

6.4 Conclusions

The pin and bolt bearing behaviour of several GLARE laminates locally reinforced with thin stainless steel strips has been studied experimentally and numerically. For all GLARE variants it was found that bearing ultimate in the bolt loaded case is quite well described by the FE model. For bearing yield this is only true for low edge distance, whereas at high distance the occurrence of delamination and buckling results in an overestimation of the model. In the latter case, bearing yield under bolt loading is better captured with the numerical results for the pin bearing case.

A comparison of specific strength properties between standard GLARE and reinforced GLARE, showed only a small increase of the specific bearing yield due to the steel strip addition. While the increase was found to be negligible for the specific bearing ultimate. The thin steel strip however results in a smaller increase in eccentricity compared to thicker aluminium sheet, where a lower eccentricity is preferable for the fatigue behaviour.

Chapter 7

The Static Joint Strength and Fatigue Behaviour

7.1 Introduction

Based on the bearing strength evaluation of GLARE laminates locally reinforced with a thin stainless steel strip in chapter 6 it can be concluded that the steel reinforcement provides several interesting characteristics compared to the standard GLARE laminates. Prior to actual application in aircraft structures it is however important to investigate the static joint strength and the fatigue behaviour of this laminate configuration.

Due to the eccentric nature of mechanical joints, the loading in a joint is a combination of bearing loading and so-called fastener pull through. For aerospace applications, where the aerodynamic requirements yield the use of countersunk fasteners, the pull through failure mode plays a major role, since the countersink actually facilitates tilting and final pull through. For monolithic metal sheet, pull through is to a large extent determined by the bending stiffness, since this prevents out-of-plane deformations. This bending stiffness is less important for FMLs and other laminated materials, due to the laminated build-up where delamination and fibre and matrix failure can result in early joint failure.

To correctly capture the strength of (countersunk) joints, a good understanding of the pull through failure is a necessity. Even though numerous sources are available on the behaviour of composite joints, very few are covering the behaviour of fastener pull through [64]. According to Banbury et al. [64] the pull through failure is characterised by substantial internal damage, consisting of matrix cracking and delaminations. The static joint strength of GLARE joints has been evaluated analytically by Slagter [13, 65], covering both bearing failure and pull through failure. This analytical model will be described in this chapter and applied to a standard GLARE laminate.

Since the Fibre Metal Laminate (FML) concept and in particular GLARE was developed for fatigue critical locations it is important to investigate the effect of the stainless steel strip on the fatigue behaviour. A detailed discussion of several empirical, analytical and finite element approaches is given by Alderliesten [66] to define a fatigue model for GLARE. He concluded that the method developed by Marissen [67] and extended by Guo and Wu [68], provides sufficient basis to accurately describe the fatigue behaviour in GLARE. The main aspects in this method are (i) the analytical description of the fibre bridging stresses, (ii) the correlated delamination growth between

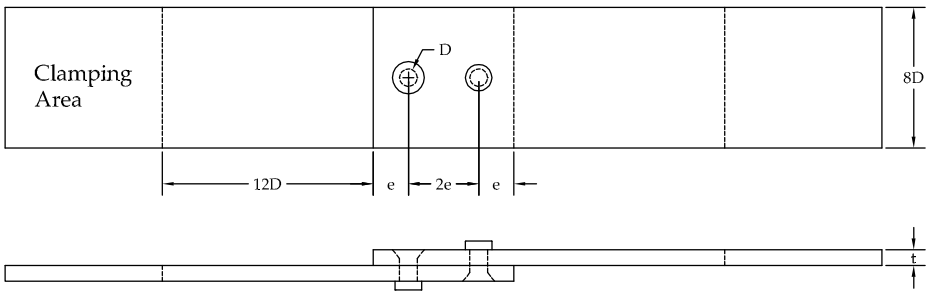

Figure 7.1: *Lay-out of the static joint specimen, which was also used for fatigue evaluation.*

aluminium and fibre layers and (iii) the crack growth in the metal layers. It is expected that the addition of a steel layer influences all these three aspects. A detailed description of the analytical model and the possible influences of the steel strip will be covered in this chapter.

The current chapter describes the experimental analysis of the static joint strength and the fatigue behaviour of standard and steel strip reinforced GLARE laminates. The static joint strength for a standard GLARE laminate and the influence of the steel strip on the fatigue behaviour are analysed analytically.

7.2 Methods

7.2.1 Experimental Setup

Static Joint Strength

The static strength of a mechanical joint is generally obtained in accordance with Military Standard 1312-4 [40]. This test standard defines a symmetrical joint with two fasteners, as shown in figure 7.1, where both fasteners are equally loaded. Even though this does not represent an actual joint configuration, still it provides the design strength for the material-fastener combination.

This test procedure was used to obtain the static strength of a standard GLARE and steel strip reinforced GLARE laminate. For the standard laminate a so-called GLARE 3-4/3-0.4 lay-up was used, which consists of four aluminium sheets of 0.4 mm thickness and three glass fibre plies of 0.254 mm thickness. The 'GLARE 3' identification defines a cross-ply fibre layer configuration, which is obtained by stacking two UD fibre layers. The steel reinforced laminate is actually a small modification of this reference laminate, since only thin stainless steel strips were added in between the cross-plied fibre layers. These steel strips were, however, only located at the joint overlap to minimise weight increase, while still improving the joint behaviour. The 'undisturbed' material is therefore the standard GLARE laminate as was described.

For the stainless steel reinforcement two different types were used. Austenitic AISI 301 spring steel with added molybdenum with a thickness of 0.1 mm and so-called Nanoflex of 0.08 mm thickness. To ensure good bonding, the AISI 301 sheet was mechanically pretreated by gritblasting with aluminium oxide particles. For the Nanoflex

sheet a 2-minute chemical pretreatment in a sulfuric acid solution was used, followed by 15 minutes immersion in nitric acid to remove the residue. The adhesion to these stainless sheets was improved by applying a 1% aqueous silane solution. Subsequently, the surface was primed with BR-127 (a corrosion inhibiting primer) to improve durability.

An important parameter for the strength of a mechanical joint is the edge distance ratio e/D of the fasteners, where e defines the distance between sheet edge and the centre of the fastener hole and D is the pin diameter. Especially the bearing strength of the joint is influenced by this parameter, as was demonstrated for both standard GLARE and steel reinforced GLARE in chapters 3 and 6, respectively. Three different edge distance ratios were evaluated for each laminate: 1.5, 2.0 and 2.5. The other dimensions were taken according to the test standard: a specimen width equal to eight times the pin diameter and sufficient specimen length.

Since fastener characteristics also play an important role, two different fastener types were used: the HL413 countersunk titanium Hi-Lok and the EN6101 D countersunk rivet. The fasteners have a comparable head and therefore they can be used to reveal the influence of fastener deformability on the joint strength. All fasteners had a diameter of 5.56 mm and the fastener holes were reamed to a clearance fit of 0 to 40 micron. The Hi-Lok fasteners were installed with an HL84 aluminium collar to a torque of approximately 3.4 Nm. The deformable rivet was heat treated prior to squeezing and then squeezed to obtain a formed head diameter approx. 1.5 times the initial rivet diameter.

The different joints were tested with displacement control up to failure, with a speed of 2 mm/min. Deformation was measured at the lap joint overlap with an extensometer, which was positioned a few millimetres ahead of the sheet edges. In accordance with the test standard the stiffness of the joint was obtained in a hysteresis loop just after passing the yield point. From this hysteresis loop the secondary modulus is obtained, which is used to obtain the yield strength of the joint.

The registered force P during loading can be expressed as joint stress with the following relation $\sigma_j = P/(Dt)$, where D is the pin diameter and t the single sheet thickness at the fastener location. Comparable to other yield parameters, the joint yield stress is defined as the stress at 2% permanent hole deformation. For a two rivet lap joint, this yield stress is the intersection between the measured joint stress curve and the secondary modulus line at an offset of $0.04D$ with respect to the origin. The strength of the joint is defined as the maximum stress level reached.

Fatigue Behaviour

Two different geometries to evaluate the fatigue behaviour were adopted: (i) the joint layout as was described in the previous section and (ii) a centre cracked tension (CCT) specimen.

Only the standard GLARE and gritblasted 301 reinforced GLARE joints described earlier were fatigued. The symmetrical layout shown in figure 7.1 was used with edge distance ratio equal to 2.0 and using countersunk Hi-Lok HL413 fasteners.

For each configuration two joints were investigated at a stress level of 80 MPa and stress ratio R equal to 0.05. This number of specimens is not enough to fully account for the amount of scatter that especially occurs in fatigue initiation. Still it is expected that enough data are obtained to crudely define trends in the fatigue behaviour. Based on an initial investigation, the joints were fatigued to no more than 100,000 cycles to prevent the crack tip to reach the specimen edges. Since cracks typically grow at the mating surface in a bolted joint, it was not possible to monitor the crack growth

Table 7.1: *Test matrix for the fatigue evaluation of standard and steel reinforced* GLARE *laminates.*

Type	Material	σ_{max} [MPa]	R [-]	N_{max} [-]
CCT	GLARE 2-2/1-0.3	120	0.05	175,000
	GLARE 3-3/2-0.3	100	0.05	175,000
Joint	GLARE 3-4/3-0.4	80	0.05	100,000

visually during testing. Only final crack length was obtained by disassembly of the joints. To investigate cracks in subsurface metal plies the laminates were heated up to decomposition.

The CCT specimen used contains a centre hole with two saw cuts perpendicular to the loading direction. Due to the presence of an initial crack, fatigue crack growth is covered with this layout. Two different steel reinforced laminate configurations were analysed for fatigue crack growth: GLARE 2-2/1-0.3 and GLARE 3-3/2-0.3.

The GLARE 2 lay-up consists of two aluminium sheets, each one with a thickness of 0.3 mm, and two, 0.127 mm thick, unidirectional glass fibre layers. In between the two fibre layers a thin stainless steel strip was used as reinforcement at the centre crack region, extending 50 mm above and below the crack. This results in a local reinforcement comparable to the bolted joint case from the previous section. The GLARE 3 laminate, with three aluminium plies of 0.3 mm thickness and two 0.25 mm thick cross ply fibre layers, was reinforced in an equal manner in between the fibre layers. All material was evaluated along the aluminium rolling direction, which for the GLARE 3 case means that the outer fibre layers are oriented in the loading direction and for GLARE 2 this applies to all fibre layers.

As for the static joint strength, AISI 301 and Nanoflex steel sheet was investigated as reinforcement material for the GLARE 3 laminate. To investigate the influence of adhesion, the 301 sheet was also pretreated with the sulfuric acid treatment, however with the etching period lengthened to 3 minutes. As was described in chapter 5 grit-blasting results in a better adhesion for AISI 301 than this treatment. For the GLARE 2-2/1-0.3 configuration, only the influence of gritblasted 301 sheet was analysed. For all cases, the adhesion and durability was improved with the application of silane and the BR-127 primer.

For each configuration only one CCT specimen was investigated with a width of 80 mm. The use of a single specimen is justified based on the stable crack growth that GLARE typically has, causing rather low scatter. The specimens were loaded up to 175,000 cycles with a stress level of 100 MPa for the GLARE 3 lay-up and 120 MPa for the GLARE 2 case, with R equal to 0.05 in both cases.

The crack extension under fatigue loading was measured visually with a computer-controlled camera. For the actual visual measurements the fatigue cycle was stopped and the specimen was loaded to the maximum stress level to obtain full crack opening. After fatigue loading the laminates were also heated up to decomposition to measure the subsurface crack lengths.

7.2.2 Static Joint Strength Analysis

Model Description

To predict the strength of a mechanical joint, which connects two equal Fibre Metal Laminates, the analytical model as defined by Slagter [13] can be used. The model is capable of describing the elastic and plastic behaviour up to failure and it can predict whether the failure mode is bearing or pull-through.

A rather simple representation of the bearing behaviour of a pin-loaded hole is obtained with a circular cylindrical beam resting on an elastic foundation. The material is in this case represented with an infinite set of parallel springs, which have a spring constant equal to K. The strain energy of this so-called Winkler foundation is given by:

$$U_{s,f} = \frac{1}{2} \sum_{i=1}^{2n_{met}-1} \int_{z_{i-1}}^{z_i} K_i v^2 dz \tag{7.1}$$

Where z defines the through-the-thickness coordinate of the different layers, n_{met} the total amount of metal layers and v is the total fastener deflection. The value of the foundation stiffness K was approximated with an FE model for an isotropic pin-loaded specimen. It was found that K is a function of the edge and width distance ratios, i.e. e/D and W/D, of the specimen and the Young's modulus of the material.

The Winkler foundation covers normal forces only, where typically also shear forces should be accounted for. The correlated shear strain energy depends on the average through-the-thickness shear modulus of the laminate $\bar{G}$ and the equivalent shear area affected by the shear deformation $\bar{A}_e$. Due to fastener tilting, bearing of the pin in a lap joint occurs in two opposite directions and therefore two different equivalent shear areas are involved. The through-the-thickness coordinate at which the sign shifts is defined by Λ, which for a lap joint is equal to $\frac{1}{3}t_{lam}$. The shear strain energy of the foundation consists of the following two parts:

$$U_{ss,f} = \frac{1}{2}\bar{G}\bar{A}_e^{(1)}\Lambda \left\{ \left[\frac{dv}{dz}^{(1)} \right]^2 \right\}_{av} + \frac{1}{2}\bar{G}\bar{A}_e^{(2)}(t_{lam} - \Lambda) \left\{ \left[\frac{dv}{dz}^{(2)} \right]^2 \right\}_{av} \tag{7.2}$$

The total deflection of a fastener in a joint can be expressed as the sum of the partial deflections due to bending and shearing. Furthermore it can be assumed that the total and partial deflections can be described as a second-order polynomial, which yields the following relation:

$$v = v_b + v_s = C_1 + C_2 z + C_3 z^2 \tag{7.3}$$

The strain energy due to bending and due to shearing of the pin are then given by:

$$U_{sb,p} = \frac{E_p I_p}{2} \int_0^t \left[\frac{\partial^2 v_b}{\partial z^2} \right]^2 dz \tag{7.4}$$

$$U_{ss,p} = \frac{\lambda_s G_p A_p}{2} \int_0^t \left[\frac{\partial v_s}{\partial z} \right]^2 dz \tag{7.5}$$

Where E_p is the Young's modulus of the pin, I_p the moment of inertia, G_p the shear modulus, A_p the cross-sectional area and λ_s is the shear coefficient to account for the circular pin shape.

The final energy component is the potential energy of the shear load P, which acts at the mating surface, so at z-coordinate equal to t_{lam}:

$$U_p = -Pv(z = t_{lam}) \tag{7.6}$$

The total energy of the system is obtained by summing these five relations. Minimising the total energy with respect to the displacement coefficients results in a non-homogeneous system of linear equations:

$$\mathbf{M} \begin{bmatrix} C_1 \\ C_2 \\ C_3 \end{bmatrix} = \underline{p} \tag{7.7}$$

This system can be solved for the deflection coefficients, C_1, C_2 and C_3, since both the symmetric matrix $\mathbf{M}$ and the force vector $\underline{p}$ are known. It is hence possible to relate the displacement of the pin to the applied load.

In the elastic range the bearing behaviour of an FML can be described with the given equations. Once yielding of the metal layer occurs, which is governed by the bearing yield stress (σ_{b_y}) of the metal, it is necessary to use a plastic foundation stiffness K_{pl}. The ratio of plastic to elastic foundation stiffness is typically expressed as:

$$\kappa = \frac{K_{pl}}{K} \tag{7.8}$$

To account for internal fibre failure, also for the fibre layers a plastic foundation stiffness is used, while for simplicity it is assumed that the fibre layer *yields* at equal displacement as the metal layer.

Failure in bearing is assumed to occur whenever the bearing ultimate stress ($\sigma_{b_{ult}}$) is reached on the outer metal sheet. It is however possible that the joint shows premature failure in fastener pull through.

The pull through failure mechanism can be characterised as a deformation into a conical surface with a circular hinge line r_e. Final failure occurs when at a critical radius r_c the maximum strain of the metal sheet (ϵ_{max}) is reached in the circumferential direction. So based on this condition a limited amount of cracking can occur before failure.

It is assumed that there is no shear deformation and hence the displacement of the sheet can be captured with a linear function $w(r)$. With the boundary conditions that the displacement is zero at radius r_e and equal to w_{max} at the pin radius r_p, this displacement function is described with:

$$w(r) = \left(\frac{r_e - r}{r_e - r_p} \right) w_{max} \tag{7.9}$$

Furthermore, the metal sheet is idealised as being perfectly plastic material. Based on this assumption the radial bending moment M_{rr} reaches the yield moment on the hinge line. The energy dissipated along the circular hinge is defined as the radial bending moment times the hinge angle, which after substitution is defined by the following relation:

$$U_c = M_{pl} \left(\frac{w_{max}}{r_e - r_p} \right) 2\pi r_e \tag{7.10}$$

Where M_{pl} is the yield moment per unit width.

Within the conical surface, the loading satisfies the yield condition for combined tension and bending. Using this condition, the energy dissipated within the conical surface between the critical radius r_c and the hinge radius r_e is defined as:

$$U_s = 2\pi M_{pl} \left(\frac{r_e - r_c}{r_e - r_p} \right) w_{max} \left[1 + \frac{w_{max}^2}{48} \left(\frac{N_{pl}}{M_{pl}} \right)^2 \left(\frac{r_e - r_c}{r_e - r_p} \right)^2 \right] \tag{7.11}$$

Where N_{pl} is the limit force in simple tension per unit width.

Last component is the potential energy of the pull through load P_t, which is defined as the load times the displacement at radius r_c:

$$U_p = -P_t \left(\frac{r_e - r_c}{r_e - r_p} \right) w_{max} \tag{7.12}$$

The total energy is obtained by summing the three energy components. To obtain the pull-through load, the total energy is minimised with respect to w_{max}. The minimum pull through strength is then obtained after minimising the pull through load with respect to r_e, resulting in:

$$P_t = \pi \left(N_{pl} \sqrt{2\epsilon_{max}} r_c + 4M_{pl} \right) \tag{7.13}$$

For the yield moment M_{pl} and the limit force in simple tension N_{pl} per unit width it is assumed that the fibre layers do not contribute to the pull through strength. Then these two properties are defined as:

$$N_{pl} = n_{met} \sigma_y t_{met} \tag{7.14}$$

$$M_{pl} = \lambda \cdot \frac{1}{4} \sigma_y t_{met}^2 \tag{7.15}$$

$$\text{with } \lambda = \begin{cases} 1 + (n_{met}^2 - 1) \left(1 + \dfrac{t_{fibre}}{t_{met}} \right) & \text{if } n_{met} \text{ is odd,} \\ n_{met}^2 \left(1 + \dfrac{t_{fibre}}{t_{met}} \right) & \text{if } n_{met} \text{ is even.} \end{cases} \tag{7.16}$$

The derivation of the pull through strength is based on a load acting perpendicular to the sheet. To obtain the strength of a lap joint at which pull through failure occurs, it is necessary to decompose the applied load into a perpendicular component and a bearing component along the sheet. It is assumed that this bearing component is equal to the joint yield strength as obtained with the bearing evaluation. The model is developed for protruding fasteners, where in the case of a countersink a reduction factor of 0.8 should be used [65].

Model Application

The analytical model will only be used to calculate the joint strength of the standard GLARE laminates, since the bearing characteristics of the steel reinforcements are not known. The model is used to investigate the influence of edge distance and of fastener type, i.e. Hi-Lok or rivet. The main difference between these two types is the presence of an interference fit for the rivet due to squeezing, which has a positive effect on the bearing yield stress of the metal.

The input parameters for the model are listed in table 7.2. The bearing yield and ultimate stress as a function of edge distance ratio e/D are taken from the aluminium bolt bearing experiments as described in chapter 3. The bearing strain hardening ratio and the critical radius for pull through are taken from the original model.

Table 7.2: *Input parameters used for the static joint strength prediction.*

Description	Symbolic	Value
Bearing Parameters		
Yield stress	σ_{b_y}	
for $e/D = 1.5$		516 MPa
for $e/D = 2.0$		640 MPa
for $e/D = 2.5$		677 MPa
Ultimate stress	$\sigma_{b_{ult}}$	
for $e/D = 1.5$		791 MPa
for $e/D = 2.0$		1018 MPa
for $e/D = 2.5$		1188 MPa
Bearing strain hardening ratio	κ	0.1
Rivet Pull Through Parameters		
Yield stress	σ_y	330 MPa
Maximum (aluminium) strain	ϵ_{max}	15%
Critical radius	r_c	5.6 mm

7.2.3 Fatigue Crack Growth Analysis

Model Description

The fatigue crack growth in Fibre Metal Laminates can be predicted with the analytical model defined by Alderliesten [66], which is defined below. This model is based on the assumption, originally made by Marissen [67], that the crack growth is defined by the stress intensity at the crack tip in the metal layer. This stress intensity consists of a crack opening component due to the far field metal stresses and a crack closing component due to the bridging stresses in the fibre layers:

$$K_{tip} = K_{ff} + K_{br} \tag{7.17}$$

The first, far field, component follows from the standard solution for a cracked monolithic metal sheet. More complicated is the second (bridging) component, which requires knowledge of the fibre bridging stress distribution and the delamination zone at the interface between metal and fibre layers. The bridging stress itself is, however, also related to the delamination zone.

For a given delamination zone it is, however, possible to obtain the bridging stress, when focussing on the crack opening of a fatigue crack in GLARE. This crack opening at any location x along the crack can be written as:

$$v(x) = v_\infty(x) - v_{br}(x) \tag{7.18}$$

Where v_∞ defines the standard solution for the crack opening in a cracked monolithic metal sheet due to the far field stresses. And v_{br} the crack closing component due to the bridging stress, which was derived based on several standard solutions for crack opening due to point loads.

The crack opening can also be described by the deformation of the fibres over the

delamination length:

$$v(x) = \delta_s(x) + \delta_e(x) \tag{7.19}$$

Where δ_s defines the shear deformation of the fibre layer due to stress redistribution from the aluminium sheet to the fibre layer, while δ_e denotes the fibre elongation due to far field fibre stress ($S_f f$) and bridging stress (S_{br}) as a function of delamination height b:

$$\delta_e(x) = \frac{S_{ff} + S_{br}(x)}{E_{FRP}} b(x) \tag{7.20}$$

The bridging stress can be obtained by equalling equations 7.18 and 7.19. After substitution of equation 7.20 and rewriting, the following relation is obtained:

$$v_\infty(x) - \delta_s(x) - \frac{S_{ff}}{E_{FRP}} b(x) = \left[\frac{b(x)}{E_{FRP}} + \frac{v_{br}(x)}{S_{br}(x)} \right] S_{br}(x) \tag{7.21}$$

This relation can be solved numerically for the bridging stress when the crack geometry is divided into equal width segments. The sum of the bridging stress acting over the segment is assumed to act at the centre of such a segment (or so-called bar element). Delamination height and crack opening are also defined at the segment centres.

From the calculated bridging stress it is now possible to obtain the stress intensity at the crack tip and hence the crack growth in the metal layer. The crack growth rate da/dN in the aluminium sheet is defined by the following Paris relation:

$$\frac{da}{dN} = C_{cg} \Delta K_{eff}^{n_{cg}} \tag{7.22}$$

Where ΔK_{eff} is the effective stress intensity range, which corrects for the stress ratio R. For thin aluminium sheets this stress ratio correction was defined empirically as:

$$\Delta K_{eff} = (1 - R^{1.35}) K_{tip} \tag{7.23}$$

Next to crack growth in the metal layer it is also important to calculate the delamination growth, since this defines the new delamination zone. Based on experiments on GLARE laminates it was concluded that the delamination growth db/dN can be described with the following Paris relation:

$$\frac{db}{dN} = C_d \left(\sqrt{G_{d,max}} - \sqrt{G_{d,min}} \right)^{n_d} \tag{7.24}$$

Where G_d defines the energy release rate at the interface between fibre and metal layer, which is depending on the bridging stress S_{br}.

For a given crack length and initial delamination zone, the model can predict the rate of growth of both the crack and the delamination zone in an iterative process.

Model Application

The fatigue crack growth model as described in the previous section cannot be directly used for the analysis of steel reinforced GLARE. This is due to the fact that the model assumes equal crack length in all metal layers as well as equal material properties. Furthermore, it should be expected that the steel strip has different crack growth characteristics than the aluminium sheet.

Table 7.3: *Input parameters used for the crack growth prediction method.*

Description	Symbolic	Value
Crack growth parameters:		
Half saw cut length	a_s	2.5 mm
Initial (half) crack length	a_0	3.0 mm
Paris law constants	C_{cg}	$2.17{\cdot}10^{-12}$
	n_{cg}	2.94
Delamination parameters:		
Initial shape		parabolic
Paris law constants	C_d	0.05
	n_d	7.5

The model can however be modified to obtain an approximation for the steel influence. Three different modifications were analysed, which are detailed below. In all three cases shear deformation was excluded from the crack opening in equation 7.19. The definition given by Alderliesten [66] is not applicable to the current laminate configuration and more importantly the component is so small that it can be omitted. For all three cases the default input parameters from table 7.3 are used.

An upper bound for the crack growth rate of the steel reinforced GLARE is obtained when it is assumed that the steel sheet does not carry any load. This actually means it is fully cracked at the location of the crack in the aluminium sheet. In this case it is not expected that delamination occurs at the interface with the steel sheet. Furthermore the influence of curing stresses due to the steel strip is expected to be negligible. For this situation the crack growth rate can be calculated by modelling the GLARE laminate without reinforcement, while the applied stress is based on the actual thickness.

In comparison, a lower bound for the crack growth rate is obtained when the steel layer does not crack. To include this extra bridging component, the steel layer properties are *mixed* with the fibre layer properties. Also in this case no extra delamination zone is created.

To capture the influence of the steel layer more accurately it can be modelled as an equivalent aluminium ply. Based on the steel stiffness E_{st} and the aluminium stiffness E_{alu} this equivalent thickness is:

$$t_{alu\ equi} = t_{st}\frac{E_{st}}{E_{alu}} \tag{7.25}$$

Where t_{st} is the actual steel thickness. It is assumed that this equivalent aluminium ply has equal crack growth characteristics to an actual aluminium ply. With this modification, the modelled thickness differs from the actual thickness and the stress level should be adapted accordingly. Due to the presence of a crack in the steel sheet, delamination also occurs at the steel interface. It is assumed that delamination does not occur for fibres perpendicular to the load, since they do not have any crack bridging capability. For the delamination growth between the steel strip and the fibre layer it is assumed that this is equal to the standard GLARE solution.

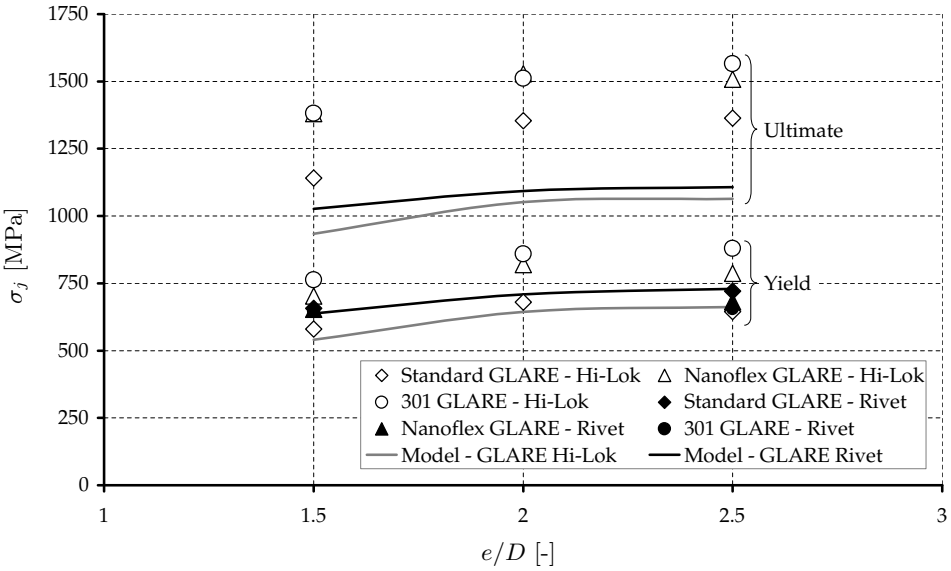

Figure 7.2: *Comparison of experimental joint strength for standard and steel reinforced* GLARE *3-4/3-0.4. For the standard* GLARE *laminates the calculated strength is also given.*

7.3 Results & Discussion

7.3.1 Static Joint Strength

The yield and ultimate stress of the standard GLARE and steel reinforced GLARE joints are given in figure 7.2 as a function of e/D. The ultimate values for the rivetted joints are not included since these joints all failed in fastener shank failure. Clearly the stainless steel reinforced joints have higher properties than the GLARE joints, which is of course related to the higher strength of these strips. Furthermore, the 301 stainless sheet has a higher tensile yield point than the Nanoflex material and hence also a higher yield for the joint.

For the rivetted case, the stiff stainless steel strip seems to have a minimal influence on the yield stress, since comparable yield values were obtained for the standard and steel reinforced GLARE laminate configurations. Apparently the squeezing process has little influence on the bearing yield stress of the steel strip, which is probably related to a larger stiffness difference. Still the squeezing process results in better hole filling, since for all the riveted joints it was seen that the secondary modulus was smaller than the primary modulus (i.e. the stiffness of the initial elastic region), while for the Hi-Loks the opposite was seen.

From the comparison between experimental and calculated GLARE results it can be seen that the joint yield strength is predicted almost perfectly for both fastener types. The difference for the ultimate strength with Hi-Loks installed is however quite large. Since the model predicted the correct failure mode for the different edge distance ratios, both bearing behaviour and pull through strength are not correctly captured for this

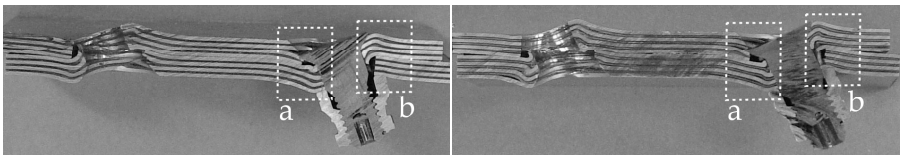

(a) GLARE **(b)** *Reinforced* GLARE

Figure 7.3: *Cross-sections half-way the joint width of the (a)* GLARE *and (b) steel reinforced* GLARE *joints with an e/D equal to 2.5, showing fastener tilting and deformation after joint failure. Indicated with rectangles are the regions, where more detailed SEM micrographs were obtained.*

laminate.

Two different failure modes were seen for the joints with Hi-Loks, which are related to the edge distance (e/D). At e/D equal to 1.5 failure was mainly due to bearing, while at higher e/D fastener pull-through was the dominant failure mode. This pull-through failure is caused by the tilting of the fastener, which results in a tensile load along the shank direction that pulls the fastener through the sheet. Figure 7.3 shows a cross-section of the standard GLARE and reinforced GLARE joints, with one fastener still installed. Clearly the tilting of the fastener and correlated pull through is easy to discern.

The specific properties, i.e. per density (where the density is based on the reinforced location for the steel reinforced GLARE), as given in figure 7.4 show that on a weight basis the GLARE joints generally have a higher ultimate stress than the steel reinforced ones. Only for e/D equal to 1.5 the specific results are comparable for all cases. As stated above, for higher e/D values the failure mode is mainly fastener pull-through and then the steel plies have much less influence. The bending stiffness of the plies and the adhesion between the different layers then play a major role.

The comparison on specific strength properties omits the aspect of local reinforcement, which only locally results in a weight increase. The influence of the steel strip weight is minimal when applied in an actual aircraft sheet, while it still has a positive influence on joint strength.

To obtain more insight into the failure behaviour of the two joint types with countersunk Hi-Loks, cross-sections were made at the joint centre (so a cut through the centre of the joint holes) for e/D equal to 1.5 and 2.5. These cross-sections were investigated with the SEM at location 'a' and 'b' from figure 7.3. For the countersunk sheet, locations 'a' and 'b' can best be characterised as the pull through and bearing side of the joint, while location 'a' is the bearing side for the non-countersunk sheet. It should be noted that the relative position of the sheets in the SEM micrographs is a reconstruction, since the fastener was too loose to keep the sheets in place.

The bearing failure is especially apparent at the sheet edge for small e/D in figures 7.5b and 7.5d, where the material is pushed outwards due to the fastener load. This results in fibre layer failure and delamination. A comparable failure patterns was also seen for bearing loading of steel reinforced GLARE in chapter 6. The damage at the sheet edge is less severe for the steel reinforced GLARE than for the standard GLARE. At the other side of the hole, figures 7.5a and 7.5c, the damage is comparable.

For a larger edge distance, the influence of the fastener load is localised around the hole and no damage was seen at the sheet edge. The micrographs show that

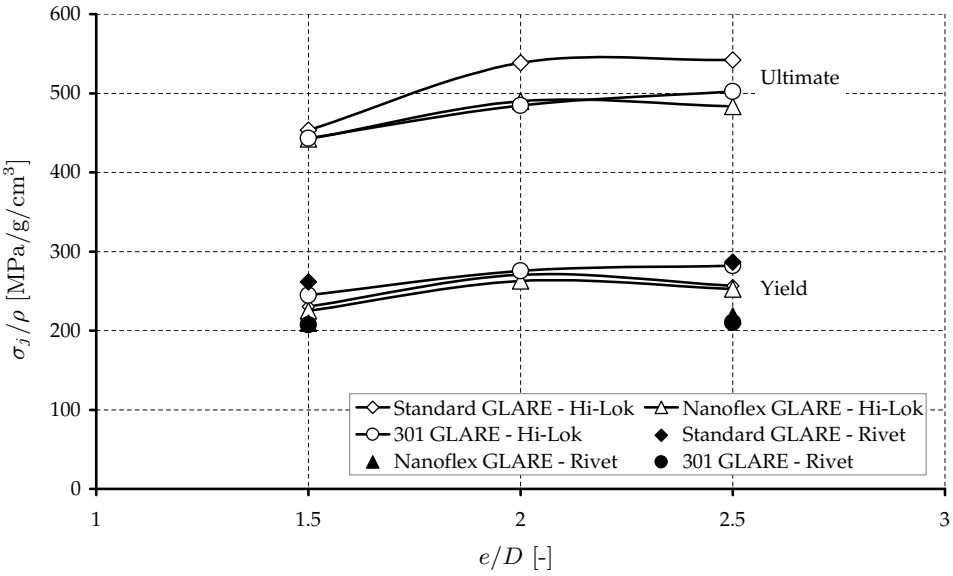

Figure 7.4: *Comparison of experimental joint strength per unit weight for standard and steel reinforced* GLARE *3-4/3-0.4.*

delamination plays a major role for failure of both laminates at higher e/D. This illustrates why the stainless steel version performs worst on a specific strength basis.

7.3.2 Fatigue Behaviour

Joints

For all fatigued joints it was seen that the cracks start from the mating sheet at the fatigue critical side, which is typically the side without a local free edge since it experiences more bending. For the tested joints, due to the symmetrical build-up, this is equivalent to crack growth at the non-countersunk side.

The (subsurface) crack investigation only revealed cracks in the mating aluminium sheets for the GLARE joints, while the steel reinforced joints also had subsurface cracks as seen in table 7.4. Especially, specimen 1 has *deeper* crack growth, which should be attributed to incorrect fastener clamping since it had crack initiation at the horizontal centre line of the hole. For all other specimens cracks initiated above the hole, followed by sideways crack growth towards the horizontal centreline of the hole. The different crack location for specimen 1 causes cracks to grow earlier/faster in the subsequent layers, since these typically also initiate at the horizontal centre line.

Although the GLARE joints only had cracks in the mating sheet, still these cracks were longer than for the steel reinforced joints. The increased eccentricity due to the steel addition is apparently counterbalanced by the higher stiffness of the steel plies. This causes a decrease in the actual loading of the aluminium plies, causing lower crack growth rates for the aluminium, but a correlated increase in crack growth for the steel layers.

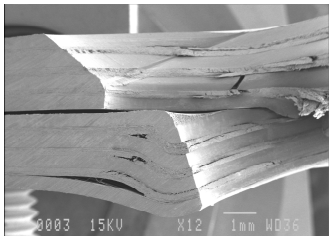

(a) *location 'a' for* GLARE

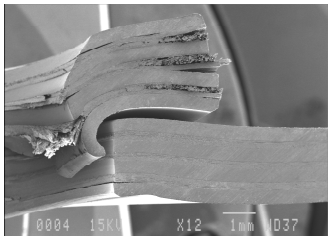

(b) *location 'b' for* GLARE

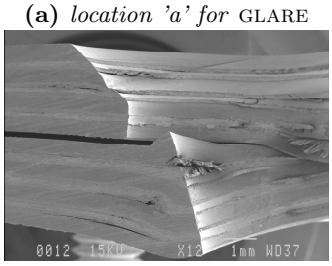

(c) *location 'a' for steel reinforced* GLARE

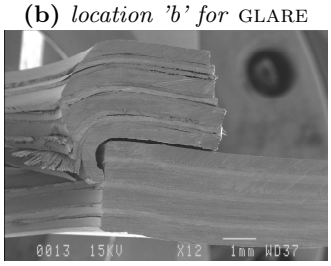

(d) *location 'b' for steel reinforced* GLARE

Figure 7.5: *Deformation at failure of the standard and steel reinforced* GLARE *joints at e/D=1.5 obtained with the SEM at location (a) and (b) from figure 7.3.*

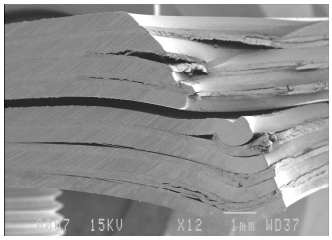

(a) *location 'a' for* GLARE

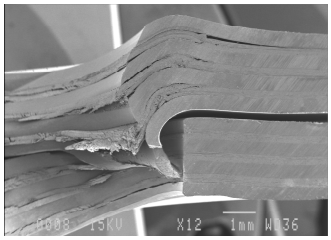

(b) *location 'b' for* GLARE

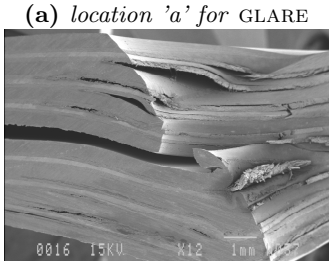

(c) *location 'a' for steel reinforced* GLARE

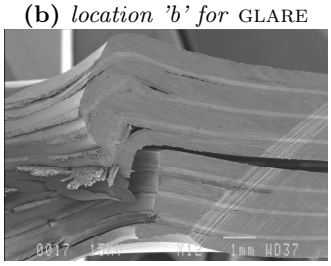

(d) *location 'b' for steel reinforced* GLARE

Figure 7.6: *Deformation at failure of the standard and steel reinforced* GLARE *joints at e/D=2.5 obtained with the SEM at location 'a' and 'b' from figure 7.3.*

Table 7.4: *Measured crack lengths in the different layers of the steel reinforced and standard* GLARE *3-4/3-0.4 joints after 100,000 cycles.*

Material	No.	Layer	$2a$ [mm]	a_{left} [mm]	a_{right} [mm]
Steel Reinforced GLARE	1A	(1) aluminium	18.5		
		(2) steel	-	4.7	4.0
		(3) aluminium	-	4.6	2.9
		(4) steel	-	2.6	3.2
	1B	(1) aluminium	21.8		
		(2) steel	-	5.9	5.4
		(3) aluminium	-	7.1	5.3
		(4) steel	-	3.4	4.3
	2A	(1) aluminium	19.7		
		(2) steel	-	3.9	2.9
	2B	(1) aluminium	20.1		
		(2) steel	-	2.3	0.0
Standard GLARE	3A	(1) aluminium	26.1		
	3B	(1) aluminium	27.6		
	4A	(1) aluminium	23.3		
	4B	(1) aluminium	23.5		

Centre Cracked Tension Specimen

The measured crack growth for GLARE 2L is compared in figure 7.7 with the calculated crack growth with the assumptions that the steel layer is either fully cracked, fully bridging or replaced by an equivalent aluminium sheet. It is seen that the experimental results are in between the calculated ones, having faster crack growth than the aluminium equivalent calculation.

The results in table 7.5, which show the crack lengths in the different layers after 175,000 cycles, indicate that the steel layer has smaller cracks and thus slower crack growth than the aluminium plies. Based on this observation it is expected that the calculation with an equivalent aluminium ply actually overestimates the experimental behaviour. The smaller crack length can however be caused by improved bridging of the inner (steel) ply compared to the outer aluminium sheets due to the bridging fibres on both sheet sides in the GLARE 2 lay-up.

It should be remarked that the outer sheet crack lengths from table 7.5 are shorter than the final measured crack length in figure 7.7. This is of course related to the better measurements with the digital camera under full crack opening compared to the microscope with manual opening.

Next to the subsurface crack growth, also the delamination zones within the laminate at the left and right crack were investigated. Unfortunately the delamination zone was not always clearly visible: out of the four active zones only three could be obtained for the GLARE 2 laminate. A comparison between the experimental and the calculated delamination zones is given in figure 7.8. From this comparison it is seen that the experimental behaviour is close to the calculated 'aluminium equivalent' one. However

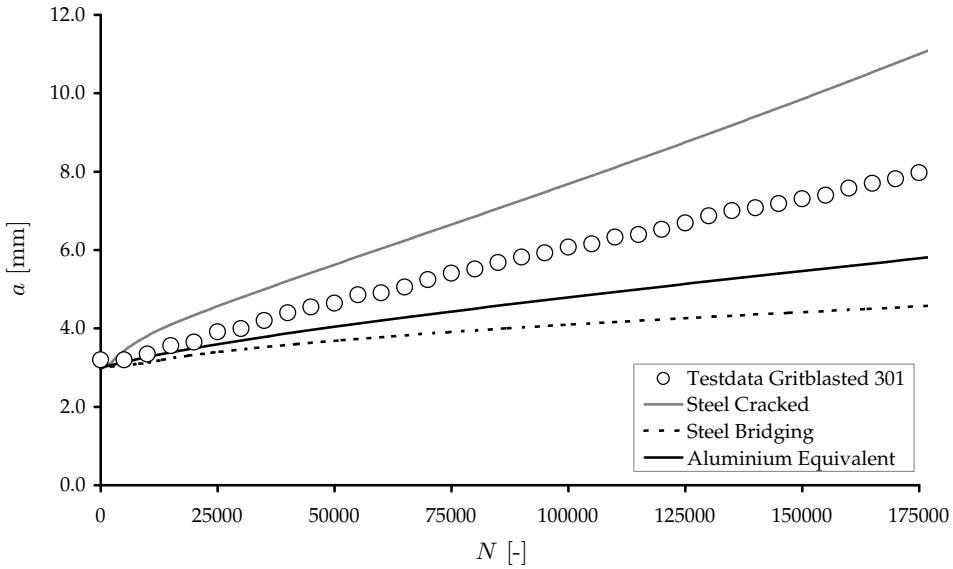

Figure 7.7: *Comparison of experimentally observed and calculated (half) crack length versus number of cycles for* GLARE *2L-2/1-0.3 reinforced with a gritblasted 301 steel strip. With* σ_{max}*=120 MPa, R=0.05, W=80 mm and* a_0*=2.5 mm.*

Table 7.5: *Measured (half) crack lengths in the different layers of the steel reinforced* GLARE *2-2/1-0.3 CCT specimens after 175,000 cycles.*

Reinforcement	Layer	a_{left} [mm]	a_{right} [mm]
Gritblasted 301	(1) aluminium	4.9	4.8
	(2) steel	4.3	4.4
	(3) aluminium	4.9	4.9

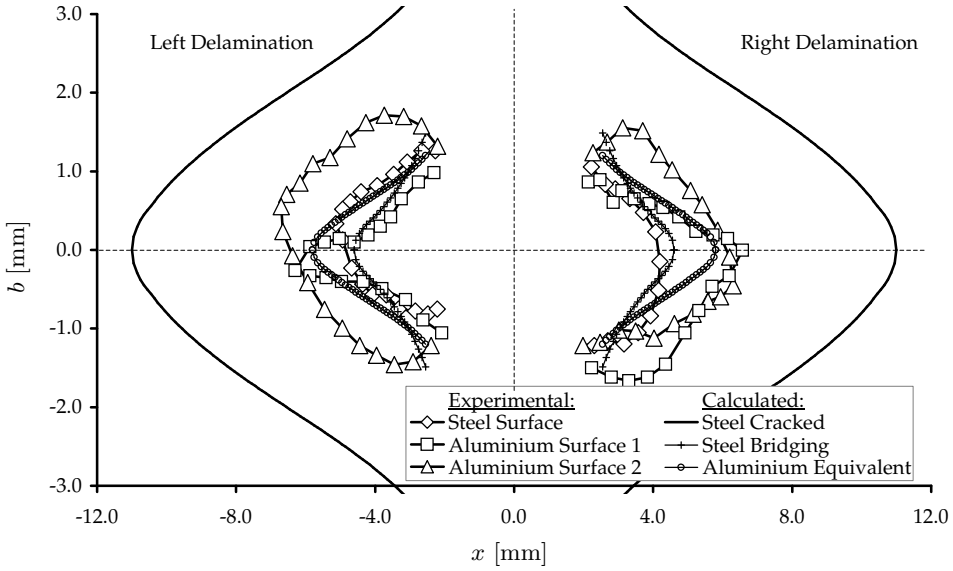

Figure 7.8: *Comparison of experimentally observed and calculated delamination zone along the crack at N=175,000 cycles for* GLARE *2L-2/1-0.3 reinforced with a gritblasted 301 steel strip. With* σ_{max}*=120 MPa, R=0.05, W=80 mm and* a_0*=2.5 mm.*

the observed shape, which was either triangular or elliptical, differs from the calculated parabolic one. This is especially apparent at the region near the saw cut root, where the calculated shape reaches its maximum, while experimentally this maximum is located at a small distance along the crack. This larger delamination at the root results in lower bridging stresses and therefore in an increase of crack growth compared to the elliptic delamination case.

The comparison between measured and calculated crack length for GLARE 3 laminates is given in figure 7.9. In this case relatively faster crack growth is seen, comparable to the assumption that the steel is fully cracked. This relatively fast crack growth for the steel reinforced GLARE 3 laminates is mainly due to the lay-up used: [Alu- ⇳ -Steel- ⇔ -Alu- ⇔ -Steel- ⇳ -Alu]. The crack-bridging fibres (i.e. fibres in the loading direction indicated with ⇳) are only located between the outer aluminium sheet and the steel strips, while especially in the centre of the laminate there is almost no crack bridging capability. This is also seen from the measured subsurface crack lengths in table 7.6, which are longer in the centre than at the outer sheet.

Also for the GLARE 3 laminates the delamination zones were obtained. Indeed no delamination was seen at the interface between metal sheet and fibres perpendicular to the loading direction (so in the centre part of the laminate). For the interfaces with the crack bridging fibres only 50% of the delamination zones could be clearly measured. These measurements and the calculated delamination zones are split into figures 7.10a and b, showing the delamination at the aluminium and steel interface respectively. Also from a delamination point of view the experimental results are quite well approached with the steel cracked assumption.

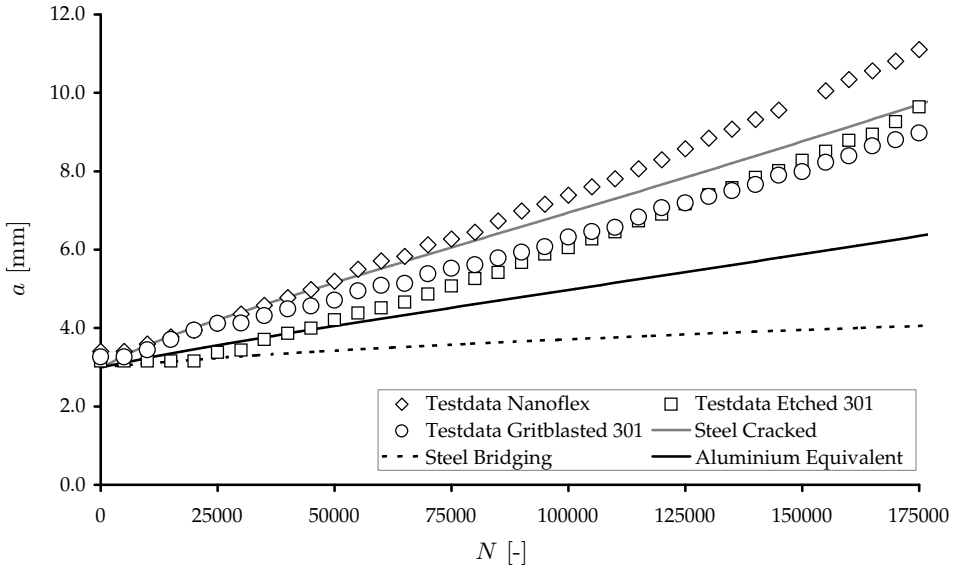

Figure 7.9: *Comparison of experimentally observed and calculated (half) crack length versus number of cycles for* GLARE *3-3/2-0.3 reinforced with either (i) gritblasted 301, (ii) etched 301 or (iii) etched Nanoflex steel strip. With* σ_{max}*=100 MPa, R=0.05, W=80 mm and* a_0*=2.5 mm.*

Table 7.6: *Measured (half) crack lengths in the different layers of the steel reinforced* GLARE *3-3/2-0.3 CCT specimens at N=175,000 cycles.*

Steel Reinforcement	Layer	a_{left} [mm]	a_{right} [mm]
Gritblasted 301	(1) aluminium	5.8	5.8
	(2) steel	6.0	6.3
	(3) aluminium	6.3	6.3
	(4) steel	6.2	6.4
	(5) aluminium	6.1	6.1
Etched 301	(1) aluminium	6.4	6.3
	(2) steel	7.0	6.9
	(3) aluminium	7.0	7.1
	(4) steel	7.1	6.9
	(5) aluminium	6.6	6.5
Nanoflex	(1) aluminium	8.0	7.1
	(2) steel	8.2	7.3
	(3) aluminium	8.0	7.7
	(4) steel	8.2	7.5
	(5) aluminium	7.4	7.3

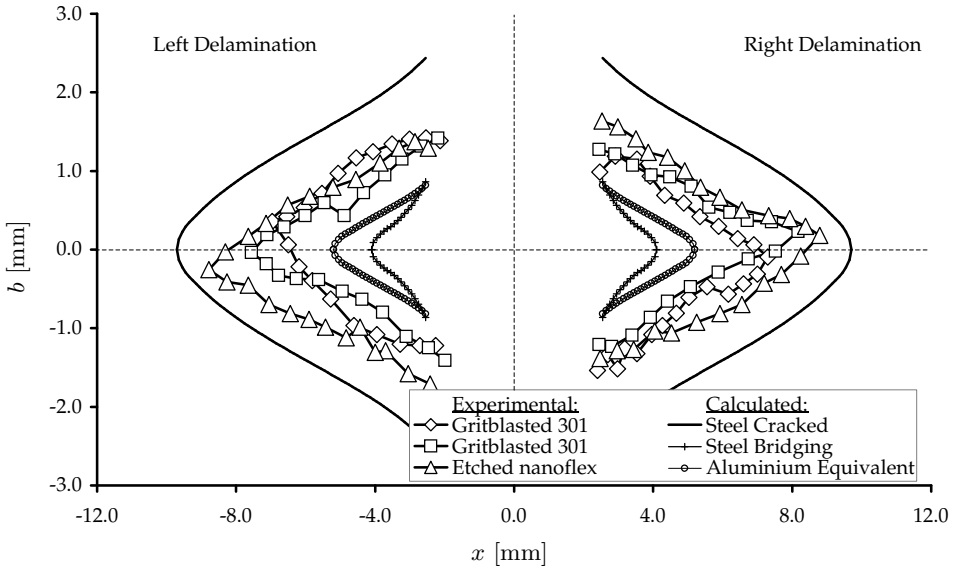

(a) *on the aluminium layers*

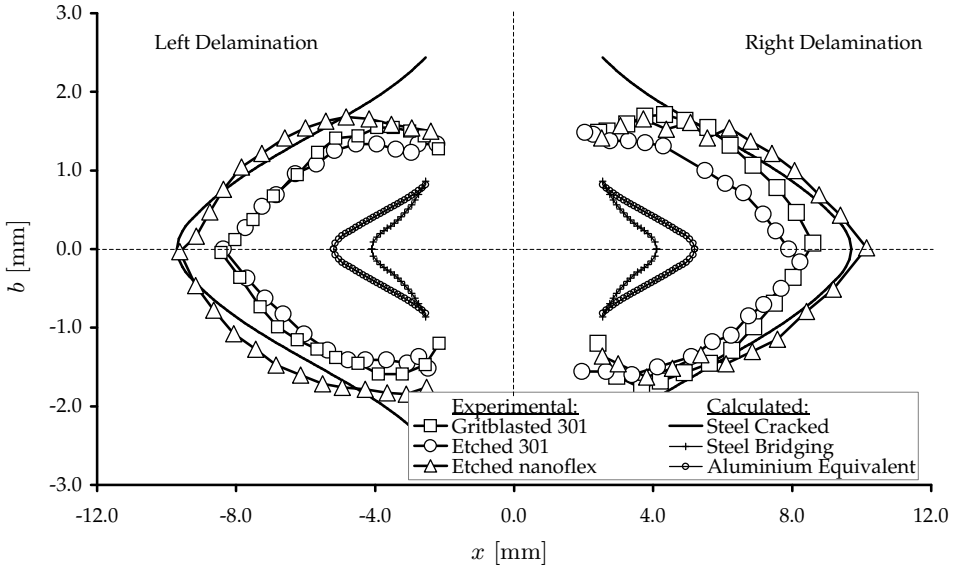

(b) *on the steel layers*

Figure 7.10: *Comparison of experimentally observed and calculated delamination zone along the crack on (a) the aluminium layers and (b) the steel layers at N=175,000 cycles for* GLARE *3-3/2-0.3 reinforced with either (i) gritblasted 301, (ii) etched 301 or (iii) etched Nanoflex steel strip. With σ_{max}=100 MPa, R=0.05, W=80 mm and a_0=2.5 mm.*

The difference in adhesion for the etched and gritblasted 301 sheet does not result in distinct differences in fatigue behaviour. There is actually only a small difference in final crack length between the etched and gritblasted 301. For small crack lengths the etched version performs better, having almost no crack growth but at larger crack lengths it shows faster growth. The delamination at the etched 301 is even slightly smaller than for the gritblasted sheet.

For the specific laminates evaluated it can be concluded that the model generally underestimates the actual behaviour. But with the model limitations and difficulties in fatigue modelling in FMLs in general, the model actually performs quite well.

7.4 Conclusions

The static joint strength of standard and steel reinforced GLARE has been evaluated. It was shown that the steel reinforcement leads to higher joint strength, but the specific strength of a GLARE laminate is higher. The main reason for this was the occurrence of large-scale delamination, which decreases the effectiveness of the steel strip. The effect of the stainless steel strip was mainly seen at the yield point of the joint, due to increased laminate stiffness. An analytical model for joint strength prediction applied to the standard GLARE laminate, performed quite well for the joint yield strength, but resulted in a rather conservative joint ultimate strength.

The fatigue evaluation of the joints has shown that the stainless steel strip results in a decrease of crack growth in the mating aluminium sheets. Compared to standard GLARE, the steel reinforced joints have however subsurface cracks after 100,000 cycles.

Evaluation of the fatigue crack growth with centre-cracked tension specimens, showed a positive influence of the steel strip on a GLARE 2 lay-up, however for the GLARE 3 lay-up increased crack growth was seen. Comparison with an analytical model for fatigue crack growth, showed that the behaviour of steel reinforced GLARE was between the predictions for a GLARE laminate locally reinforced with an aluminium sheet and that of a GLARE reinforced with a cracked steel strip.

Summary & Conclusions

Bearing Strength Characteristics of Standard and Steel Reinforced GLARE

by Reinout van Rooijen

Fibre Metal Laminates (FMLs) are hybrid materials, which consist of thin metal sheets bonded together with alternating (unidirectional) fibre layers. This material concept has resulted in superior fatigue characteristics with respect to the metallic counterpart. Several static characteristics (specifically tension, shear, bearing, blunt and sharp notch behaviour) are however negatively influenced in absolute numbers due to the fibre addition.

Property Optimisation
To define possible improvements of these static strength characteristics, the influence of constituent properties on these characteristics was investigated in chapter 2. The available analytical models were reviewed and if necessary the specific failure mechanisms were described. Using these models and available test data, trend lines were obtained, which indicate the effects of the principal parameters and quantify potential improvements.

It was concluded that carbon, M5 and steel fibres can result in increased properties compared to the currently used glass fibres in GLARE. Likewise, the use of different aluminium alloys or materials like (stainless) steel, titanium and nickel were presented as replacements for the 2024-T3 aluminium in standard GLARE.

Bearing Strength Investigation
Based on the investigation in chapter 2 it was concluded that the knowledge about bearing strength characteristics (i.e. the behaviour of a pin or bolt loaded hole) of FMLs is rather limited. The main part of this thesis, therefore focussed on the description of bearing strength of FMLs and based on the acquired knowledge, a solution was presented to improve the bearing strength. The so-called bolt bearing test is generally applied to composite materials, where lateral restraint is provided to prevent or minimise delamination around the hole. In this thesis also the behaviour of an FML under pin loading, so without lateral restraint, was investigated.

Bolt Bearing Strength of GLARE
The bolt bearing strength, in particular the edge distance sensitivity, of several FMLs of the GLARE family was evaluated experimentally in chapter 3. The behaviour of

the fibre layer with increasing bolt displacement was investigated in detail to obtain a better understanding of its failure mode. In parallel with these experiments, the bearing behaviour was studied using an FE model. Plasticity in the metal layers, failure of the fibre layers and friction between pin and laminate, were all implemented in the model.

A comparison between experimental and FE results showed a good resemblance in both bearing yield and bearing ultimate strength. On a detailed level the damage pattern of the fibre layer compared quite well between experiment and analysis. The elastic stiffness was however underestimated and at high edge distance ratio (e/D) the occurrence of early delamination started to play a role, which results in larger differences in load versus displacement behaviour.

Pin Bearing Strength of GLARE

The occurrence of delamination in GLARE due to a pin load was investigated on a more detailed level in chapter 4. To correctly model this failure mechanism with the FE model, an interface element with mixed mode delamination capabilities was included at the interface between the different layers. The model was validated against experimental data of several FMLs and a bonded aluminium laminate.

A good agreement was obtained both for the load displacement behaviour and the pin bearing strength. The assumption that delamination occurs at the interface between the different layers was seen to be quite close to reality. The model predicts that pin bearing strength can be improved by increasing the interfacial shear strength. Increase in the interfacial tensile strength is shown to play a minor role, while the influence of energy release rates is almost negligible.

Improvement of Bearing Strength

The introduction of GLARE as fuselage material to replace monolithic aluminium structures has led to a higher sensitivity to fastener holes at mechanical joints. To improve the strength of these mechanical joints and in particular the bearing strength, thin stainless steel sheets with high strength were selected to be used as local reinforcement. To allow incorporation of such sheets in FMLs their adhesion to epoxies used in aerospace applications should be at a high level. The adhesion of AISI 301 steel sheets was investigated in chapter 5 for several chemical and mechanical pretreatments. Based on an investigation with the floating roller peel test, it was concluded that gritblasting followed by a silane treatment for adhesion promotion yields the best properties.

Bearing Strength of Steel Reinforced GLARE

Chapter 6 describes the research on the bearing strength of GLARE laminates internally reinforced with thin stainless steel grades. Besides the AISI 301 steel sheet described in the previous chapter also Nanoflex maraging steel was used, which has a lower yield point and tensile strength. These laminates have been experimentally and numerically investigated with both a pin and bolt loaded test setup. The main difference with respect to the FE models from chapter 3 and 4 was the inclusion of a local stainless steel strip.

For the bolt loaded case it was seen that the bearing yield and the force versus pin displacement behaviour were incorrectly captured when the FE model does not allow delamination to occur. Comparable to the GLARE behaviour in chapter 3, early delamination and ply buckling was observed in the experiments. Still the FE model predicted the bearing ultimate strength of the bolt-loaded case quite well. Furthermore the pin bearing behaviour and the bearing yield in the bolt-loaded case was quite well

captured when delamination was accounted for in the model.

Compared to standard GLARE the stainless steel reinforcement resulted in a large increase in bearing strength capabilities. However, based on specific strength properties it was shown that the improvement in bearing strength can also be reached using an aluminium reinforcement layer. The thin steel strip especially offers a smaller increase in thickness and hence a lower eccentricity, which is beneficial for actual joints in real aircraft structures. But also from a production perspective the lower thickness increase is preferable, since it for example requires less stiffener joggling.

Static Joint Strength and Fatigue Behaviour

Prior to application in aircraft structures the static joint strength and fatigue behaviour of these laminates requires further attention. In chapter 7, these characteristics were investigated experimentally for GLARE laminates, reinforced with the two stainless steel grades. The influence of the steel strip on the fatigue behaviour was also studied analytically with a fatigue crack growth model specifically developed for regular GLARE variants.

The presence of the steel strip led to a higher static joint strength, but for the geometry used the increase in yield and ultimate strength level was modest due to large-scale delamination around the hole. The behaviour of these joints under fatigue-loading was improved due to the steel strip, since it results in smaller cracks at the mating sheet. For centre cracked tension specimens the reinforced laminates did not reveal improved characteristics, but this can be attributed to the laminate lay-up.

Samenvatting

Vlaktedrukeigenschappen van Standaard en Staalversterkt GLARE

door Reinout van Rooijen

Vezel Metaal Laminaten (VML) zijn hybride materialen, bestaande uit dunne metaal lagen verlijmd met unidirectionele vezellagen. Dit materiaalconcept heeft geresulteerd in superieure vermoeiingseigenschappen ten opzichte van monolithisch metaal. Verscheidene statische eigenschappen (met name: treksterkte, afschuiving, vlaktedruk en de invloed van stompe en scherpe scheuren) worden in absolute getallen echter negatief beinvloed door de toevoeging van de vezellagen.

Optimalisatie van Eigenschappen
De invloed van de verschillende bestanddelen op de statische eigenschappen van een VML zijn onderzocht in hoofdstuk 2, om via een parameterstudie de haalbare verbeteringen van deze eigenschappen af te schatten. Hiervoor zijn de beschikbare analytische modellen en indien nodig de specifieke faalmechanismen beschreven. Gebaseerd op deze modellen en beschikbare testdata zijn trendlijnen verkregen, waarmee het effect van de belangrijkste eigenschappen en mogelijke verbeteringen beschreven kunnen worden.

Op basis van deze trendlijnen kunnen koolstof, M5 en staal vezels mogelijk leiden tot verbeterde eigenschappen ten opzichte van de huidige glasvezels in GLARE. En 2024-T3 aluminium zou vervangen kunnen worden door andere aluminiumlegeringen, (roestvast) staal, titanium of nikkel.

Vlaktedrukeigenschappen
Zoals bleek in hoofdstuk 2 is de kennis over vlaktedrukeigenschappen (het gedrag van een pen- of bout-belast gat) van VML redelijk beperkt. Dit proefschrift concentreert zich daarom met name op de vlaktedruksterkte van VML. Gebaseerd op de verkregen kennis wordt een oplossing aangedragen om deze eigenschap te verbeteren. De vlaktedrukeigenschappen van composietmaterialen worden normaal gesproken gemeten aan een bout-belast gat, waarbij het materiaal zijdelings wordt ondersteund om delaminatie rond het gat te voorkomen. In dit proefschrift wordt ook het gedrag beschreven van een pen-belast gat, waarbij geen zijdelingse ondersteuning wordt aangebracht.

Bout-Belast Gat in GLARE
De sterkte van enkele GLARE laminaten met een bout-belast gat en met name de invloed

van de randafstand van dit gat is experimenteel onderzocht in hoofdstuk 3. Het gedrag van de vezellaag als functie van toenemende boutverplaatsing is onderzocht om een beter begrip te krijgen van het faalmechanisme. Parallel aan deze experimenten zijn de vlaktedrukeigenschappen onderzocht met een eindige elementen (EE) model. Dit model bevat zowel plasticiteit in de metaallagen, het bezwijken van de vezellaag als wrijving tussen de bout en het laminaat.

De vergelijking tussen experimentele en numerieke resultaten toont een klein verschil aan voor het vloeipunt en de breuksterkte onder vlaktedruk. Ook het voorspelde schadepatroon van de vezellaag komt redelijk overeen met de werkelijkheid. De stijfheid in het elastische gebied wordt echter onderschat en voor grote randafstand (e/D) begint vroegtijdige delaminatie een rol te spelen wat resulteert in verschillen in het kracht-verplaatsingsverloop.

Pen-Belast Gat in GLARE

Het optreden van delaminatie in GLARE rond het pen-belaste gat is nader onderzocht in hoofdstuk 4. Om dit faalmechanisme correct te beschrijven met een EE model, is een zogenaamd 'interface' element met 'mixed mode' delaminatie gedrag toegevoegd tussen de verschillende lagen. Dit model is gevalideerd met experimenten op enkele vezel metaal laminaten en een gelijmd aluminium laminaat.

Zowel voor het kracht-verplaatsingsverloop als de vlaktedruksterkte was het model redelijk nauwkeurig. De aanname, dat delaminatie optreedt bij de overgang tussen de verschillende lagen, bleek redelijk overeen te komen met de werkelijkheid. Met behulp van het model is de invloed van de eigenschappen van het grensvlak bepaald. Hieruit bleek dat verbetering van de vlaktedruksterkte met name verkregen kan worden door een toename van de afschuifsterkte. De treksterkte van de interface heeft een kleinere invloed, terwijl de invloed van de 'energy release rate' parameters te verwaarlozen is.

Verbetering van de Vlaktedruksterkte

De toepassing van GLARE als rompmateriaal in plaats van monolitisch aluminium heeft geleid tot een grotere (negatieve) invloed van verbindingsgaten bij mechanische verbindingen. Door dunne roestvast stalen strips met hoge sterkte in te lijmen in standaard GLARE wordt naar verwachting de vlaktedruksterkte van mechanische GLARE verbindingen verbeterd. Voor succesvolle toepassing van deze strips in een VML is het echter noodzakelijk dat ze voldoende hechting hebben met standaard vliegtuigbouw epoxies. De hechting van AISI 301 staal strips is onderzocht in hoofdstuk 5 voor verschillende chemische en mechanische voorbehandelingen. Op basis van testresultaten met de 'floating roller' afpel test, bleek gritstralen gevolgd door een silaan behandeling het beste resultaat op te leveren.

Vlaktedruksterkte van Staalversterkt GLARE

Hoofdstuk 6 beschrijft het onderzoek naar de vlaktedruksterkte van GLARE laminaten versterkt met dunne roestvast staalsoorten. Naast het AISI 301 staal van het vorige hoofdstuk is ook Nanoflex staal gebruikt, wat een lager vloeipunt en een lagere breukspanning heeft. Het gedrag van deze laminaten onder invloed van zowel een bout- als een pen-belast gat is zowel experimenteel als numeriek onderzocht. Grootste verschil met het EE model uit hoofdstuk 3 en 4 is de toevoeging van de lokale roestvast stalen strip.

Voor het bout-belaste gat bleek het EE model zowel het vloeipunt als het kracht-verplaatsingsverloop niet goed te beschrijven tenzij delaminatie werd toegestaan. Net als voor standaard GLARE in hoofdstuk 3, treden delaminatie en het verder uitknikken

van de lagen vroegtijdig op tijdens de experimenten. De resultaten voor de sterkte van het laminaat komen echter redelijk overeen. Het gedrag van een pen-belast gat en het vloeipunt voor een boutbelasting wordt beter beschreven als delaminatie wordt toegestaan.

Ten opzichte van standaard GLARE zorgt de roestvast stalen versterking voor een grote toename in vlaktedruksterkte. Gebaseerd op specifieke eigenschappen is het ook mogelijk om deze toename te verkrijgen met een extra aluminium laag. De dunne staal strip veroorzaakt echter met name een kleinere diktetoename en hierdoor een lagere eccentriciteit, wat een voordeel is voor mechanische verbindingen in echte vliegtuigconstructies. Maar ook gezien vanuit een productiestandpunt is de lagere dikte een voordeel, aangezien het leidt tot een vlakker oppervlak.

Statische Verbindingsterkte en Vermoeiingsgedrag
Voordat staalversterkt GLARE toegepast kan worden in een vliegtuigconstructie is het noodzakelijk dat de statische verbindingssterkte en de vermoeiingseigenschappen onderzocht worden. Deze eigenschappen zijn nader experimenteel beschouwd in hoofdstuk 7, voor enkele GLARE laminaten versterkt met de twee staalvarianten. De invloed van de staalversterking is verder ook onderzocht met een scheurgroeimodel dat specifiek voor standaard GLARE varianten is ontwikkeld.

Ten opzichte van standaard GLARE heeft de staalversterkte variant een hogere verbindingssterkte, maar voor de gebruikte laminaatopbouw is de toename in vloeipunt en breukspanning gering ten gevolge van grootschalige delaminatie rond het gat. De vermoeiingseigenschappen van deze verbindingen zijn verbeterd door de stalen strip, aangezien het leidt tot kleinere scheurlengtes. Voor de vermoeiingsproefstukken met een centrale scheur leidde de staalversterking niet tot betere eigenschappen, maar ook dit is te wijten aan de laminaatopbouw.

Bibliography

[1] L.B. Vogelesang and A. Vlot. Development of Fibre Metal Laminates for Advanced Aerospace Structures. *Journal of Materials Processing Technology*, 103:1–5, 2000.

[2] A. Vlot. Impact Loading on Fibre Metal Laminates. *International Journal of Impact Engineering*, 18:291–307, 2000.

[3] B.A. Burianek. *Mechanics of Fatigue Damage in Titanium-Graphite Hybrid Laminates*. PhD thesis, Massachusetts Institute of Technology, 2001.

[4] C.A.J.R. Vermeeren. The Application of Carbon Fibres in ARALL Laminates. Technical Report LR 658, Delft University of Technology, 1991.

[5] P. Cortés and W.J. Cantwell. The Tensile and Fatigue Properties of Carbon Fiber-Reinforced PEEK-Titanium Fiber-Metal Laminates. *Journal of Reinforced Plastics and Composites*, 23:1615–1623, 2004.

[6] A. Afaghi-Khatibi, G. Lawcock, L. Ye, and Y.W. Mai. On the Fracture Mechanical Behaviour of Fibre Reinforced Metal Laminates (FRMLs). *Computer Methods in Applied Mechanics and Engineering*, 185:173–190, 2000.

[7] C.T. Lin, P.W. Kao, and F.S. Yang. Fatigue Behaviour of Carbon Fibre-Reinforced Aluminium Laminates. *Composites*, 22:135–141, 1991.

[8] P. Cortés and W.J. Cantwell. Fracture Properties of a Fiber-Metal Laminates Based on Magnesium Alloy. *Journal of Materials Science*, 39:1081–1083, 2004.

[9] F.L. Matthews, A.A. Roshan, and L.N. Phillips. The Bolt Bearing Strength of Glass/Carbon Hybrid Composites. *Composites*, 13:225–227, 1982.

[10] E.W. Godwin and F.L. Matthews. A review of the strength of joints in fibre-reinforced plastics - Part 1. Mechanically fastened joints. *Composites*, 11:155–160, 1980.

[11] P.P. Camanho and F.L. Matthews. Stress-Analysis and Strength Prediction in FRP Joints: a Review. *Composites Part A*, 28:529–547, 1997.

[12] T.J. de Vries. *Blunt and Sharp Notch Behaviour of* GLARE *Laminates*. PhD thesis, Delft University of Technology, 2001.

[13] W.J. Slagter. *Static Strength of Riveted Joints in Fibre Metal Laminates*. PhD thesis, Delft University of Technology, 1993.

[14] P.P. Camanho and C.G. Davila. Mixed-Mode Decohesion Finite Elements for the Simulation of Delamination in Composite Materials. Technical Report TM-2002-211737, NASA, 2002.

[15] G.H.J.J. Roebroeks. *Towards* GLARE- *the Development of a Fatigue Insensitive and Damage Tolerant Aircraft Material*. PhD thesis, Delft University of Technology, 1991.

[16] M. Hagenbeek. Shear Yield Strength. In A. Vlot and J.W. Gunnink, editors, *Fibre Metal Laminates an Introduction*. 2002.

[17] B. Okutan, Z. Allan, and R. Karakuzu. A Study of the Effects of Various Geometric Parameters on the Failure Strength of Pin-Loaded Woven-Glass-Fiber Reinforced Epoxy Laminate. *Composites Science and Technology*, 61:1491–1497, 2001.

[18] B.M. Içten and R. Karakuzu. Progressive Failure Analysis of Pin-Loaded Carbon-Epoxy Woven Composite Plates. *Composites Science and Technology*, 62:1259–1271, 2002.

[19] C.A.J.R. Vermeeren. *The Residual Strength of Fibre Metal Laminates*. PhD thesis, Delft University of Technology, 1995.

[20] J.S. Hidde and C.T. Herakovich. Inelastic Response of Hybrid Composite Laminates. *Journal of Composite Materials*, 26, 1992.

[21] M. Kawai, M. Morishita, S. Tomura, and K. Takumida. Inelastic Behaviour and Strength of Fibre-Metal Hybrid Composite: GLARE. *International Journal of Mechanical Sciences*, 40:183–198, 1998.

[22] T.J. de Vries, A. Vlot, and F. Hashagen. Delamination Behaviour of Spliced Fiber Metal Laminates. Part 1. Experimental Results. *Composite Structures*, 46:131–145, 1999.

[23] J. Schijve and J. Snijder. The Effect of Blunt Notches and Saw Cuts on the Static Strength of 2024-T3 and 7075-T6 Sheet Material. Technical Report LR 313, Delft University of Technology, 1981.

[24] G.D. Lawcock, L. Ye, Y.W. Mai, and C.T. Sun. Effects of Fibre/Matrix Adhesion on Carbon-Fibre-Reinforced Metal Laminates - I. Residual Strength. *Composites Science and Technology*, 57:35–45, 1997.

[25] J.C.F.N. van Rijn. The Use of Composite Fracture Models to Describe the Blunt Notch Behaviour of Metal Laminates. Technical Report NLR TP 92061 U, 1992.

[26] J.M.M. de Kok. *Deformation, Yield and Fracture of Unidirectional Composites in Transverse Loading*. PhD thesis, Technische Universiteit Eindhoven, Eindhoven, 1995.

[27] F.L. Matthews. The Static Strength of Bolted Joints in Fibre Reinforced Plastics. In *Behaviour and Analysis of Mechanically Fastened Joints in Composite Structures 9*, number CP-427. 1988.

[28] R.L. Moore and C. Wescoat. Bearing Strength of Some Wrought-Aluminium Alloys. Technical Report NACA TN 901, NACA, 1943.

[29] C. Wescoat and R.L. Moore. Bearing strengths of 75S-T aluminum-alloy sheet and extruded angle. Technical Report NACA TN-974, NACA, 1945.

[30] Department of Defence. Military Handbook 5H. Technical report, Department of Defence, United States of America, 1998.

[31] Th. de Jong. Stresses around pin-loaded holes in elastically orthotropic or isotropic laminates. *Journal of Composite Materials*, 11:313–331, 1977.

[32] C.L. Hung and F.K. Chang. Bearing Failure of Bolted Composite Joints. Part II: Model and Verification. *Journal of Composite Materials*, 30:1359–1399, 1996.

[33] P. Perugini, A Riccio, and F. Scaramuzzino. Three-Dimensional Progressive Damage Analysis of Composite Joints. In B.H.V. Topping, editor, *Proceedings of the Eigth International Conference on Civil and Structural Engineering Computing*, 2001.

[34] K.I. Tserpes, P. Papanikos, and Th. Kermanidis. A three-dimensional progressive damage model for bolted joints in composite laminates subjected to tensile loading. *Fatigue Fracture Engineering Material Structures*, 24:663–675, 2001.

[35] F.K. Chang, R.A. Scott, and G.S Springer. Strength of Mechanically Fastened Composite Joints. *Journal of Composite Materials*, 16:470–494, 1982.

[36] J.M. Whitney and R.J. Nuismer. Stress Fracture Criteria for Laminated Composites Containing Stress Concentrations. *Journal of Composite Materials*, 8:253–265, 1974.

[37] H.F. Wu, L.L. Wu, and W.J. Slagter. An investigation on the bearing test procedure for fibre-reinforced aluminum laminates. *Journal of Material Science*, 29:4592–4603, 1994.

[38] ASTM. Standard Test Method for Pin-Type Bearing Test of Metallic Materials E238-84. In *Annual Book of ASTM Standards*. ASTM, 1984.

[39] ASTM. Standard Test Method for Bearing Strength of Plastics, D953-92. In *Annual Book of ASTM Standards*. ASTM, 1992.

[40] Department of Defence. Military Standard 1312, Fasteners, Test Methods, Test 4, Joint Shear Strength. Technical report, Department of Defence, United States of America.

[41] Z. L. Zhang, M. Hauge, J. Ødegård, and C. Thaulow. Determining material true stress-strain curve from tensile specimens with rectangular cross-section. *International Journal of Solids and Structures*, 36:3497–3516, 1999.

[42] Y. Ling. Uniaxial True Stress-Strain after Necking. *AMP Journal of Technology*, 5:37–48, 1996.

[43] F.K. Chang and L.B. Lessard. Damage Tolerance of Laminated Composites Containing an Open Hole and Subjected to Compressive Loadings: Part I - Analysis. *Journal of Composite Materials*, 25:2–43, 1991.

[44] J.H.A. Schipperen. An Anisotropic Damage Model for the Description of Transverse Matrix Cracking in a Graphite-Epoxy Laminate. *Composite Structures*, 53:295–299, 2001.

[45] P.P. Camanho, C.G. Davila, and M.F. De Moura. Numerical Simulation of Mixed-Mode Progressive Delamination in Composite Materials. *Journal of Composite Materials*, 37:1415–1438, 2003.

[46] F. Hashagen. *Numerical Analysis of Failure Mechanisms in Fibre Metal Laminates*. PhD thesis, Delft University of Technology, 1998.

[47] ABAQUS. A Finite Element System, Version 6.3. User's Manual, 2002.

[48] I. Eriksson. On the Bearing Strength of Bolted Graphite/Epoxy Laminates. *Journal of Composite Materials*, 24:1246–1269, 1990.

[49] Cytec Industries Inc. *FM94 datasheet*, 1997.

[50] M. Vesco and J. Sinke. Response and Damage Evolution in GLARE Laminates under Indentation Loads - Experimental Results. Technical Report B2V-05-01, Delft University of Technology, 2005.

[51] F. ParíS. A Study of Failure Criteria of Fibrous Composite Materials. Technical Report NASA/CR-2001-210661, NASA, 2001.

[52] Standard Guide for Preparation of Metal Surfaces for Adhesive Bonding - D2651. In *Annual Book of ASTM Standards*. 2001.

[53] F. Bouquet, J.M. Cuntz, and C. Coddet. Influence of Surface Treatment on the Durability of Stainless Steel Sheets Bonded with Epoxy. *Journal of Adhesion Science and Technology*, 6:233–242, 1992.

[54] G.B. Gaskin, G.J. Pilla, and S.R. Brown. Preparation of Stainless Steel Adherends for Adhesive Bonding. *Journal of Testing and Evaluation*, 22:222–225, 1994.

[55] Standard Specification for Chemical Passivation Treatments for Stainless Steel Parts - A967. In *Annual Book of ASTM Standards*. 2001.

[56] K.L. Mittal, editor. *Silanes and Other Coupling Agents*, volume 2. VSP, Utrecht, (2000).

[57] K.L. Mittal, editor. *Silanes and Other Coupling Agents*, volume 3. VSP, Utrecht, (2004).

[58] Standard Test Method for Floating Roller Peel Resistance of Adhesives - D3167. In *Annual Book of ASTM Standards*. 2003.

[59] J.R. Davis. *Corrosion - Understanding the Basics*. ASM International, Metals Park, Ohio, 2000.

[60] R. Li, D. Kelly, and A. Crosky. Strength Improvement by Fibre Steering around a Pin Loaded Hole. *Composite Structures*, 57:377–383, 2002.

[61] P. Camanho and F.L. Matthews. Bonded Metallic Inserts for Bolted Joints in Composite Laminates. In *Proceedings of the I MECH E Part L Journal of Materials: Design and Applications*, volume 214, pages 33–40, 2000.

[62] S. Nilsson. Increasing Strength of Graphite/Epoxy Bolted Joints by Introducing an Adhesively Bonded Metallic Insert. *Journal of Composite Materials*, 23:642–650, 1989.

[63] A. Fink and B. Kolesnikov. Hybrid Titanium Composite Material Improving Composite Structure Coupling. Website: www.dlr.de.

[64] A. Banbury and D.W. Kelly. A Study of Fastener Pull-Through Failure of Composite Laminates. Part 1: Experimental. *Composite Structures*, 45:241–254, 1999.

[65] W.J. Slagter. On the Tensile Strength of Rivets in Thin Sheet Materials and Fibre Metal Laminates. *Thin-Walled Structures*, 21:121–145, 1995.

[66] R.C. Alderliesten. *Fatigue Crack Propagation and Delamination Growth in* GLARE. PhD thesis, Delft University of Technology, 2005.

[67] R. Marissen. *Fatigue Crack Growth in* GLARE*, A Hybrid Aluminium-Aramid Composite Material, crack growth mechanisms and quantitative predictions of the crack growth rate.* PhD thesis, Delft University of Technology, 1988.

[68] Y.J. Guo and X.R. Wu. Bridging Stress Distribution in Center-Cracked Fiber Reinforced Metal Laminates: Modelling and Experiment. *Engineering Fracture Mechanics*, 63:147–163, 1999.

Publications

R.G.J. van Rooijen, J. Sinke, T.J. de Vries and S. van der Zwaag, Property Optimisation in Fibre Metal Laminates, *Applied Composite Materials*, Volume 11, Number 2, pp. 63-76, 2004.

R.G.J. van Rooijen, J. Sinke and S. van der Zwaag, Improving the Adhesion of Thin Stainless Steel Sheet for FML Applications, *Journal of Adhesion Science Technology*, Volume 19, Number 16, pp. 1387-1396, 2005.

R.G.J. van Rooijen, J. Sinke, T.J. de Vries and S. van der Zwaag, The Bearing Strength of Fibre Metal Laminates, *Journal of Composite Materials*, Volume 40, Number 1, pp. 5-19, 2006.

R.G.J. van Rooijen, R. Benedictus and S. van der Zwaag, The Pin Bearing Strength of Fibre Metal Laminates, *submitted to Journal of Composite Materials*.

R.G.J. van Rooijen, R. Benedictus and S. van der Zwaag, The Bearing Strength of Steel Reinforced GLARE, *to be submitted*.

R.G.J. van Rooijen, R. Benedictus and S. van der Zwaag, The Static Joint Strength and Fatigue Behaviour of Steel Reinforced GLARE, *to be submitted*.

Acknowledgements

The supervision that I received during my PhD from my promotor professor Sybrand van der Zwaag is something that I will cherish all my life. Thank you for your different way of thinking, for keeping up with my short style of writing and for being always available to comment on my work. Due to circumstances, I could not always benefit from the useful comments of Tjerk de Vries, but his 'practical' view on things was really valuable to me. I started this PhD work under the supervision of professor Ad Vlot, but unfortunately I was never able to benefit from this, but he is in my memory as the person that gave me the chance to start this work. I am furthermore grateful for the supervision that I received from Jos Sinke and professor Rinze Benedictus. And I should not forget to mention the good (working) environment that the NIMR provided: the courses and the social events made it a great 'company' to work for.

Finite elements became a lot more clear during the development of the delamination model, for which I especially thank Joris Remmers for providing me this insight. For the research on fatigue that I performed, I want to thank René Alderliesten for providing me with his crack growth model. On the pretreatment of stainless steel, the useful discussions with the people from the Adhesion Institute (especially Jeroen Hofstede) were important for my understanding. And Peter de Regt and Michel Badoux thank you for priming the stainless steel sheets after those many pretreatment trials. And of course I want to thank Ludwig Padji for performing several bearing experiments.

On the experimental side, things would not have run as smoothly without the help of the people in the *Vliegtuighal*. For tools, help with drilling the numerous holes or just for easy tips there were always Bertus van der Stok, Ed Roesen, Kees Paalvast and especially Herman Werges available to help me out. For deep analysis and for the dirty part of my research (pretreatment of my stainless steel material) the help of but also the discussions with Frans Oostrum were really valuable. And whenever I needed an acoustic analysis of my material or specimens, there was always Serge van Meer to give me quick answers on this. Controlling the test machines (both static and fatigue) was not always an easy job, but I am happy that Jeroen Los taught me several tricks to work with them. And Niels Jalving, thank you for having almost always the machines available whenever I needed to perform a test. A large part of this thesis contains research on GLARE material, for which I am happy that Rob Leonard helped me out with both standard sheet and the steel reinforced case. Due to circumstances the *Vliegtuighal*, was not always fully operational, but I was lucky that Jan Boomstra at Materials Science helped me out with gritblasting my stainless steel sheets. Finally I want to pay gratitude to the person that made sure that we had enough oxygen to keep our brain working: thank you Hans Weerheim for watering the plants.

During my research I have used a lot of different materials and I could not have done this without the support of several people. The main contribution in this respect was

the help of Remco Jongen from Sankvik and Huib Blaauw and Tjamme de Vries from Philips DAP, who helped me enormously with the stainless steel sheet and with the discussions on pretreatment. Even though it is not treated in this PhD thesis, still the stainless steel fibres that I received from Bekaert and the perforated nickel foil from Stork Prints were valuable in my research.

During my PhD work I was lucky to have a roommate like Chris Randell. In my opinion we were a perfect combination: the valuable discussions about experiments and FE models, but also the chats about 'world politics' and just the friendship made it a great time. Roommate for a while, Mario Vesco, thank you for the entertaining moments. Furthermore I should really thank Jens de Kanter, Tjarko de Jong, Arjan Woerden and Pieter van Nieuwkoop, who helped me out with the 'laatste loodjes', graphics, material pretreatment, finite element questions and with keeping up the spirit.

And now it is time to thank the most important people in my life, three generations that supported me in different ways. Mum thank you for your support and just for being you and Dad thanks for the moral support up from your cloud. Lisanna, although now, when I write this, you are still too young to understand what your father did in your first year and the three years before, one day you will. The research did not get more difficult with you around, maybe in a way it just got easier. It was probably good that you drew my attention more towards full diapers, baby toys and having fun with such a little girl. Ioana, yes we did it, the work is done and I stress that WE did it, thank you for the support during those difficult moments and of course also during the easy ones. It is more than obvious that in some countries they address the partner of the 'dr.' also with this title.

About the Author

Reinout van Rooijen was born on the 23rd of October 1976 in the village Werkhoven (the Netherlands), which is part of the municipality Bunnik. He attended the Athenaeum (pre-university education) in Doorn at the Revius Lyceum from 1989 till 1995.

Subsequently, he started the study Aerospace Engineering at Delft University of Technology. Parallel to this study he worked for 2 to 3 days per week as a software tester at a Dutch-Romanian company. During the final part of his study at the department of Aerospace Materials he tackled two different subjects: The 'Behaviour of Fasteners under Tensile Loads' as preliminary project and the 'Feasibility Study for GLARE as Pressure Bulkhead Material' as final graduation project. This was shortly interrupted in the spring of 2001 for an internship at Stork Fokker.

Soon after graduation in October 2001, the author started a PhD study in the framework of the NIMR at the Faculty of Aerospace Engineering. Under the supervision of prof. dr. ir. S. van der Zwaag he finalised his PhD thesis in 2006. The research has resulted in a patent on the reinforcement of GLARE material with stainless steel strips.